BRAZOS RIVER FLOOD SEDIMENT DEPOSITION, REMOBILIZATION AND CONTINENTAL SHELF PATHWAYS

A Thesis

by

ANDREW BRIAN MCGUFFIN

Submitted to the Office of Graduate and Professional Studies of
Texas A&M University
in partial fulfillment of the requirements for the degree of

MASTER OF SCIENCE

Chair of Committee,	Timothy Dellapenna
Committee Members,	Peter Santschi
	Peter van Hengstum
Head of Department,	Shari Yvon-Lewis

May 2018

Major Subject: Oceanography

ABSTRACT

The Brazos River flows through central Texas and empties into the northwestern Gulf of Mexico. Brazos River discharge is highly variable and is controlled in part by the El Niño Southern Oscillation (ENSO). The Brazos River reached historic discharge levels in 2015 and 2016, including the second highest discharge event ever recorded, concurrent with a strong El Niño. Following these floods, several boxcore sampling cruises between February 2016 and September 2016 captured the temporal and spatial evolution of flood sediment deposited along the continental shelf near the mouth of the Brazos River. Additional boxcores and vibra-cores were collected farther downcoast in the Texas Mud Blanket (TMB), a continental shelf depocenter, in an attempt to determine preservation potential of Brazos River sediments. Brazos River flood sediments were identified in nearshore boxcores using ^{7}Be activities, grain size, porosity and x-radiograph data. Vibra-cores were analyzed using grain size, porosity, X-ray fluorescence (XRF), ^{210}Pb geochronology, x-radiography and photography. Flood deposits are homogeneous, generally coarsen upwards, with relatively enriched ^{7}Be inventories. Flood deposit thicknesses ranged from 2.5 to 40 cm and thicken with increasing water depth and distance from the Brazos River mouth. TMB sedimentation rates range from 0.21 to 0.59 cm yr^{-1} in the TMB, with evidence of Brazos River sourced sediment preservation and temporal variability of Brazos River sediment supply to the TMB. Flood deposits are reworked on an intra-annual, inter-flood timescale, with significant remobilization during fall and winter due to strong, westward currents, which likely play a role in sediment preservation within the TMB.

ACKNOWLEDGEMENTS

I would like to thank my committee chair, Dr. Timothy Dellapenna, and my committee members, Dr. Peter Santschi and Dr. Peter van Hengstum for their mentorship. I am grateful to Dr. Joseph Carlin, who paved the way for this research and helped it develop into this document. I am in debt to Dr. Peng Lin, Dr. Kathleen Schwehr and Dr. Chen Xu for their assistance and guidance on radioisotope methods. I am grateful to the Texas Sea Grant and National Science Foundation for providing funding for this research.

Special recognition goes to my peers. You all have been a joy to work with and have made this experience one that I will not forget. Thank you for sharing all the good times (and bad) with me. You've helped me become a better scientist and person and this research would not have been completed if I you hadn't been so supportive.

Lastly I'd like to thank my family for their encouragement and support in my pursuit of my education. They have been incredibly magnanimous in my undergraduate, graduate and professional careers. I aim to make them proud as a son, brother and significant other because I admire all of them for their exemplary personal and professional qualities.

CONTRIBUTORS AND FUNDING SOURCES

This work was supervised by the following committee members: Timothy Dellapenna and Peter van Hengstum of the Departments of Oceanography and Marine Sciences and Dr. Peter Santschi of the Department of Marine Sciences. XRF and TMB boxcore gamma spectroscopy was completed by Dr. Joseph Carlin at California State University, Fullerton. The remainder of the thesis work was completed independently by the student at Texas A&M University.

This research was funded in part by a National Science Foundation Rapid Grant (#1548598).

TABLE OF CONTENTS

Page

LIST OF FIGURES

Page

LIST OF TABLES

1. INTRODUCTION

Flooding is an important process for sediment delivery to coastal environments, including deltas, flood plains, estuaries, and barrier islands. Floods are also globally significant sources of sediment to shelf and slope and are typically driven by increases in rainfall over short-timescales (Wheatcroft, 2000, Milliman and Meade, 1983). Coastal communities, representing >37% of the human population, are at risk of inundation due to rising sea levels (Syvitski et al., 2005). With increased dam construction and soil erosion controls, fluvial sediment supply has drastically decreased (Meade and Moody, 2009, Blum and Roberts, 2009). Anthropogenic changes in natural sediment transport pathways have resulted in the reduction of sediment delivered to the coast by 1.4 BT/yr from pre-human load levels (Syvitski et al., 2005). Understanding the fate of sediment delivered to coastal environments is important in developing mitigation techniques for coastal land loss.

This study aims to answer the following questions: 1) How do modern Brazos River flood deposits change in thickness and spatial extent over intra-annual timescales? 2) Is there evidence of varying Brazos River sediment input preserved in the Texas Mud Blanket (TMB)? Brazos River flood sediment should be discernable using the methods proposed below. Flood sediment should be deposited near the mouth of the river and remobilized on an inter-flood timescale. Brazos River sediment layers should be preserved and identifiable in the TMB. These questions will test the hypotheses that Brazos River flood deposits are distinguishable and stratigraphically significant in the nearshore environment and Brazos River deposits are preserved in the TMB with evidence of temporal variability in sediment supply.

1.1 Study Area

A likely depocenter of Brazos River flood sediment is the TMB, located on the continental shelf offshore central and southern Texas (Weight et al., 2011). Currents offshore the Brazos River are predominantly westward, advecting sediment towards the TMB (Cochrane and Kelly, 1986, Jarosz and Murray, 2013). The TMB has retained Brazos River sediment for at least the past 3 ka (Weight et al., 2011). Due to these westward currents and the relatively short distance (~75 km) between the eastern edge of the TMB and the Brazos River mouth, preservation potential of Brazos River flood layers in the TMB is high. Previous research has found that Brazos River flood deposits are readily mobilized in under a year after initial deposition near the mouth of the river (Carlin and Dellapenna, 2014).

The Brazos River flows through eastern New Mexico, central Texas and into the northeastern Gulf of Mexico (GOM). One of the strongest El Niño's on record occurred from late-2014 to mid-2016, during which Texas received record rainfall and the Brazos River experienced several flooding events. Seven distinct flooding events exceeded the National Weather Service's Flood Stage of 13.11 m at the Rosharon, TX river gauge station during this period. The three largest of these were on June 4th, 2015, April 24th, 2016 and June 4th, 2016, each with a respective peak discharge of 1917 m^3/s, 1914 m^3/s and 3172 m^3/s. The June 4th, 2016 flooding event was the second highest daily discharge ever recorded at the Rosharon, TX river gage station (USGS 08116650).

The Brazos River drainage basin encompasses 118,000 km^2 (Fraticelli, 2006). The river is subject to a variety of climates, ranging from arid to subhumid, as it flows from eastern New Mexico, through central Texas and eventually into the Gulf of Mexico (GOM) near Freeport,

TX. (Fraticelli, 2006). On average, the river delivers 16 x 10^6 t yr^{-1} of sediment to the GOM and forms a wave-dominated delta on the Texas coast (Milliman and Meade, 1983). Discharge from the river is highly variable and dependent on precipitation patterns related to the El Niño-Southern Oscillation (ENSO). During El Niño periods, Texas, and consequently the Brazos River, experiences higher precipitation and flooding, and during La Niña periods Texas experiences drought conditions (Fraticelli, 2006, Labat, 2008) The Brazos River is currently the only riverine source of sand in the northwest GOM, however, its sand delivery is minimal (Anderson et al., 2014). Brazos River sediment delivery has decreased over the past millennium, in part due to anthropogenic influences such as dams and river diversions (Anderson et al., 2014, Carlin and Dellapenna, 2015).

The TMB is a mid-continental shelf depression that acts as a depocenter for fluvial-sourced sediment entering the shelf. The TMB began to accumulate sediment about 20 ka when global sea level was at a lowstand (Weight et al., 2011). Brazos River sediment has been accumulating in the TMB for at least the last 3 ka (Weight et al., 2011). The primary, modern contributing rivers to TMB sedimentation are the Brazos, Rio Grande and Mississippi Rivers, with reworked shelf sediments also contributing significantly to accumulation rates (Weight et al., 2011, Anderson et al., 2016).

1.2 Regional Oceanography and Meteorology

The Louisiana-Texas Coastal Current (LTCC) is a coastal current situated in the northeast GOM, offshore Texas and Louisiana. During the late summer the LTCC experiences a weak reversal of mean flow eastward and upcoast, but a westward, downcoast mean flow is dominant

during fall, spring and winter. (Cochrane and Kelly, 1986, Jarosz and Murray, 2013). The LTCC transports Brazos and Mississippi River sediment to the TMB (Weight et al., 2011). The potential for preservation of Brazos flood sediment in the TMB is high due to the LTCC, the

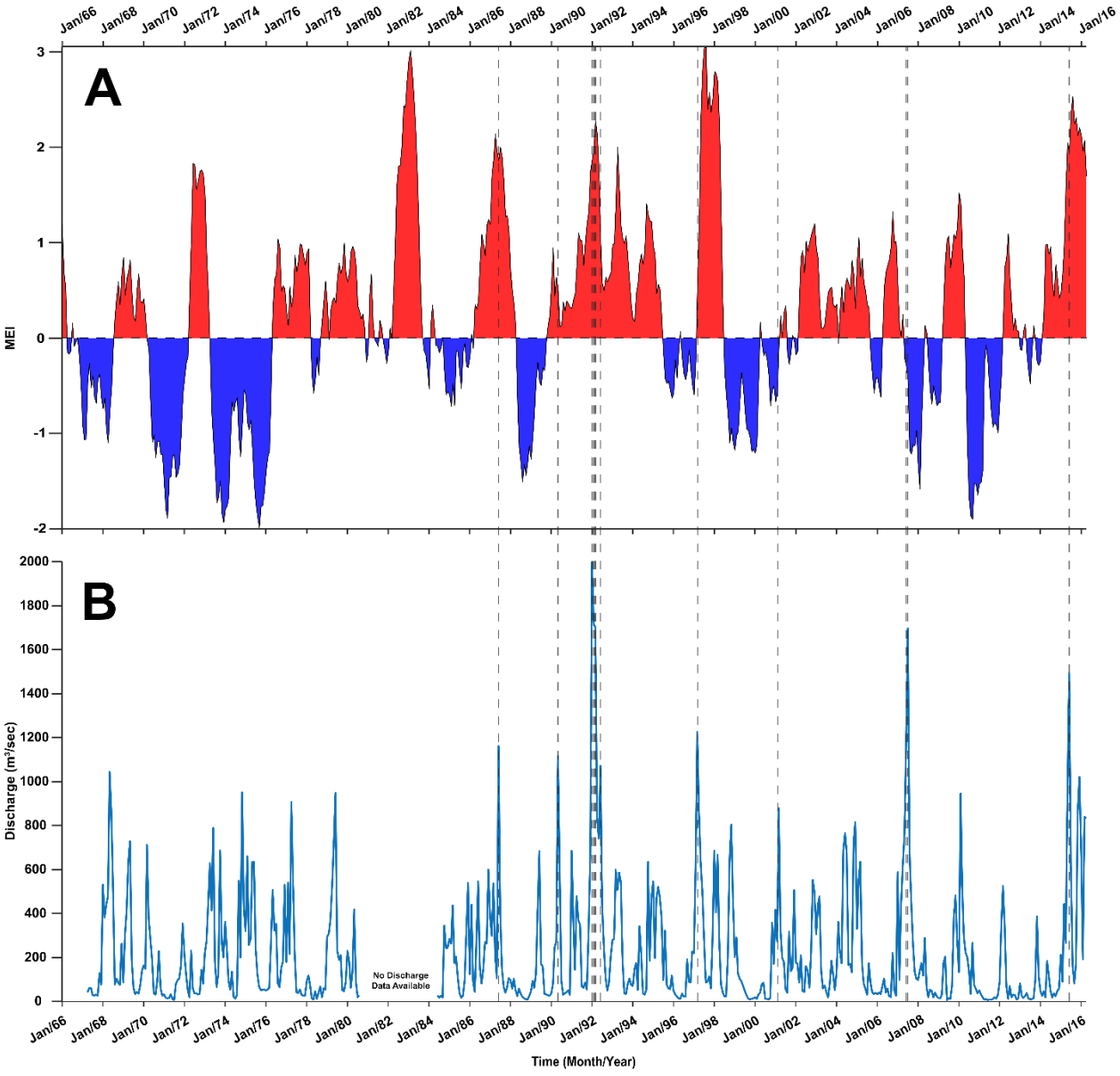

Figure 1: (A) Monthly mean multivariate ENSO Index (MEI) where red indicates El Niño conditions, while blue indicates La Niña conditions. Data sourced from NOAA Earth Systems Research Laboratory (B) Monthly mean Brazos River discharge. No discharge data available between Sep. 1980 and May 1984. Data sourced from USGS Gage Station at Roscharon, TX (08116650). Dashed lines indicate the 10 highest monthly mean discharges.

proximal location of TMB (~75 km southwest of the Brazos River mouth). During periods of high discharge, significant portions (44-100%) of Brazos River sediment discharge is exported to the continental shelf (Carlin et al., 2015).

El Niño events are characterized by a reduction in trade-wind intensity, which reduce upwelling in the eastern Pacific Ocean, and a subsquent warming of equitorial Pacific Ocean surface waters, extending eastwards towards the South American coast. This surface water warming drives an eastward shift in the Walker circulation, a zonal atmospheric circulation pattern, which in turn drives an eastward preciptiation pattern shift, resulting in increased precipitation in North and South America (Bjerknes, 1969, Ropelewski and Halpert, 1986). Storms in North America track along the subtropical jet stream which shifts southward during El Niño events to cover the southern United States (D'Aleo and Grube, 2002, Fraticelli, 2006). Texas precipitation patterns are controlled in part via ENSO conditions. Texas, on average, recieves 120-180% more precipitation from December through March during strong El Niños (NOAA, 1997). Brazos River discharge increases subsequently due to increases in precipitation during El Niño conditions, as do other Gulf Coast rivers, such as the Mississppi (Munoz and Dee, 2017). High monthly mean discharges correspond to high monthly mean multivariate ENSO index (MEI) (Figure 1). Figure 1 illustrates this relationsip and specifically indicates the 10 highest monthly mean discharges, 8 of which correspond to moderate to strong El Niños.

1.3 Identifying and Tracing Flood Sediment Packages

Identifying and tracking flood sediment requires event-response sampling. Sampling must occur within weeks of peak flooding in order to capture the initial flood deposit, after which deposits may be dispersed to slope regions (Wheatcroft, 2000).

Previous studies have used x-radiographs, water content and grain size to delineate fresh flood deposits (Wheatcroft and Borgeld, 2000, Wheatcroft et al., 2006, Carlin and Dellapenna, 2014, Bentley and Nittrouer, 2003). Changes in grain size, porosity and sedimentary structures can be detected with X-radiography. Offshore flood deposits typically exhibit internal

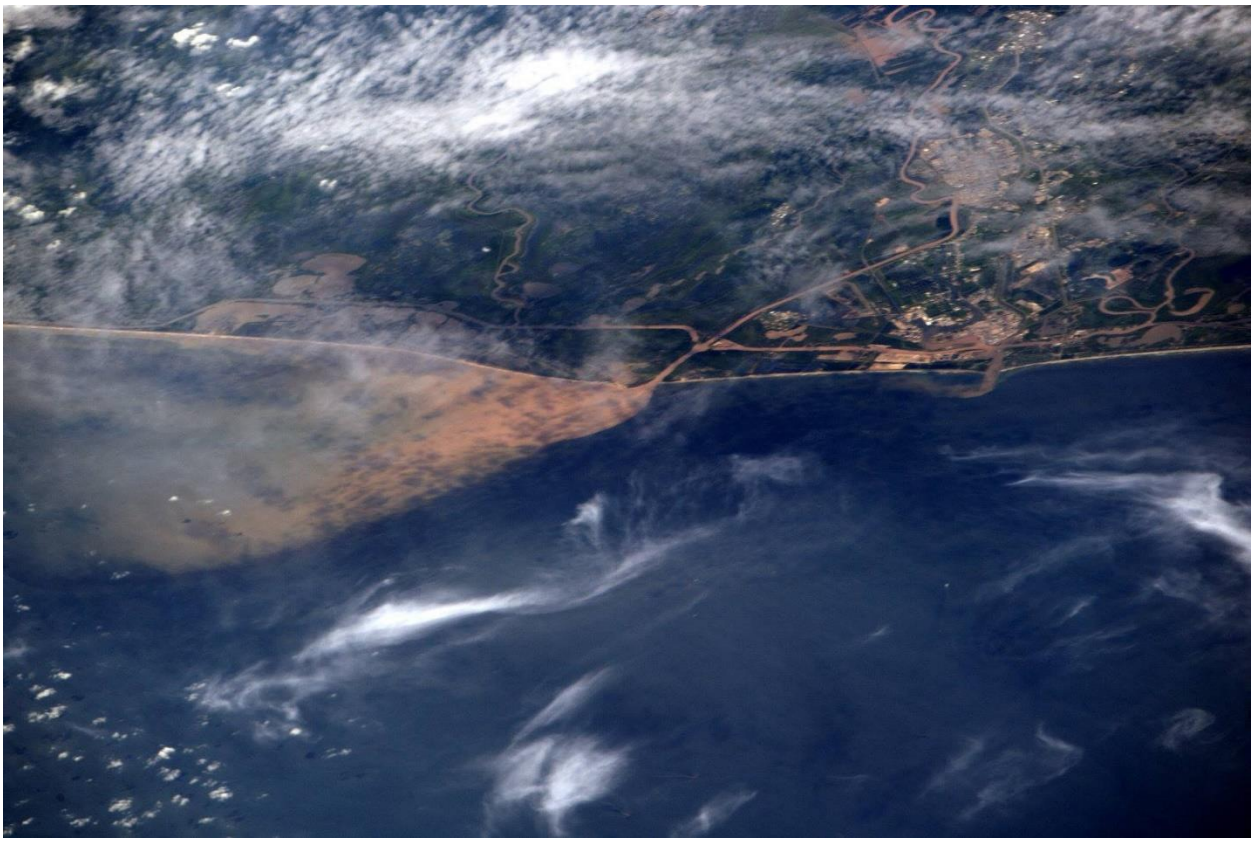

Figure 2: Photographic image of the Brazos River taken on March 20, 2016 from the International Space Station. Photo taken by Jeff Williams, NASA.

homogeneity and sharp contact with underlying pre-flood deposits. Deposits less than a few weeks old will exhibit lesser degrees of bioturbation than pre-flood deposits, or may even exhibit a complete lack of bioturbation (Wheatcroft et al., 2006, Palinkas et al., 2005). Flood beds may exhibit a fining upward or coarsening upward trend, with the later suggesting an increase in riverine transport capacity at peak river discharge (Wheatcroft, 2006). Flood deposits may exhibit high water content (>80%) due to elevated clay content and rapid deposition, but this decreases with time due to compaction, reworking and eventual accumulation (Wheatcroft et al., 1996, Wheatcroft et al., 2006).

Beryllium-7 (^{7}Be) is a short-lived ($T_{½}$ = 53 days) radionuclide formed in the atmosphere via cosmic ray spallation of nitrogen and oxygen atoms (Arnold and Al-Salih, 1955, Kaste and Baskaran, 2012). The radionuclide is drawn out of the atmosphere and delivered to the Earth's surface primarily during rainfall events (Todd et al., 1989, Olsen et al., 1985, Baskaran et al., 1993). Storm events act to integrate a watershed's ^{7}Be inventory and focus it in rivers, which leads to elevated, coastal ^{7}Be inventories near river mouths (Du et al., 2012). ^{7}Be residence time in coastal waters is dependent on suspended particulate matter concentrations, coastal water depth and the residence time of suspended particulate matter in the water column. Riverine flooding events introduce large quantities of suspended particulate matter and large ^{7}Be inventories to coastal regions. Since ^{7}Be readily sorbs onto sediment particles, residence times in the water column are on the order of days to weeks (Kaste and Baskaran, 2012).

The particle-reactive, short-lived nature of ^{7}Be makes it an ideal tracer for modern river flood sediment over day to month timescales (Allison et al., 2000, Sommerfield et al., 1999, Palinkas et al., 2005). Sommerfield et al. (1999) was the first study to apply ^{7}Be as a flood sediment tracer. The study introduced a box-model to describe the complex ^{7}Be source-sink

pathways. The model suggests that during non-flooding events, when riverine inputs are negligible, the local, atmospheric ^{7}Be flux (F_a) and suspended sediment concentrations are low. Therefore, ^{7}Be will likely decay in the water column before being deposited ($\lambda I \gg rI$). During flooding events, large riverine fluxes of ^{7}Be (F_r) and suspended sediment result in rapid ^{7}Be scavenging ($rI \gg \lambda I$) and deposition within flood sediments, leaving a traceable flood signature (Sommerfield et al., 1999).

1.4 Identifying Brazos River Flood Sediment

Previous work has found modern Brazos River sediments to be fine grained, red to brown in color and enriched in calcium relative to potassium (Carlin and Dellapenna, 2014). The red to brown colored sediment is eroded from Triassic red beds in northwestern Texas and northeastern New Mexico (Rodriguez et al., 2000). Enriched calcium in Brazos River sediments is a result of eroded calcium carbonate sourced from central Texas (Carlin and Dellapenna, 2014, Rice, 2009). In contrast, the Mississippi River's sediment is enriched in potassium relative to calcium due to weathering of potassium-rich clay minerals (Rice, 2009, Weight et al., 2011).

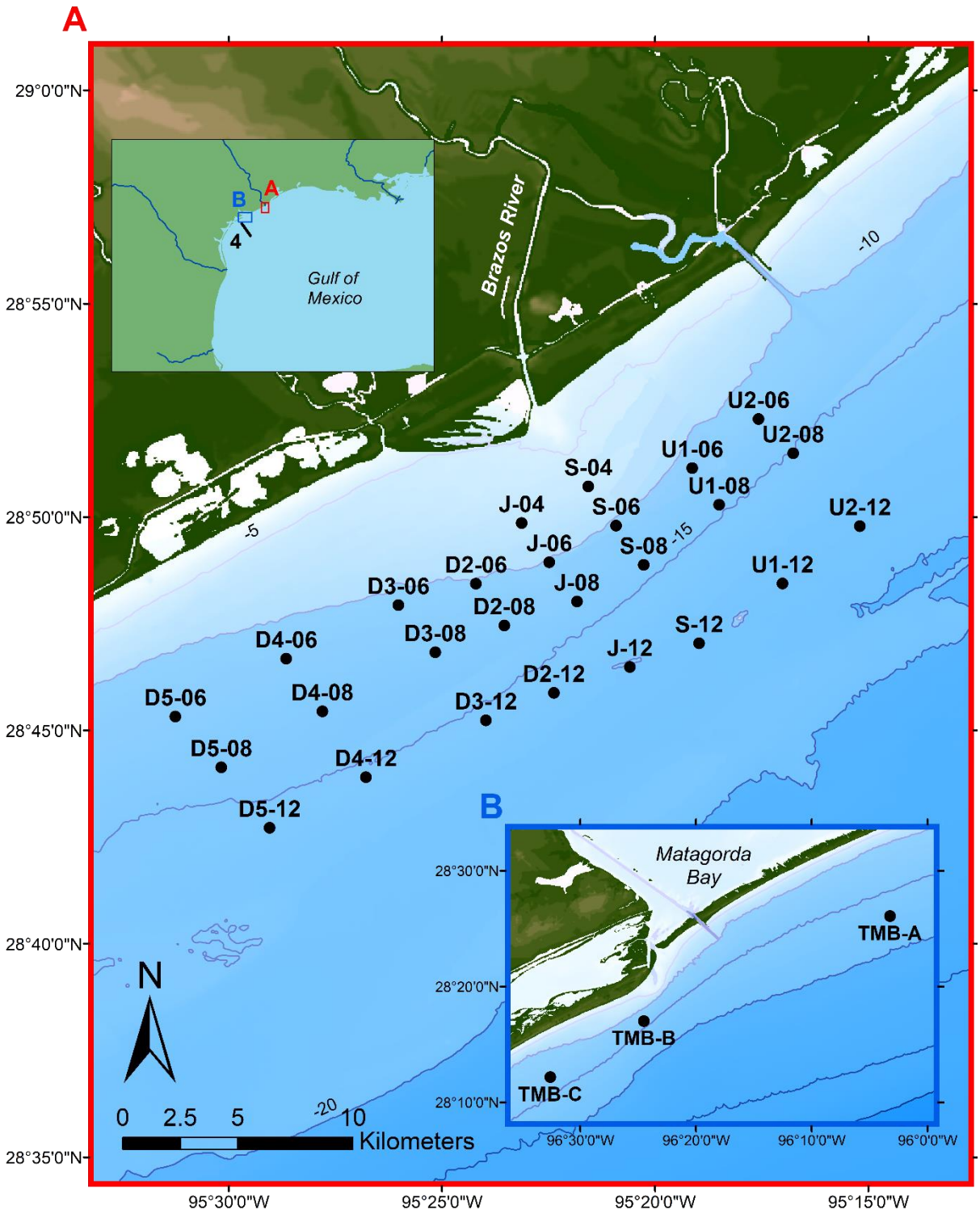

Figure 3: Map showing location of offshore Brazos River boxcores and TMB vibra-cores. Top insert shows setting of Brazos River (A) and TMB (B, bottom insert) sampling sites. Line 4 marks the aerial extent of seismic line shown in Figure 5 (Weight et al., 2011).

2. METHODS

2.1 Sampling Techniques

Sediment samples were collected according to an established grid offshore the Brazos River (Figure 3). The grid covers a roughly 190 km^2 area proximal to the mouth of the Brazos River and consists of 26 sampling locations. The number in each sample name refers to the distance located offshore in kilometers (e.g. J-04 is 4 km offshore). Sites were resampled during multiple research cruises using TAMUG's R/V *Trident*. Sediment samples were collected using a GOMEX style box corer. Between February 2016 and September 2016, four offshore sampling trips were conducted at the mouth of the Brazos River and at what is believed to be an ultimate sink, the TMB (Figure 4). A total of 45 boxcores were collected near the mouth of the Brazos River (Table 1). Most boxcores were sampled with an X-radiograph tray and a PVC coring tube. However, some boxcores were only subsampled with an X-radiograph tray due to an insufficient amount of PVC coring tubes, including U1-06, U2-06, U1-08, U2-08, S-08 during the February 2016 cruise. Box cores were sub-sampled using 15.24 cm (6 in) diameter PVC coring tubes and plexiglass trays for X-radiography. PVC coring tube sediment samples were extruded and homogenized in 1 cm intervals. Immediately following homogenization, samples were weighed, oven-dried for at least 24 hours at 70°C, and reweighed to calculate water content.

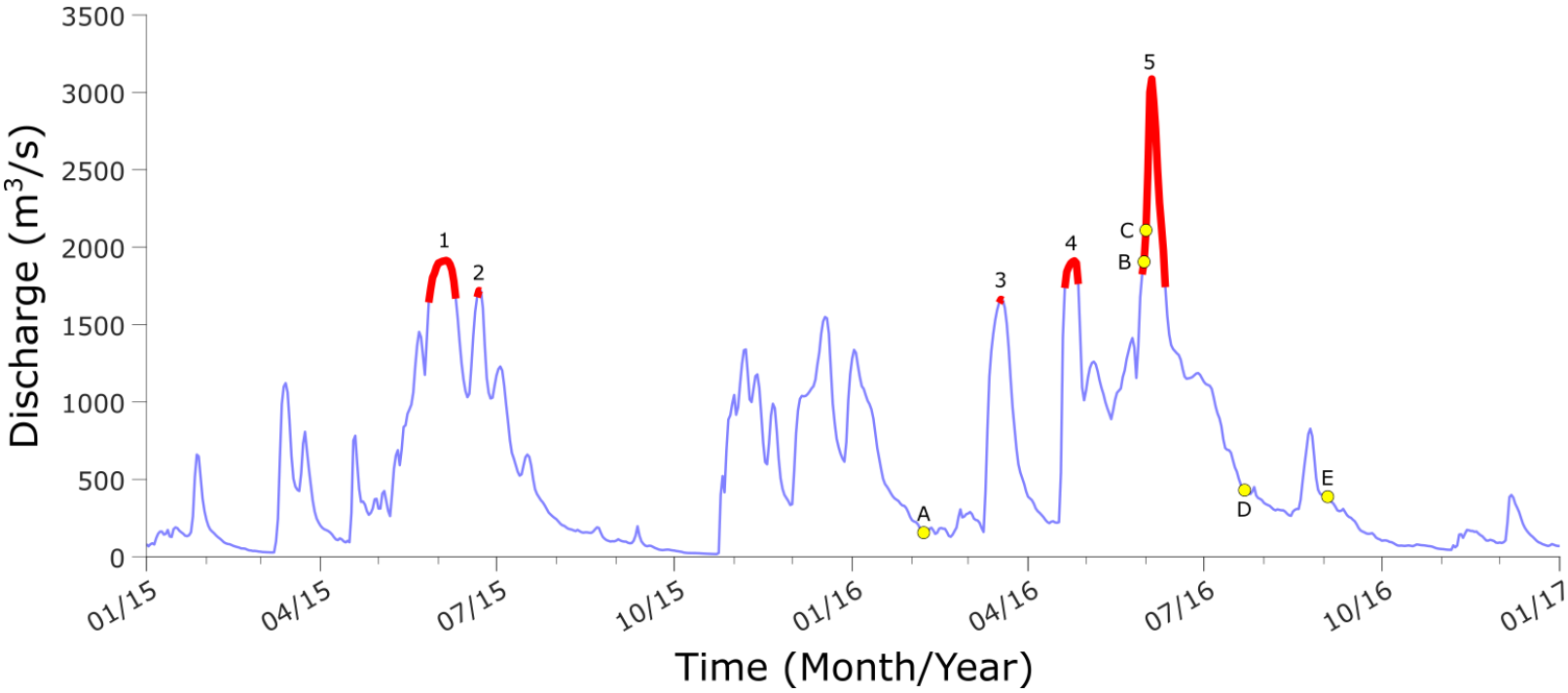

Figure 4: Daily discharge of the Brazos River from Jan 1, 2015 to Jan 1, 2017. Red lines represent periods when the Brazos River exceeded moderate flood stage (14.33 m gauge height) and individual flooding events are numerically labelled. Yellow circles represent dates during which boxcore or vibra-core sampling occurred and are alphabetically labelled as A) Feburary 7, B) May 31, C) June 1, D) July 22, E) September 3. Data sourced from USGS Gage Station at Roscharon, TX (08116650).

Table 1: Location and water depth information for all boxcores collected offshore the mouth of the Brazos River. Longitude and latitude are represented as decimal degrees.

Date Collected	Core Name	Longitude	Latitude	Water Depth (m)	Flood Deposit Thickness (cm)
February 7, 2016	D2-06	−95.40340	28.80727	12.3	3
February 7, 2016	D2-08	−95.39226	28.79095	14.8	7
February 7, 2016	D2-12	−95.37287	28.76464	18.4	17.5
February 7, 2016	D3-06	−95.43371	28.79894	11.2	5
February 7, 2016	D3-08	−95.41921	28.78049	13.8	9
February 7, 2016	D3-12	−95.39948	28.75390	17.4	9
February 7, 2016	D4-08	−95.46333	28.75740	13.5	13
February 7, 2016	D4-12	−95.44637	28.73169	16.6	4.5
February 7, 2016	D5-06	−95.52088	28.75538	11.6	4
February 7, 2016	D5-08	−95.50292	28.73554	14.1	8
February 7, 2016	D5-12	−95.48400	28.71195	16.8	6
February 7, 2016	J-04	−95.38552	28.83094	11.4	3
February 7, 2016	J-06	−95.37468	28.81564	10.7	4.5
February 7, 2016	J-12	−95.34318	28.77477	19.5	15
February 7, 2016	S-08	−95.33777	28.81464	14.3	10
February 7, 2016	S-12	−95.31611	28.78402	19.8	40
February 7, 2016	U1-06	−95.31881	28.85246	15.0	8.5
February 7, 2016	U1-08	−95.30832	28.83811	17.0	8.5
February 7, 2016	U1-12	−95.28357	28.80737	19.6	9
February 7, 2016	U2-06	−95.29294	28.87156	15.1	4
February 7, 2016	U2-08	−95.27939	28.85824	16.8	4
February 7, 2016	U2-12	−95.25333	28.82977	19.7	3
June 1, 2016	U2-06	−95.28960	28.87605	14.9	2.5
June 1, 2016	U1-06	−95.31882	28.85332	13.4	2.5
June 1, 2016	S-06	−95.34812	28.82995	13.7	9.5
July 22, 2016	D3-06	−95.43401	28.79869	11.2	5
July 22, 2016	D2-06	−95.40396	28.80762	12.3	3
July 22, 2016	J-04	−95.38416	28.83382	10.9	16.5
July 22, 2016	J-06	−95.37462	28.81545	14.0	6
July 22, 2016	S-04	−95.35858	28.84525	11.9	9
July 22, 2016	S-06	−95.34873	28.83033	14.3	5
July 22, 2016	U1-06	−95.31829	28.85289	14.4	3
July 22, 2016	U2-06	−95.29380	28.87187	14.6	4.5

Table 1: (Continued)

Date Collected	Core Name	Longitude	Latitude	Water Depth (m)	Flood Deposit Thickness (cm)
September 3, 2016	U1-12	−95.28971	28.80583	18.3	17.5
September 3, 2016	S-12	−95.31697	28.78480	19.0	38.5
September 3, 2016	D2-12	−95.37188	28.76386	17.3	9
September 3, 2016	D5-08	−95.50239	28.73448	13.2	7.5
September 3, 2016	D4-08	−95.46442	28.76043	12.2	17
September 3, 2016	D3-08	−95.41977	28.77879	13.1	8.5
September 3, 2016	D2-08	−95.39284	28.79048	13.9	4
September 3, 2016	J-08	−95.36539	28.79927	15.1	6.5
September 3, 2016	J-06	−95.37394	28.81647	13.1	5.5
September 3, 2016	S-06	−95.34809	28.83003	13.4	4.5
September 3, 2016	D5-06	−95.51983	28.75417	10.9	3

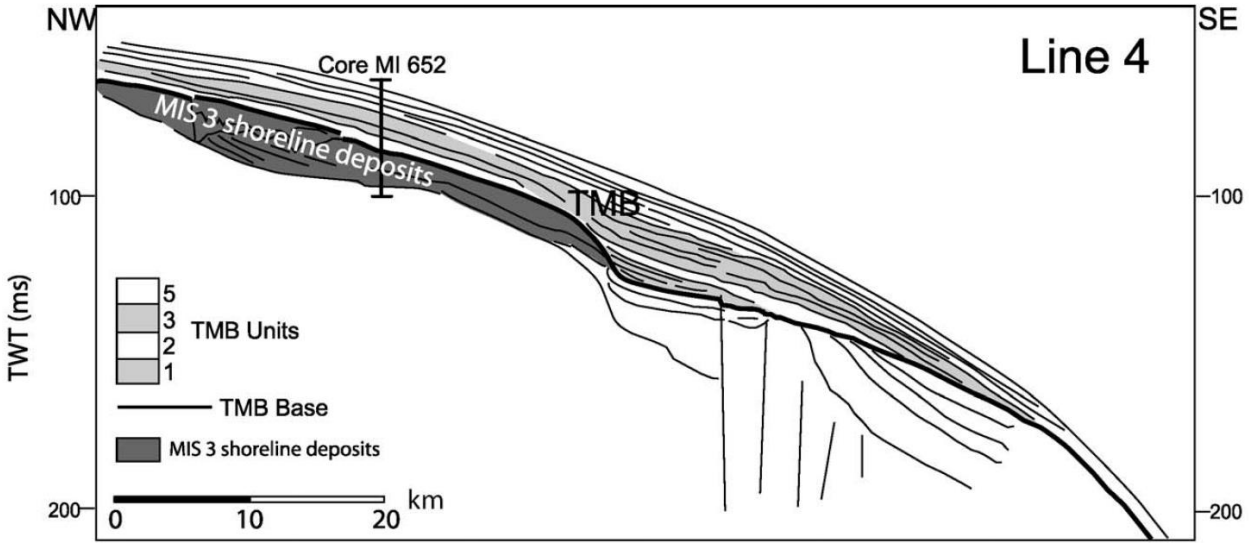

Figure 5: Interpreted seismic line corresponding to Line 4 in Figure 3. TMB sediments are roughly 10 m thick in Core MI 652. Reprinted from Weight et al. (2011).

Three additional boxcores and two vibra-cores were collected further downcoast in the TMB (Table 2). TMB sediments are roughly 10 m thick in TMB-B and TMB-C vibracore sampling locations as evidenced by interpreted seismic lines from Weight et al. (2011) (Figure

5). Core MI 625, taken approximately 60 km offshore, shows influence of shoreface and storm processes as interpreted by Weight et al. (2011) due to the presence of coarse (>31 μm) material. TMB-A, TMB-B and TMB-C sampling locations are 5-8 km offshore and may also show evidence of nearshore processes. Vibra-cores were collected using a PVL Technologies, Inc. submersible vibra-corer and 7.62 cm (3 in) diameter aluminum core barrels. Vibra-cores were split, photographed, logged and X-rayed. One half of each core was archived and used for X-ray fluorescence (XRF) analysis and the other was sub-sampled for grain size, porosity and radioisotopic analysis. Vibra-cores were stored in a refrigerated core repository.

Table 2: Location and water depth information for all boxcores and vibra-cores (*) collected in the TMB.

Date Collected	Core Name	Longitude	Latitude	Water Depth (m)
May 31, 2016	TMB-A	−96.05375	28.43458	18.2
May 31, 2016	TMB-B	−96.40833	28.28352	18.3
May 31, 2016	TMB-C	−96.54328	28.20287	15.1
June 1, 2016	TMB-B*	−96.40668	28.28277	16.0
June 1, 2016	TMB-C*	−96.53108	28.19968	15.4

2.2 Gamma Spectroscopy

Gamma spectroscopy were used to determine ^{7}Be inventories of dry bulk sediment samples. ^{7}Be activities were measured in cores . Two High Purity Germanium Detectors (HPGe), one at TAMUG and the other at California State University at Fullerton (CSUF), were used to measure radioactivity. Between 5 to 10 mL of dry, bulk sediment were ground using a mortar and pestle and measured between 42-48 hours. Identical counting vials were used to maintain

counting geometry. Counting efficiency was determined by measuring a ^{7}Be standard of known activity. The standard was measured in ten aliquots starting with 1 mL of standard and adding 1mL for each subsequent measurement up to 10 mL. A linear regression allows for volumetric calibration of instrument counting efficiency.

Measured ^{7}Be inventories were calculated using the following equation from Sommerfield et al. (1999):

$$I = \sum \rho_s \, X_i \, (1 - \phi_i) \, A_i$$

Where I is the inventory (dpm cm^{-2}), ρ_s is the sediment density (2.4 g cm^{-3}), X_i is the sampling interval thickness (cm), ϕ_i is the porosity, and A_i is the specific activity (dpm g^{-1}) of the sampling interval.

2.3 ^{210}Pb Geochronology

^{210}Pb geochronology was used to determine accumulation rates of sediment in the TMB and the age of Brazos River flood packages in the TMB in TMB-B and TMB-C vibracores. ^{210}Pb geochronology is a well-established tool for dating marine sediments up to 150-200 years old (Noller, 2000, Appleby, 2001, Nittrouer et al., 1979). Samples were wet sieved through a 63 μm screen and 1-2 g of dried silt and clay fractions were retained in Teflon containers and spiked with 0.25 μl of a 4M HNO_3 solution containing ^{209}Po (22.2 dpm/ml). Activity of ^{210}Pb can be determined through measuring the activity of its isotopic granddaughter, ^{210}Po, assuming they are in secular equilibrium (Nittrouer et al., 1979). After being spiked, samples were digested using 15 mL of HCl and HNO_3 and added to a HotBlock at 165°C until samples are near desiccated.

The previous step was repeated a second time with 15 mL of HCL and HNO_3 and a third time with 15 mL of HCL. 50 mL of HCl and 1 cm^3 of ascorbic acid were added to the sample and stirred with a glass rod. A 1 cm^2 silver planchet was added to the solution and stirred for 24 hours. The planchet was removed and counted for 24 hours using an α spectroscopy surface barrier detector. The difference between total ($^{210}Pb_{total}$) and supported activity ($^{210}Pb_{sup}$) yields the excess activity of ^{210}Pb ($^{210}Pb_{xs}$) which can be used to calculate sediment accumulation rate using a logarithmic regression (Appleby, 2001). $^{210}Pb_{sup}$ was determined for each vibra-core by averaging ^{210}Pb constant activities downcore. Due to the flashy discharge and variable sediment supply rate of the Brazos River, a constant sedimentation rate in the TMB cannot be assumed. Therefore, the constant rate of supply (CRS) model was used to date ^{210}Pb activities and determine sedimentation rates. This model assumes the rate of $^{210}Pb_{xs}$ to sediments is constant, that ^{210}Pb is rapidly sorbed onto particles and that $^{210}Pb_{xs}$-laden sediments have not been reworked (Appleby, 2001). The rate of $^{210}Pb_{xs}$ to sediments is likely not constant in the TMB due to fluctuations in supporting river discharge, however this model has been effectively used in marine sediments (Appleby, 2008). Flood deposit layer reworking can be assessed using x-radiographs to determine bedding patterns. The following equation was used to calculate sedimentation rate (S) of age *t* (yr):

$$S = \frac{\lambda z}{\ln\left(\frac{A_0}{A_z}\right)}$$

Where, λ is the ^{210}Pb decay constant (0.031 yr^{-1}), z is the sediment depth (cm), A_0 is the total, integrated excess ^{210}Pb activity, A_z is the integrated, excess ^{210}Pb activity below depth *z*. Sedimentation rates were calculated for each measured sample depth and averaged to determine

a mean sedimentation rate. Depths used in ^{210}Pb sedimentation rate calculations were corrected for porosity and average sediment density (2.65 g cm^{-3}).

2.4 Grain Size Distributions

Wet, homogenized sediment samples were analyzed using a Malvern Mastersizer 2000 particle size analyzer to determine grain size distributions. Boxcores were sampled at 1 cm intervals, and vibra-cores were sampled at 2 cm intervals Sample aliquots were mixed with a sodium hexametaphosphate dispersant and sieved at 2mm. The Malvern Mastersizer 2000 uses reverse osmosis water as its suspension medium and is capable of measuring particle sizes between 0.02-2000 μm. The Malvern Mastersizer 2000 uses laser diffraction to accurately quantify clay (<0.002 mm) through sand (0.063-2000 mm) sized particles.

2.5 Elemental Abundance

The relative elemental abundance of vibra-cores TMB-B and TMB-C were determined by using a XRF core scanner at Scripps Institute of Oceanography. Measurements were made every 0.5 cm for the entire length of the vibra-core. Archived halves of the vibra-cores were used for XRF analysis.

2.6 Isopach Mapping

Isopach mapping was performed in ArcMap using the “Spline Interpolation” tool. Isopach maps were calculated using interpreted flood thicknesses for each boxcore collected within the proximal sampling area. Maximum extent of interpolation was set as a bounding box extending 2 km beyond boundary sampling locations, which is approximately half the minimum distance between any sampling location. Interpolation extent included a larger, 4-6 km extent between the shoreline and sampling locations proximal to the mouth of the Brazos River. Shoreline points were assigned a flood deposit thickness of zero.

3. RESULTS

3.1 Sediment Characteristics

Silt particles dominate boxcore grain size distribution (Table 3). Silt makes up 29.3-67.3% of any given boxcore's total grain size distribution, with a mean of 52.1%. Sand particles make up between 1.2-50.4% of any given boxcore's total grain size distribution, with a mean of 15.4%. Clay particles make up between 20-44% of any given boxcore's total grain size distribution, with a mean of 32.5%. Boxcore grain size distribution exhibits a fining upwards trend, with 62% of the boxcores with grain size data exhibiting a fining upwards trend. The remaining 38% do not exhibit a clear trend in grain size.

Boxcore x-radiographs show a variety of downcore trends. However, most x-radiographs reveal a homogenized, thin to laminated bed up to 15 cm thick at the surface of the sample. Sediment beneath this surface layer may also exhibit thin, homogenous beds, but typically show evidence of bioturbation and potential reworking of sediment.

Table 3: Depth-averaged statistics for all boxcores collected offshore the mouth of the Brazos River. Sand, silt and clay fractions are represented as percetnages of the total grain size distribution (2000-0.01μm).

	Sand	Silt	Clay (0.01-4.00 μm)	Porosity (%)
Minimum	1.2	29.3	20.3	87.9
Maximum	50.4	67.3	44.0	44.3
Average	15.4	52.1	32.5	69.4

Boxcores generally exhibit decreasing porosity with depth. Values for total, depth-averaged porosity ranges between 44.3-87.9%. Boxcore surface sediments typically exhibit porosity values >65% in homogenous layers, with relatively equal values that sharply decrease with depth at the base of the homogenous layer.

Vibra-cores exhibit wide ranges of grain size, porosity and sedimentary fabric trends with depth. Sand content of both vibra-cores ranged between 3-85% (Figure 6, 7). TMB-B had a higher average sand content (42%) than TMB-C (35%). Both vibra-core x-radiographs show evidence of bioturbation and shell debris in the upper 50 cm with occasional intact bedding. TMB-C vibra-core x-radiograph also suggest a thin, sand-rich (>50%) surface layer (<2cm thick) with mottled bioturbed sediment. Beneath this upper 50 cm surface layer, bioturbation becomes almost nonexistent and clear, intact bedding dominates. TMB-C x-radiographs suggest better preservation, with evidence of parallel thin beds (1-5 cm thick) with sharp contacts from 79 cm to 125 cm (Figure 7). Interbedded are sandy, high porosity beds versus silty, low porosity beds.

3.2 ^{7}Be Activities and Inventories

^{7}Be activities were detected in all cores which were sampled for gamma radiation counting. Average daily NOAA precipitation values along the northeastern Texas coast were used to calculate local bulk atmospheric ^{7}Be deposition for a period of 76 days (^{7}Be mean lifetime) prior to the date of sampling. ^{7}Be inventories were calculated using Baskaran et al. (1993) values for wet and dry deposition (106 dpm l^{-1}) in Galveston, TX. Local atmospheric input of ^{7}Be inventories were 2.0 dpm cm^{-2} in February, 2016, 4.5 dpm cm^{-2} in May/June 2016, 4.3 dpm cm^{-2} in July, 2016, and 4.4 dpm cm^{-2} in September, 2016.

Surface ^{7}Be activities (0-1 cm) of boxcores collected from near the mouth of the Brazos River ranged from 0.18 dpm g^{-1} to 29.00 dpm g^{-1}, with an average of 10.78 dpm g^{-1}. Average surface inventories were 6.1 dpm cm^{-2}. When compared to estimated locally sourced ^{7}Be atmospheric inputs, measured inventories were nearly double, suggesting strong influence from other (riverine) sources on ^{7}Be sediment inventories. Boxcores taken at the same location as TMB vibra-cores exhibited relatively low ^{7}Be surface activities (<5.48 dpm g^{-1}), compared to boxcores collected near the mouth of the Brazos River, and penetrate between 2-8 cm. ^{7}Be activities for these boxcores generally decrease with increasing distance from the mouth of the Brazos River.

3.3 XRF

Brazos River sourced sediments were delineated in TMB vibra-cores using Ca/K elemental abundance ratios. Ca/K ratios for the TMB-B vibra-core ranged between 0.81-4.00, with a mean ratio of 1.41 (Figure 6). TMB-C Ca/K ratios ranged between 0.65-4.29, with a mean ratio of 1.55 (Figure 7). Using the Ca/K value from Carlin and Dellapenna (2014), interpreted ratios above 1.5 are considered to have significant Brazos River sourced sediment. Both vibra-cores have high Ca/K ratios in the upper 6 cm (TMB-B) and 10 cm (TMB-C). Peaks vary from 1 cm to 6 cm in thickness for TMB-B and are located at 60-63 cm and a series of interbedded peaks from 150 cm to 185 cm. The interval from 184 cm to 195 cm was unable to be measured due to equipment limitations. TMB-C vibra-core has more Ca/K peaks than TMB-B, suggesting more influence from the Brazos River. TMB-B Ca/K peaks are difficult to correlate with strata revealed by photograph and x-radiograph data. However, TMB-C Ca/K peaks are supported by

photograph and x-radiograph data, correlating well with homogeneous layers with sharp, parallel contacts, especially from 79 cm to 125 cm.

3.4 ^{210}Pb Geochronology

Excess ^{210}Pb activities were measured for both vibra-cores up to 2.33 dpm g^{-1} and logarithmic regressions were calculated from these data (Figure 8). Sedimentation rates were calculated at each measured ^{210}Pb sample depth (Figure 9). Excess ^{210}Pb activities in both cores decreased rapidly in the upper 10 centimeters, suggesting surface sediment was not significantly reworked. Excess ^{210}Pb activities were integrated above 68 cm for TMB-B and above 47 cm for TMB-C. Excess ^{210}Pb activities below these depths were interpreted as erroneous data points and were not factored into calculations of sedimentation rates. Activities above the excess ^{210}Pb base with values less than or equal to zero were excluded from the logarithmic regression. Excess ^{210}Pb activities for TMB-B dropped from 0.37 dpm g^{-1} at 59.4 cm to background levels at 96.3 cm. A value of 68 cm was used as the base of excess ^{210}Pb activity, as this was the approximate value the logarithmic regression became asymptotic. Sedimentation rates ranged between 0.35-0.59 cm yr^{-1} for TMB-B and 0.21 cm yr^{-1} – 0.49 cm yr^{-1} for TMB-C (Figure 9). These values are in agreement with sedimentation rates (0.1-0.5 cm yr^{-1}) calculated using $^{210}Pb_{xs}$ and ^{137}Cs by Carlin and Dellapenna (2014). Average sedimentation rates were calculated by taking the mean of derived sedimentation rates at each sample depth. Average sedimentation rates were 0.49 cm yr^{-1} for TMB-B and 0.40 for TMB-C. Sedimentation rates therefore decreased with increasing distance from the Brazos River's mouth.

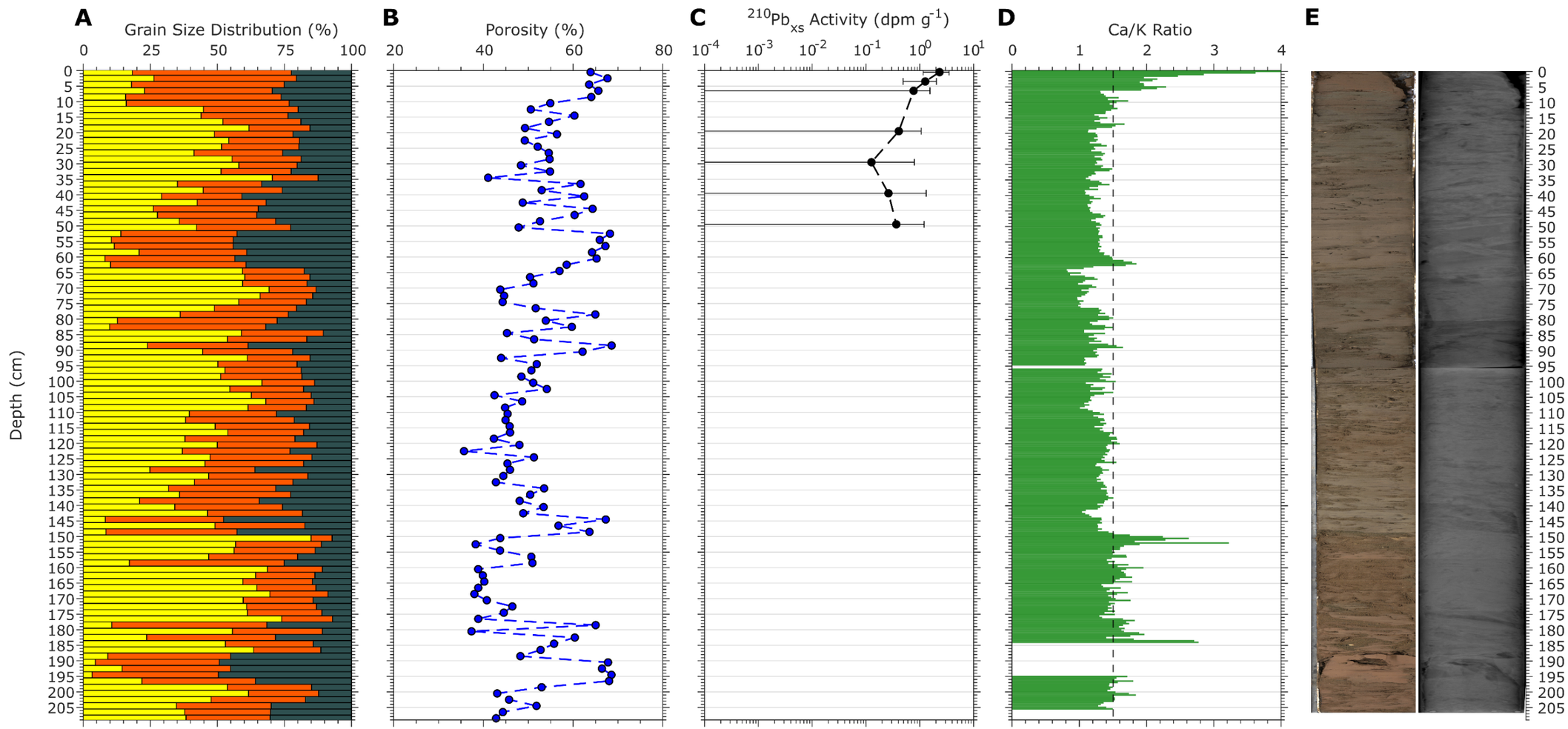

Figure 6: TMB-B vibra-core data compilation with: A) Grain size distribution demonstrating ratio of sand (yellow), silt (orange), and clay (black) with depth B) Porosity (blue) percentages with depth C) $^{210}Pb_{xs}$ activity with depth D) Ca/K elemental abundance ratio (green) with depth and dashed line at 1.5 indicating Brazos River influence E) Photograph and X-radiograph.

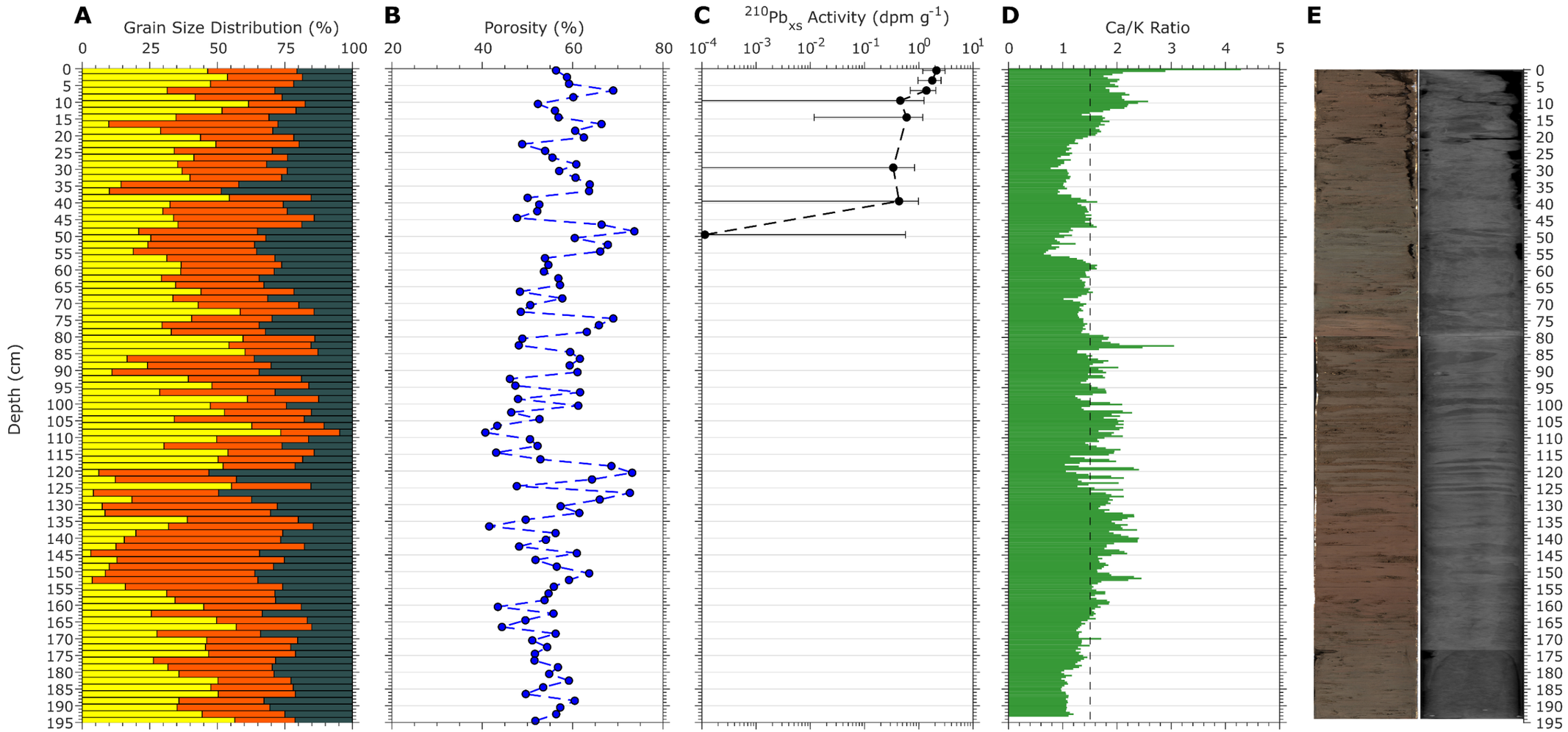

Figure 7: TMB-C vibra-core data compilation with: A) Grain size distribution demonstrating ratio of sand (yellow), silt (orange), and clay (black) with depth B) Porosity (blue) percentages with depth C) $^{210}Pb_{xs}$ activity with depth D) Ca/K elemental abundance ratio (green) with depth and dashed line at 1.5 indicating Brazos River influence E) Photograph and X-radiograph.

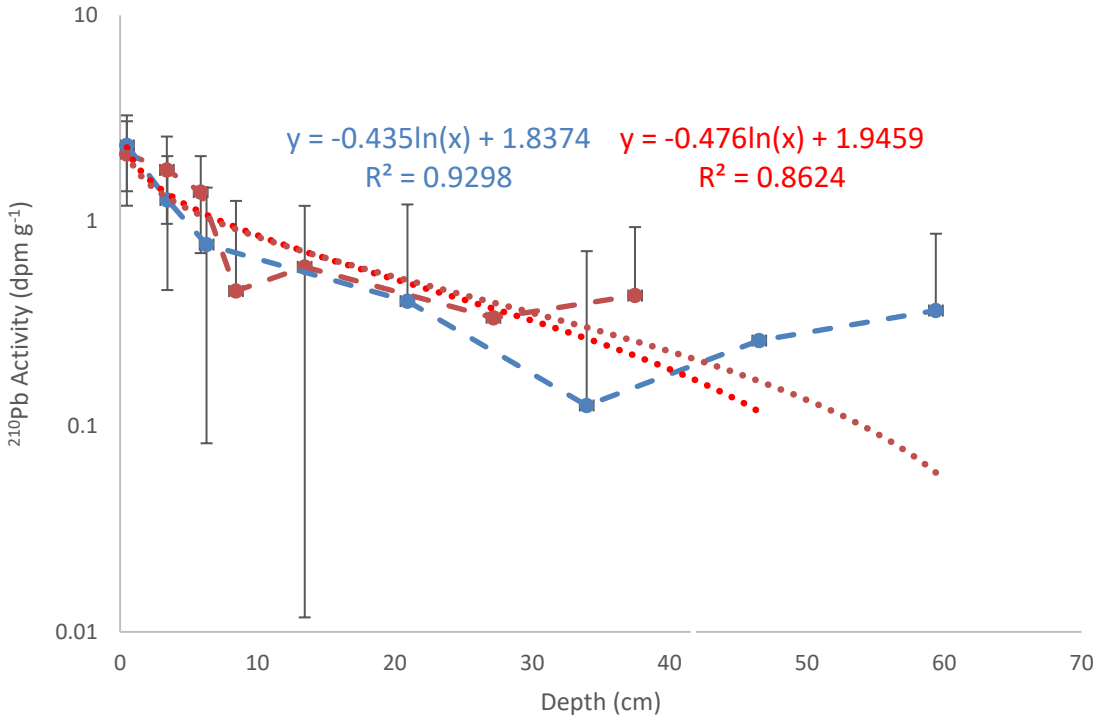

Figure 8: Corrected depth versus 210Pbxs activity for TMB vibra-cores. TMB-B (blue) and TMB-C (red) are plotted with their respective logarithmic regression equations.

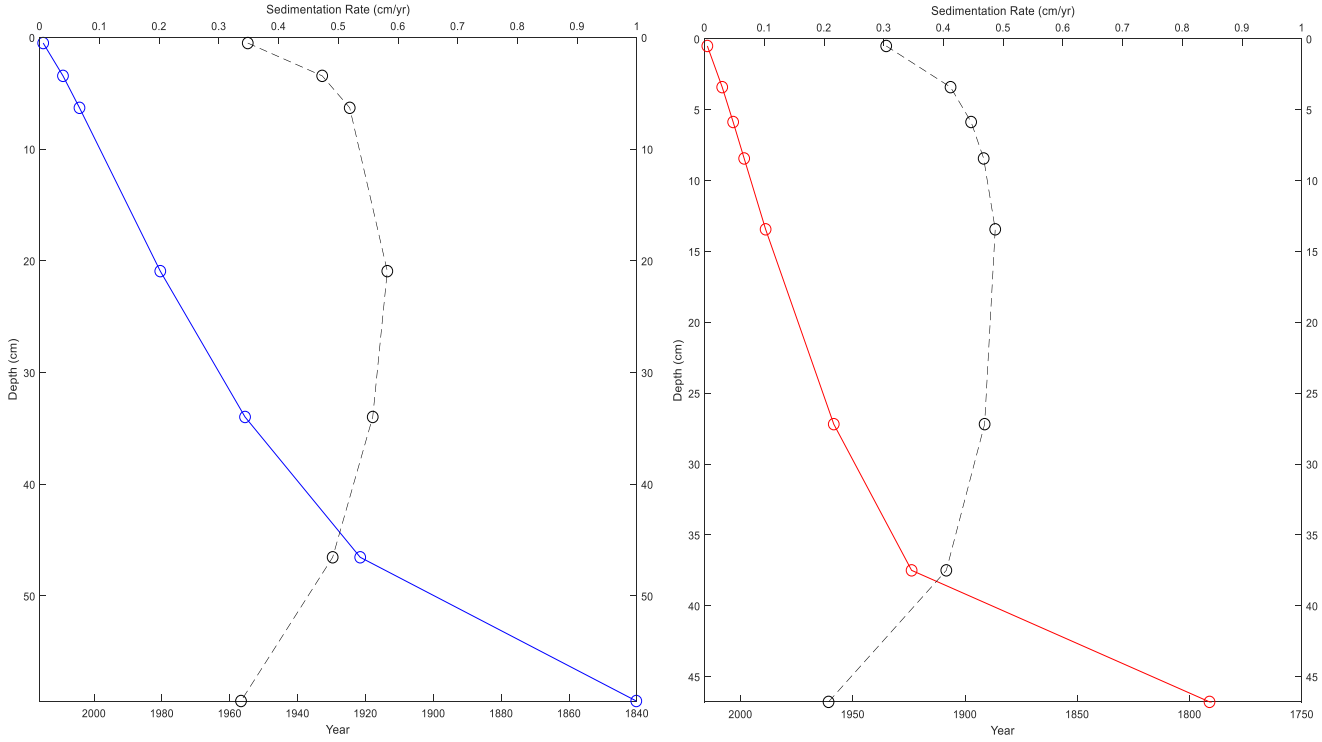

Figure 9: Time (solid) and sedimentation rate (dashed) with depth for TMB-B (left, blue) and TMB-C (right, red) derived from measured ^{210}Pb activities.

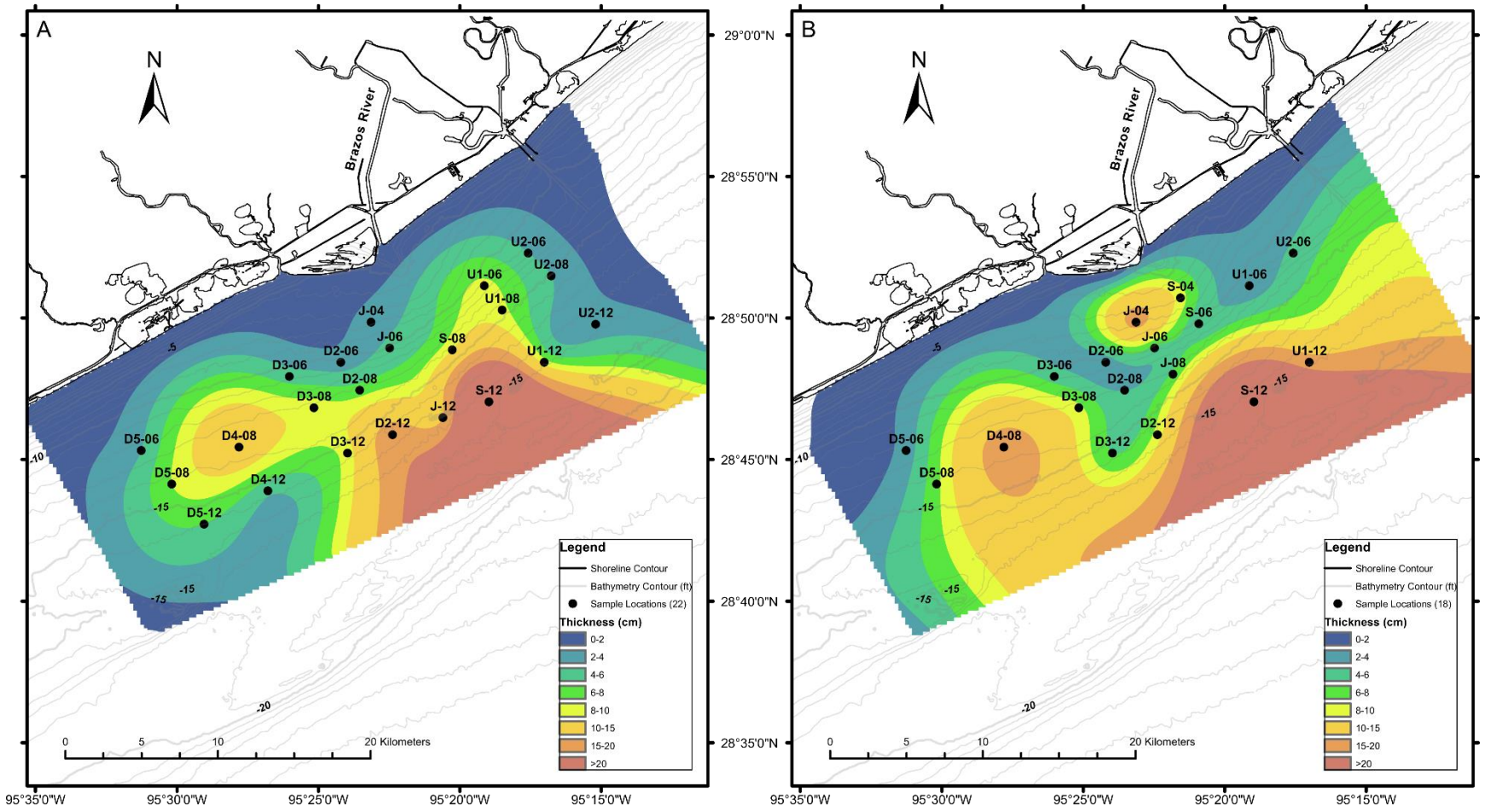

Figure 10: Isopach maps of recent flood deposit thickness (cm) from February 7, 2016 (A) sampling cruise and merged July 22, 2016 and September 9, 2016 (B) sampling cruises. The

4. DISCUSSION

4.1 Interpreted Flood Layer Thickness

Boxcore flood layer thickness was interpreted using various data, including ^{7}Be activity, grain size, porosity and x-radiographs. ^{7}Be activities were used as the primary data source to determine flood layer thickness, with grain size, porosity and x-radiographs acting as complementary data sets. In cores where ^{7}Be activities were not measured, x-radiographs, grain size and porosity were used in conjunction to determine flood deposit thickness. ^{7}Be activities decreased with depth, but were relatively constant in recent, surficial flood deposits. Depths at which ^{7}Be activities were undetectable marked the base of the flood deposit. Fining upwards grain size trends indicate coarse particles from the flood plume settled out of suspension and accumulated before fine particles, which is to be expected. A sharp contact with coarse particles overlying fine particles is interpreted to indicate the base of the flood deposit. Relatively high, constant porosity values in homogenous surface sediments indicate rapid and fresh accumulation of unconsolidated sediment. The depth at which porosity values rapidly decrease is interpreted to be the base of the flood deposit. These grain size and porosity trends both indicate a relatively homogenous flood deposit at the surface of the boxcores. The boxcore x-radiographs also suggest a homogeneous flood deposit with a sharp contact at the base. Parallel laminations and bedding suggest that flood deposits have not been subject to physical mixing (Figure 11).

4.2 Temporal and Spatial Depositional Trends at the Mouth of the Brazos River

Interpreted flood deposit thicknesses (Table 1) for each boxcore were mapped (Figure 10). Isopach maps were created via spline interpolation. The July and September 2016 sampling cruises were merged for isopach analysis as core locations, J-06 and S-06, which were sampled during both cruises yielded similar flood deposit thicknesses, suggesting that flood deposits were not remobilized between July and September. These interpolated maps provide a basis to determine qualitative changes in flood sediment thickness and morphology. Flood deposit thickness increases with increasing offshore distance, as suggested by isopach maps. This suggests that the flood sediment plume rapidly advects sediment offshore.

Sample locations J-06 and U1-06 were sampled during three separate cruises and provide evidence for changes in flood deposit stratigraphy with time (Figure 11). Flood layers interpreted for February 2016 boxcores are likely sourced from the December 2015 flood, which had a peak discharge of 1540 $m^3 s^{-1}$ and was above flood stage (13.11 m) for 5 consecutive days (Figure 4).

The February J-06 core has a homogenous 4.5 cm surficial flood layer with thin, parallel laminae at the base. Beneath this surface layer there is a shell debris and evidence of bioturbation. The July J-06 boxcore has a 5.5 cm thick flood deposit with similar stratigraphic trends. The September J-06 core shows significant stratigraphic changes at the surface, however. ^{7}Be activities, which do not decrease steadily with depth, and the x-radiograph suggest extensive reworking in the upper 5 cm of the September boxcore. The presence of ^{7}Be however, does suggest that these reworked surface sediments are not sourced from the December 2015 flood, which had reached peak discharge 260 days prior.

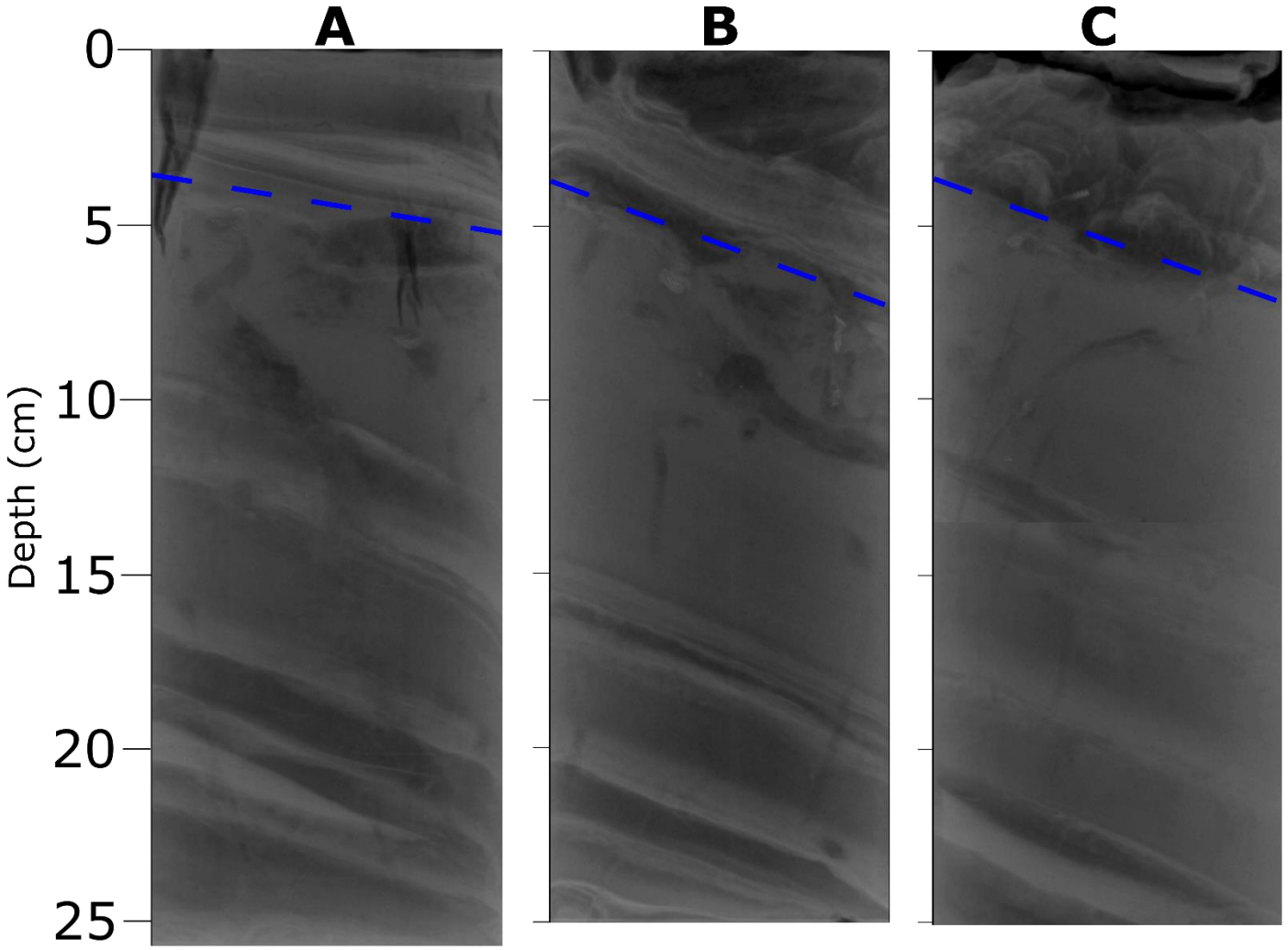

Figure 11: X-radiographs from sample location J-06 taken on February 7, 2016 (A), July 22, 2016 (B) and September 3, 2016 (C). The blue dashed line indicates the contact between recent flood sediment and underlying bioturbated sediment.

U1-06 displays similar trends to J-06. The February boxcore flood thickness is 8.5 cm. This is determined solely by x-radiograph which displays a homogenous bed at the surface and heavily reworked sediment with shell debris beneath the flood layer. The May boxcore flood thickness is 2.5 cm, suggesting the February deposit has been at least partially eroded. The 2.5 cm flood deposit is likely sourced from either the March 2016 or April 2016 floods. Beneath this flood layer is an older flood deposit with minor burrowing. This is likely the remainder of the February deposit which has been eroded from 8.5 cm to 2.5 cm.

Two boxcore locations, J-04 and D5-06 were resampled during different sampling cruises and both cores were analyzed for ^{7}Be activity, providing a basis to match flooding event with a flood deposit and to see the timescales of deposition and resuspension.

J-04 was sampled in February and July 2016 and both cores were analyzed for ^{7}Be activities. The February core has a 3 cm thick flood deposit with shells, likely sourced from the December 2015 flooding event. The maximum penetration depth of ^{7}Be is 3 cm. The flood deposit overlays two homogenous beds. The deeper of these two beds is 7-8 cm thick and shares a sharp contact with the bed beneath it. This contact contains significant shell debris. The July core has a 4.5 cm flood deposit with no evidence for bioturbation. The flood deposit contains thin laminae and overlies a reworked sediment layer with some bedding remaining intact, roughly 10 cm thick. Beneath this reworked sediment layer is the top of the February flood deposit at 14 cm with shells. ^{7}Be activities were measured up to 11 cm in the July boxcore and were higher than the ^{7}Be activity measured in the February boxcore. 14 cm of sediment was therefore deposited between February 2016 and July 2016.

D5-06 was sampled in February 2016 and September 2016 and both cores were analyzed for ^{7}Be activities, with flood deposit thicknesses of 4 cm and 3 cm, respectively. Both boxcores

have similar grain size and porosity. The upper 2 cm of both the February and September core have roughly equivalent ^{7}Be activities. Equivalent ^{7}Be activities with 209 days between sampling suggests that these surface flood deposits are sourced from different flooding events. The coarse, reworked layer beneath these flood deposits retains its thickness between the February and September cores. The September core x-radiograph reveals a second flood layer beneath the surface flood layer that is only 1-2 cm thick. This is interpreted to be the February flood layer. This suggests the February flood deposit has been at least partially eroded between February and September. Three distinct floods in March, April and June occurred between these samples (Figure 4).

4.3 Preservation of Brazos River Sediment in TMB

TMB vibra-cores indicate the presence of Brazos River sourced sediment. Ca/K ratios above 1.5 were interpreted as Brazos River sourced sediment and both vibra-cores contain thin beds of Brazos River sourced sediment. TMB-C has a higher average Ca/K ratio than TMB-B and a larger distribution over the entire core length of Ca/K peaks than TMB-B. Bedding revealed by x-radiograph and photograph data better correspond to Ca/K peaks in TMB-C than in TMB-B. This implies that TMB-C has better preserved Brazos River sourced sediment than TMB-B.

The upper 20 cm of TMB-C is dominated by Brazos River sourced sediment. The boxcore taken at this location shows ^{7}Be activity penetration for at least the upper 4 cm. These deposits have low ^{7}Be inventories but likely are sourced from the March 2015 Brazos River flood, which reached peak discharge 74 days prior, due to their high Ca/K ratios and high

porosity. TMB-A, TMB-B and TMB-C boxcore ^{7}Be activities decrease with increasing distance from the Brazos River mouth. If the flood deposits in TMB-A, TMB-B and TMB-C were sourced from direct deposition from the river plume, it would follow that ^{7}Be activities for these three cores would be relatively equal. Direct river plume sedimentation should happen coevally, relative to ^{7}Be half-life, between these three sites. ^{7}Be activities decreasing with increasing distance from the river mouth suggest that these deposits are from remobilized flood deposits from closer to the mouth of the Brazos River, potentially being resuspended and advected further downcoast by the LTCC.

TMB-C shows Brazos River sourced sediment in interbedded layers with Mississippi River derived sediment from 79-155 cm. The Brazos River sourced beds are coarser, which is to be expected because the Brazos River is the only source of sand to the northwestern GOM (Anderson et al., 2014). These beds are likely sourced from the Brazos River because of their texture and Ca/K ratios. Interbedded Brazos River sediment indicates changes in river sediment supply or resuspension of nearshore Brazos River deposits. Although, ^{210}Pb dating does not extend to this depth in the core, using the average ^{210}Pb sedimentation rate of 0.40 cm yr^{-1} and assuming it is applicable further downcore, these thin beds may represent annual records of Brazos River sediment sourcing to the TMB.

The area sampled off the mouth of the Brazos River likely did not capture the entirety of the nearshore flood deposit, as evidenced by flood deposit thickness increasing offshore. Aerial imagery and field observations suggest that the Brazos River flood sediment plume extends offshore more than 12 km and increases in width with distance from the river mouth. Flood sediment thickness likely increases beyond the extent of the sampling area. Despite not sampling a large volumetric portion of the flood deposit, the sampling area of this study is still considered

to be representative of overall trends in Brazos River flood deposit deposition, erosion and remobilization. Implications drawn from the vibra-cores may not be applicable to the entirety of the TMB. Additional cores taken in the TMB would further support evidence of Brazos River sediment preservation and delineation of flood sediment facies. Vibra-cores taken further offshore may reveal increased Brazos River sediment preservation.

5. CONCLUSION

This study revealed the timescales and depositional patterns of flood sedimentation off the mouth of the Brazos River as well as the preservation potential of Brazos River floods in the TMB. Brazos River flooding events result in 2 cm to 38 cm thick deposits near the mouth of the Brazos River. These deposits are reworked and at least partially remobilized on an intra-annual, inter-flood timescale. The abnormally high discharge events of the Brazos River between 2015 and 2016 have allowed for clear delineation of flood deposits near the river mouth. Brazos River sourced deposits are recorded in the TMB, likely through remobilization of nearshore deposits. Brazos River deposits are preserved in the TMB, potentially after seasonal reworking of spring and summer flood layers in the fall and winter. Further work should take additional cores in the TMB, perhaps further offshore to increase chances of Brazos River sediment preservation. Additional dating techniques are recommended to further constrain the age of Brazos River sourced sediment in the TMB. Further dating constraints should allow for historical Texas precipitation patterns to be determined from Brazos River sediment in the TMB.

REFERENCES

ALLISON, M. A., KINEKE, G. C., GORDON, E. S. & GOÑI, M. A. 2000. Development and reworking of a seasonal flood deposit on the inner continental shelf off the Atchafalaya River. *Continental Shelf Research,* 20**,** 2267-2294.

ANDERSON, J. B., WALLACE, D. J., SIMMS, A. R., RODRIGUEZ, A. B. & MILLIKEN, K. T. 2014. Variable response of coastal environments of the northwestern Gulf of Mexico to sea-level rise and climate change: Implications for future change. *Marine Geology,* 352**,** 348-366.

ANDERSON, J. B., WALLACE, D. J., SIMMS, A. R., RODRIGUEZ, A. B., WEIGHT, R. W. R. & TAHA, Z. P. 2016. Recycling sediments between source and sink during a eustatic cycle: Systems of late Quaternary northwestern Gulf of Mexico Basin. *Earth-Science Reviews,* 153**,** 111-138.

APPLEBY, P. G. 2001. Chronostratigraphic Techniques in Recent Sediments. *In:* LAST, W. M. & SMOL, J. P. (eds.) *Tracking Environmental Change Using Lake Sediments: Basin Analysis, Coring, and Chronological Techniques.* Springer Netherlands.

APPLEBY, P. G. 2008. Three decades of dating recent sediments by fallout radionuclides: a review. *The Holocene,* 18**,** 83-93.

ARNOLD, J. R. & AL-SALIH, H. A. 1955. Beryllium-7 Produced by Cosmic Rays. *Science,* 121**,** 451-3.

BASKARAN, M., COLEMAN, C. H. & SANTSCHI, P. H. 1993. Atmospheric depositional fluxes of7Be and210Pb at Galveston and College Station, Texas. *Journal of Geophysical Research,* 98**,** 20555.

BENTLEY, S. J. & NITTROUER, C. A. 2003. Emplacement, modification, and preservation of event strata on a flood-dominated continental shelf: Eel shelf, Northern California. *Continental Shelf Research,* 23**,** 1465-1493.

BJERKNES, J. 1969. Atmospheric Teleconnections from the Equatorial Pacific1. *Monthly Weather Review,* 97**,** 163-172.

BLUM, M. D. & ROBERTS, H. H. 2009. Drowning of the Mississippi Delta due to insufficient sediment supply and global sea-level rise. *Nature Geoscience,* 2**,** 488-491.

CARLIN, J. A. & DELLAPENNA, T. M. 2014. Event-driven deltaic sedimentation on a low-gradient, low-energy shelf: The Brazos River subaqueous delta, northwestern Gulf of Mexico. *Marine Geology,* 353**,** 21-30.

CARLIN, J. A. & DELLAPENNA, T. M. 2015. The evolution of a subaqueous delta in the Anthropocene: A stratigraphic investigation of the Brazos River delta, TX USA. *Continental Shelf Research,* 111**,** 139-149.

CARLIN, J. A., DELLAPENNA, T. M., STROM, K. & NOLL, C. J. 2015. The influence of a salt wedge intrusion on fluvial suspended sediment and the implications for sediment transport to the adjacent coastal ocean: A study of the lower Brazos River TX, USA. *Marine Geology,* 359**,** 134-147.

COCHRANE, J. D. & KELLY, F. J. 1986. Low-frequency circulation on the Texas-Louisiana continental shelf. *Journal of Geophysical Research,* 91**,** 10645.

D'ALEO, J. S. & GRUBE, P. G. 2002. *The Oryx Resource Guide to El Niño and La Niña,* Westport, Conn, Greenwood Publishing Group.

DU, J. Z., ZHANG, J. & BASKARAN, M. 2012. Applications of Short-Lived Radionuclides (7Be, 210Pb, 210Po, 137Cs and 234Th) to Trace the Sources, Transport Pathways and Deposition of Particles/Sediments in Rivers, Estuaries and Coasts. *In:* BASKARAN, M. (ed.) *Handbook of Environmental Isotope Geochemistry: Vol I.* Berlin, Heidelberg: Springer Berlin Heidelberg.

FRATICELLI, C. M. 2006. Climate Forcing in a Wave-Dominated Delta: The Effects of Drought-Flood Cycles on Delta Progradation. *Journal of Sedimentary Research,* 76**,** 1067-1076.

JAROSZ, E. & MURRAY, S. P. 2013. Velocity and Transport Characteristics of the Louisiana-Texas Coastal Current. *Circulation in the Gulf of Mexico: Observations and Models.*

KASTE, J. M. & BASKARAN, M. 2012. Meteoric 7Be and 10Be as Process Tracers in the Environment. *In:* BASKARAN, M. (ed.) *Handbook of Environmental Isotope Geochemistry: Vol I.* Berlin, Heidelberg: Springer Berlin Heidelberg.

LABAT, D. 2008. Wavelet analysis of the annual discharge records of the world's largest rivers. *Advances in Water Resources,* 31**,** 109-117.

MEADE, R. H. & MOODY, J. A. 2009. Causes for the decline of suspended-sediment discharge in the Mississippi River system, 1940-2007. *Hydrological Processes***,** n/a-n/a.

MILLIMAN, J. D. & MEADE, R. H. 1983. World-Wide Delivery of River Sediment to the Oceans. *Journal of Geology,* 91**,** 1-21.

MUNOZ, S. E. & DEE, S. G. 2017. El Nino increases the risk of lower Mississippi River flooding. *Sci Rep,* 7**,** 1772.

NITTROUER, C. A., STERNBERG, R. W., CARPENTER, R. & BENNETT, J. T. 1979. The use of Pb-210 geochronology as a sedimentological tool: Application to the Washington continental shelf. *Marine Geology,* 31**,** 297-316.

NOAA, C. P. C. 1997. *ENSO Discussion: Texas* [Online]. National Centers for Environmental Prediction. Available: http://www.cpc.ncep.noaa.gov/products/predictions/threats2/enso/elnino/tx_disc.html [Accessed 2018].

NOLLER, J. S. 2000. Lead-210 geochronology. *Quaternary Geochronology: Methods and Applications.*

OLSEN, C. R., LARSEN, I. L., LOWRY, P. D., CUTSHALL, N. H., TODD, J. F., WONG, G. T. F. & CASEY, W. H. 1985. Atmospheric fluxes and marsh-soil inventories of7Be and210Pb. *Journal of Geophysical Research: Atmospheres,* 90**,** 10487-10495.

PALINKAS, C. M., NITTROUER, C. A., WHEATCROFT, R. A. & LANGONE, L. 2005. The use of 7Be to identify event and seasonal sedimentation near the Po River delta, Adriatic Sea. *Marine Geology,* 222-223**,** 95-112.

RICE, D. 2009. *Major Changes Over Minor Distances: An Offshore Micro-Stratigraphic Study of a Modern Asymmetric Wave-Influenced Delta The Brazos Delta, Texas Gulf Coast USA.* University of Houston.

RODRIGUEZ, A. B., HAMILTON, M. D. & ANDERSON, J. B. 2000. Facies and Evolution of the Modern Brazos Delta, Texas: Wave Versus Flood Influence. *Journal of Sedimentary Research,* 70**,** 283-295.

ROPELEWSKI, C. F. & HALPERT, M. S. 1986. North American Precipitation and Temperature Patterns Associated with the El Niño/Southern Oscillation (ENSO). *Monthly Weather Review,* 114**,** 2352-2362.

SOMMERFIELD, C. K., NITTROUER, C. A. & ALEXANDER, C. R. 1999. ^{7}Be as a tracer of flood sedimentation on the northern California continental margin. *Continental Shelf Research,* 19**,** 335-361.

SYVITSKI, J. P., VOROSMARTY, C. J., KETTNER, A. J. & GREEN, P. 2005. Impact of humans on the flux of terrestrial sediment to the global coastal ocean. *Science,* 308**,** 376-80.

TODD, J. F., WONG, G. T. F., OLSEN, C. R. & LARSEN, I. L. 1989. Atmospheric depositional characteristics of beryllium 7 and lead 210 along the southeastern Virginia coast. *Journal of Geophysical Research,* 94**,** 11106.

WEIGHT, R. W. R., ANDERSON, J. B. & FERNANDEZ, R. 2011. Rapid Mud Accumulation On the Central Texas Shelf Linked To Climate Change and Sea-Level Rise. *Journal of Sedimentary Research,* 81**,** 743-764.

WHEATCROFT, R., BORGELD, J., BORN, R., DRAKE, D., LEITHOLD, E., NITTROUER, C. & SOMMERFIELD, C. 1996. The Anatomy of an Oceanic Flood Deposit. *Oceanography,* 9**,** 158-162.

WHEATCROFT, R. A. 2000. Oceanic flood sedimentation: a new perspective. *Continental Shelf Research,* 20**,** 2059-2066.

WHEATCROFT, R. A. 2006. Time-series measurements of macrobenthos abundance and sediment bioturbation intensity on a flood-dominated shelf. *Progress in Oceanography,* 71**,** 88-122.

WHEATCROFT, R. A. & BORGELD, J. C. 2000. Oceanic flood deposits on the northern California shelf: large-scale distribution and small-scale physical properties. *Continental Shelf Research,* 20**,** 2163-2190.

WHEATCROFT, R. A., STEVENS, A. W., HUNT, L. M. & MILLIGAN, T. G. 2006. The large-scale distribution and internal geometry of the fall 2000 Po River flood deposit: Evidence from digital X-radiography. *Continental Shelf Research,* 26**,** 499-516.

APPENDIX

February 7, 2016 Boxcores

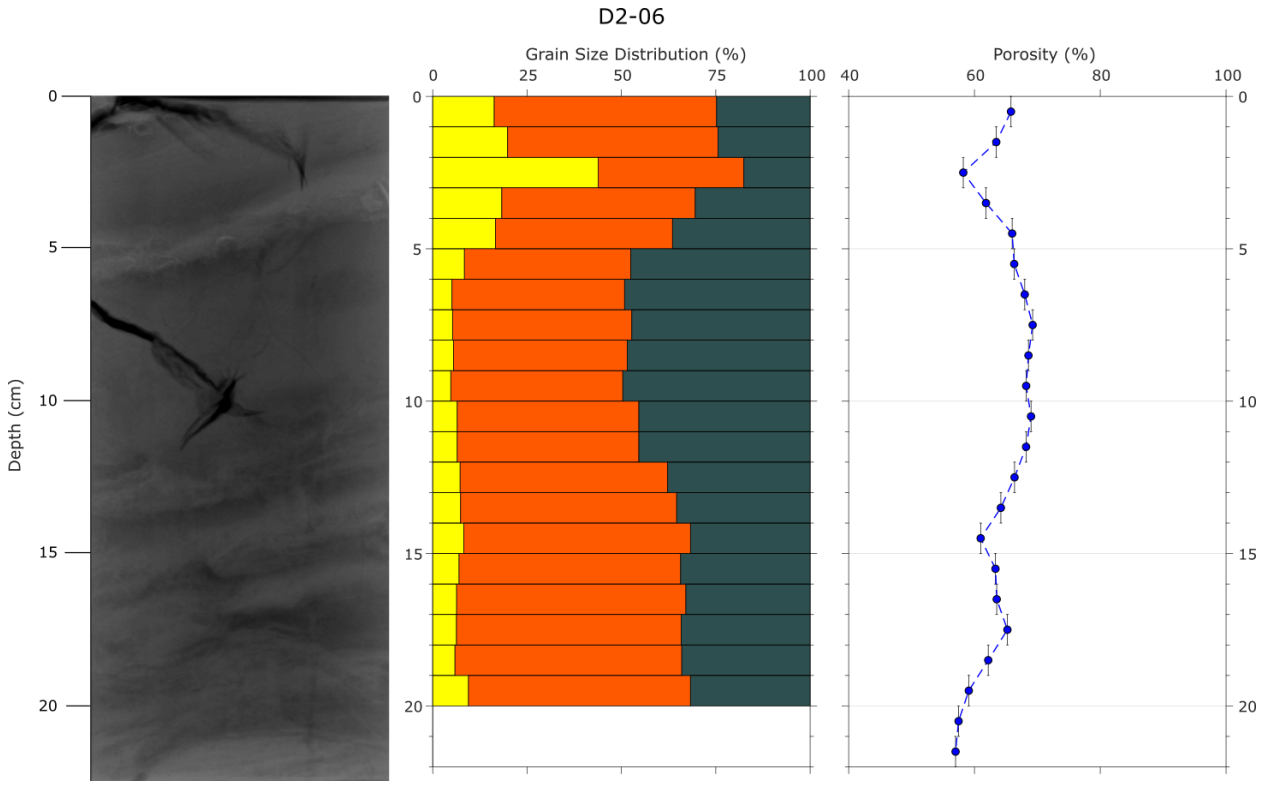

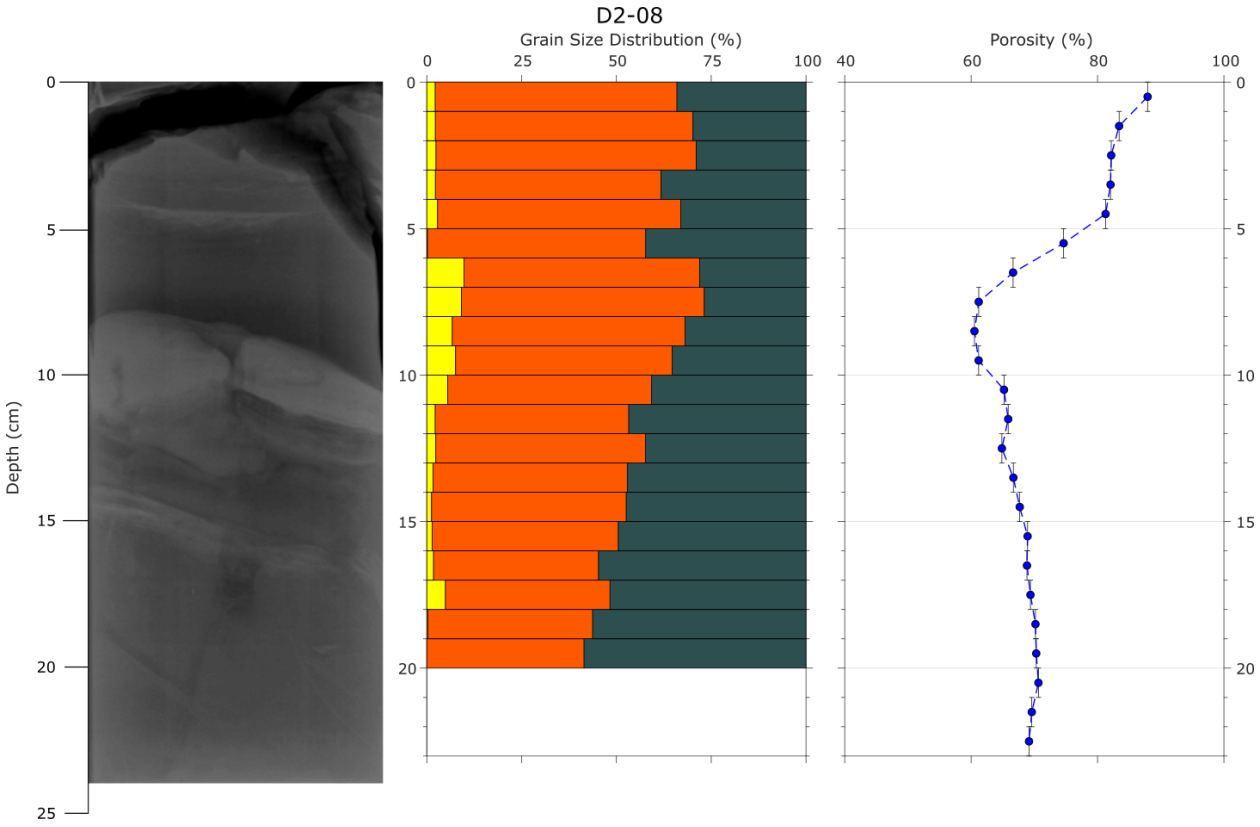
D2-08
Grain Size Distribution (%)
Porosity (%)
Depth (cm)
0
25
50
75
100
40
60
80
5
10
15
20

D2-12

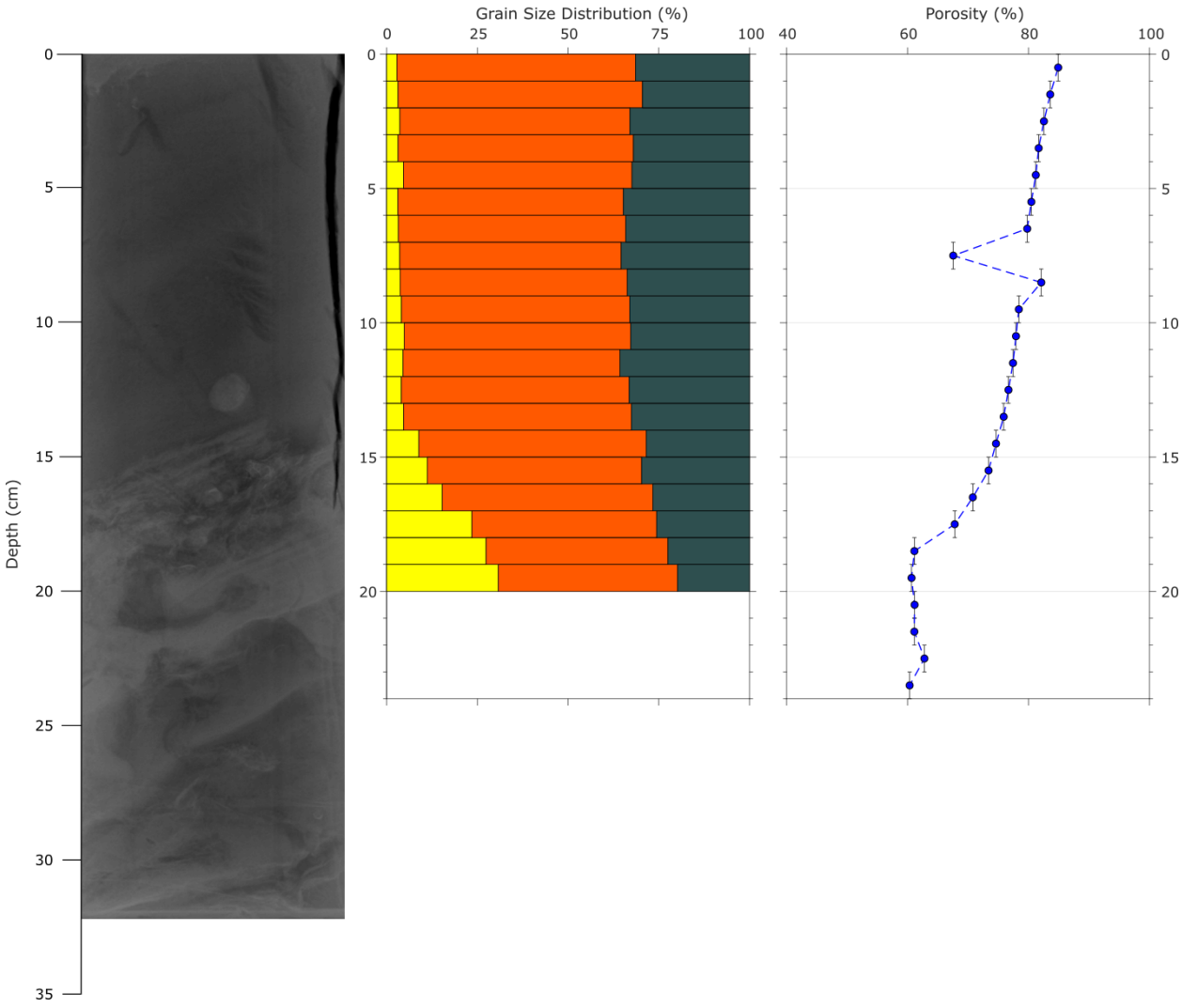
Grain Size Distribution (%)
Porosity (%)
Depth (cm)
0
5
10
15
20
25
30
35
40
60
80
100
0
25
50
75
100

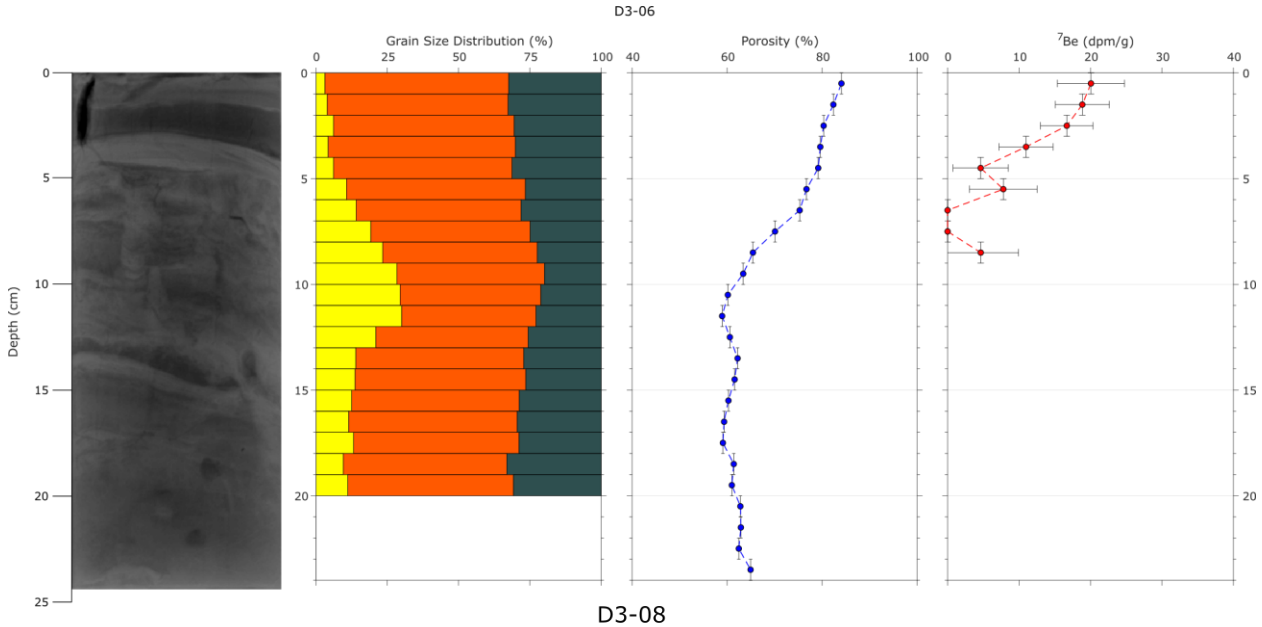
D3-06
Grain Size Distribution (%)
Porosity (%)
^{7}Be (dpm/g)
Depth (cm)

D3-08

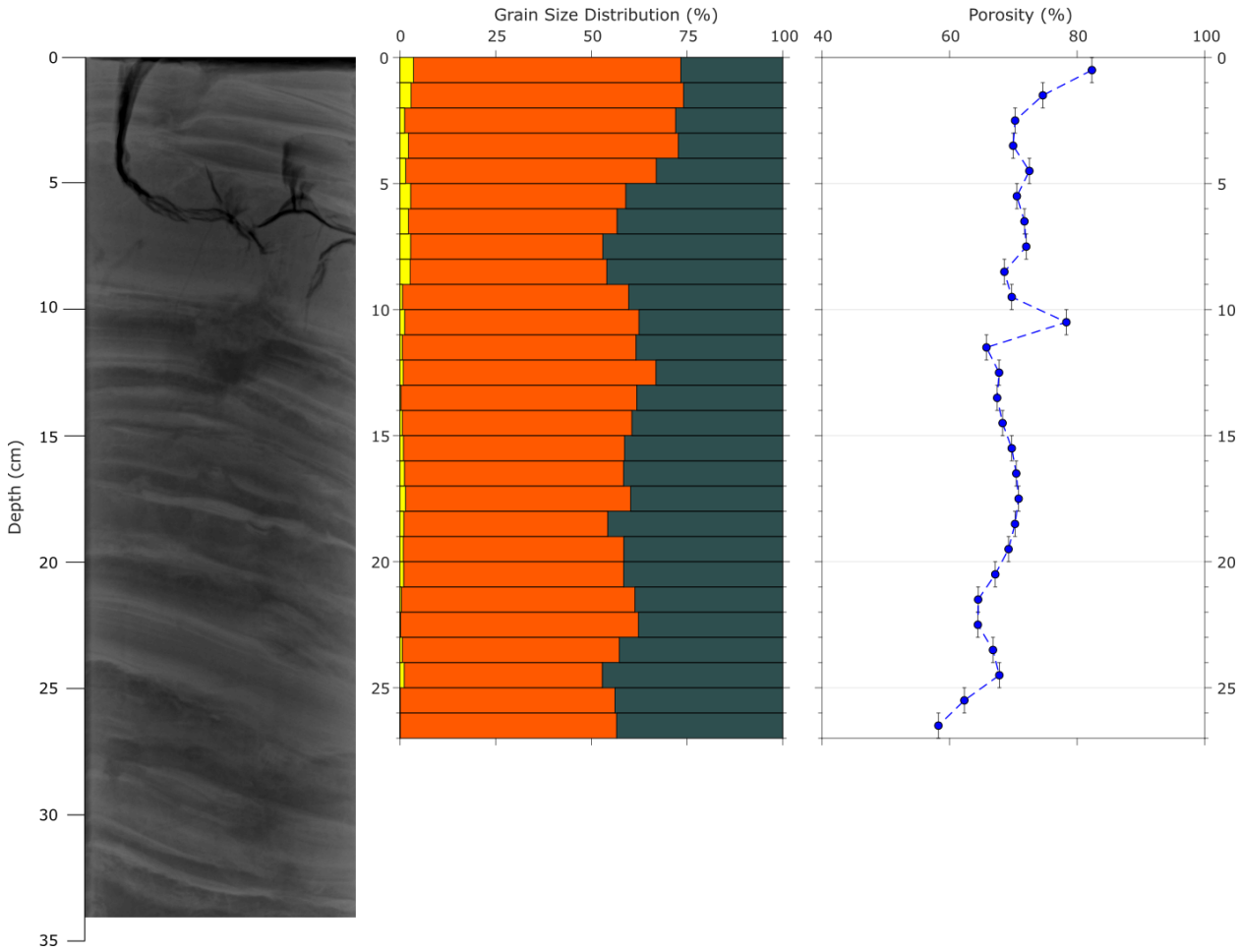
Grain Size Distribution (%)
Porosity (%)
Depth (cm)

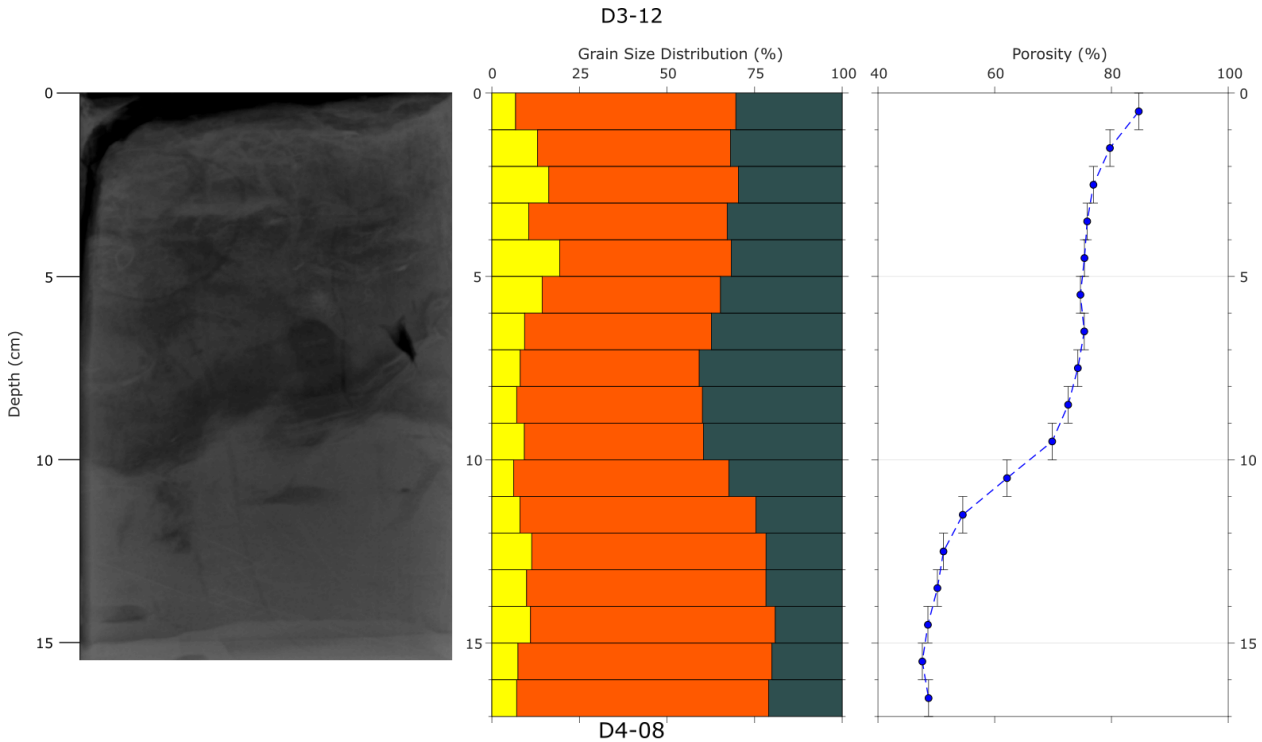
D3-12
Grain Size Distribution (%)
Porosity (%)
Depth (cm)
0
5
10
15
0
25
50
75
100
40
60
80

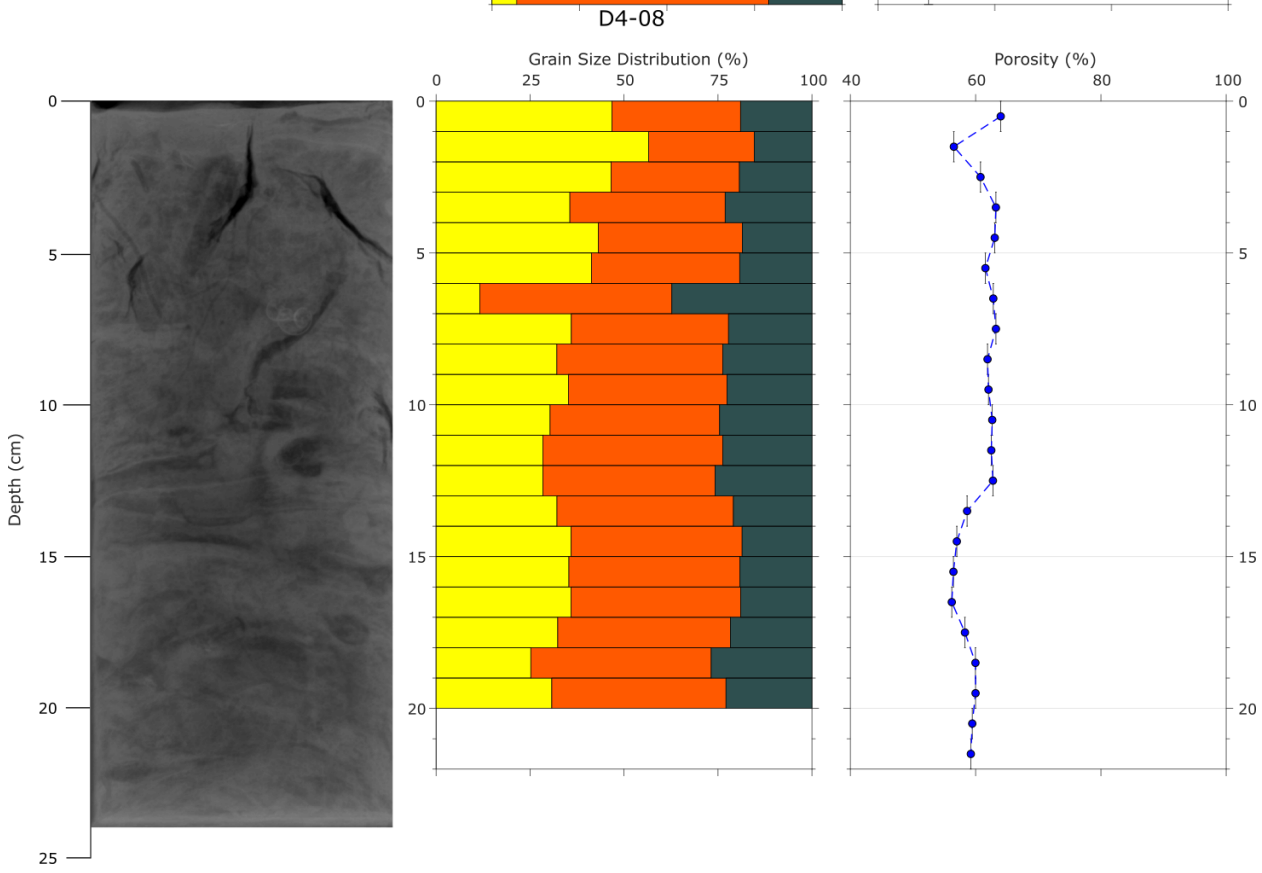
D4-08
Grain Size Distribution (%)
Porosity (%)
Depth (cm)
0
5
10
15
20
25
0
25
50
75
100
40
60
80

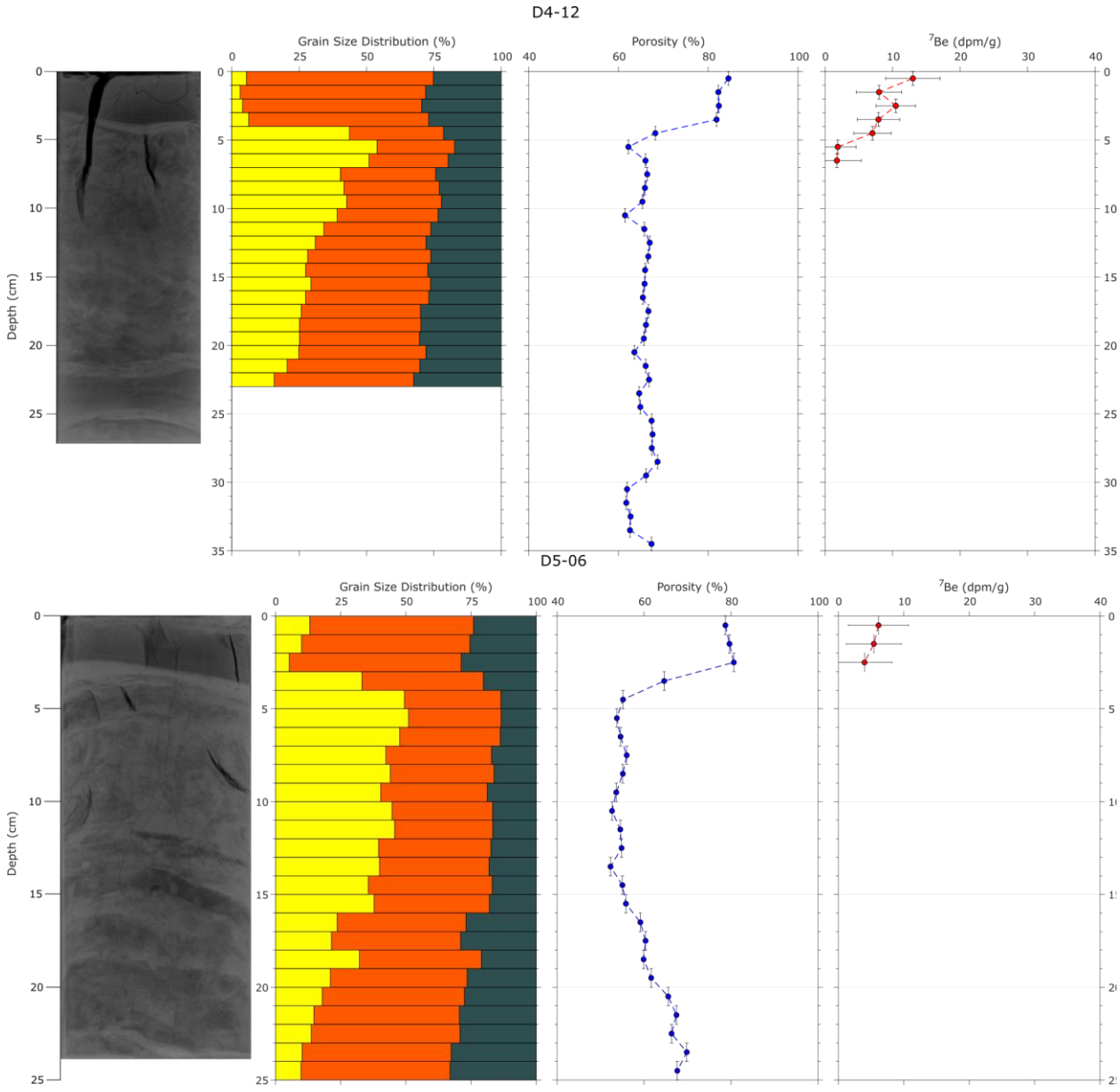
D4-12
Grain Size Distribution (%)
Porosity (%)
^{7}Be (dpm/g)
Depth (cm)
D5-06
Grain Size Distribution (%)
Porosity (%)
^{7}Be (dpm/g)
Depth (cm)

D5-08

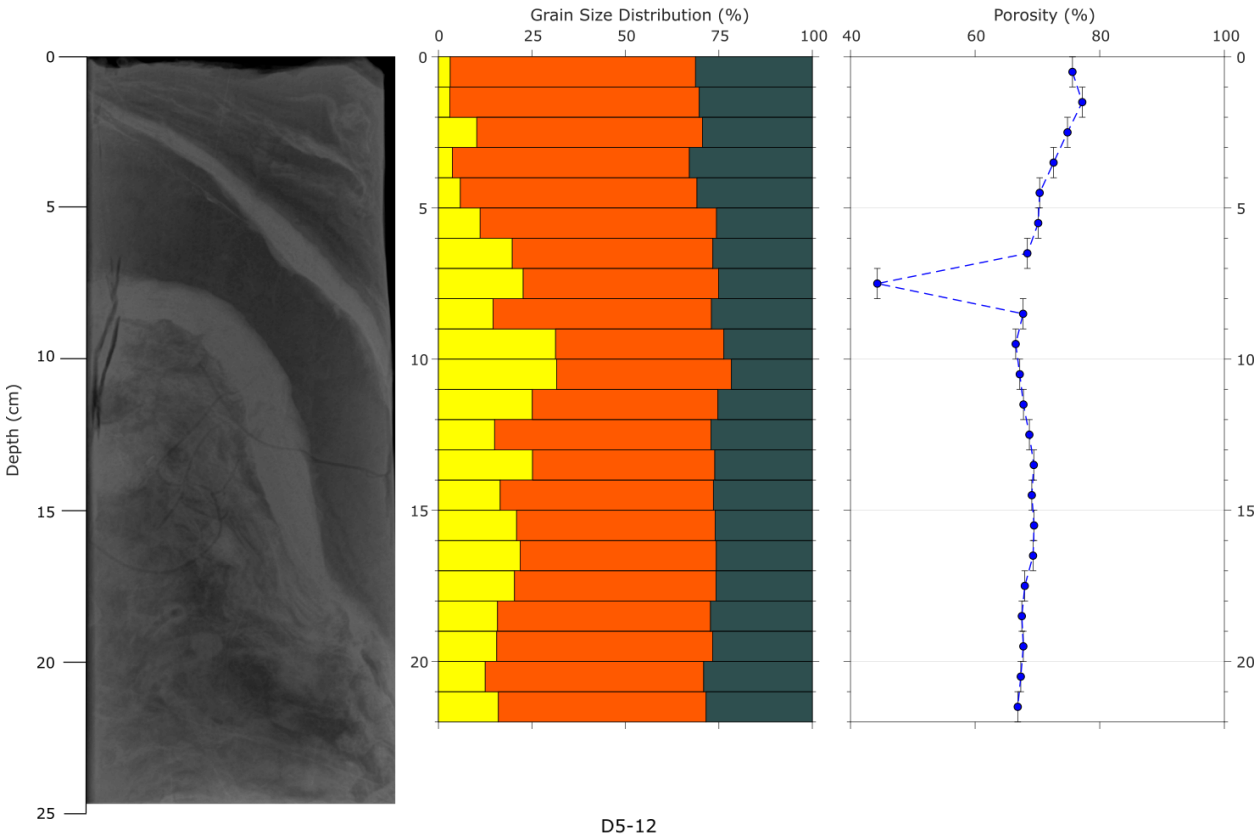
Grain Size Distribution (%)
Porosity (%)
Depth (cm)
0
25
50
75
100
40
60
80
5
10
15
20

D5-12

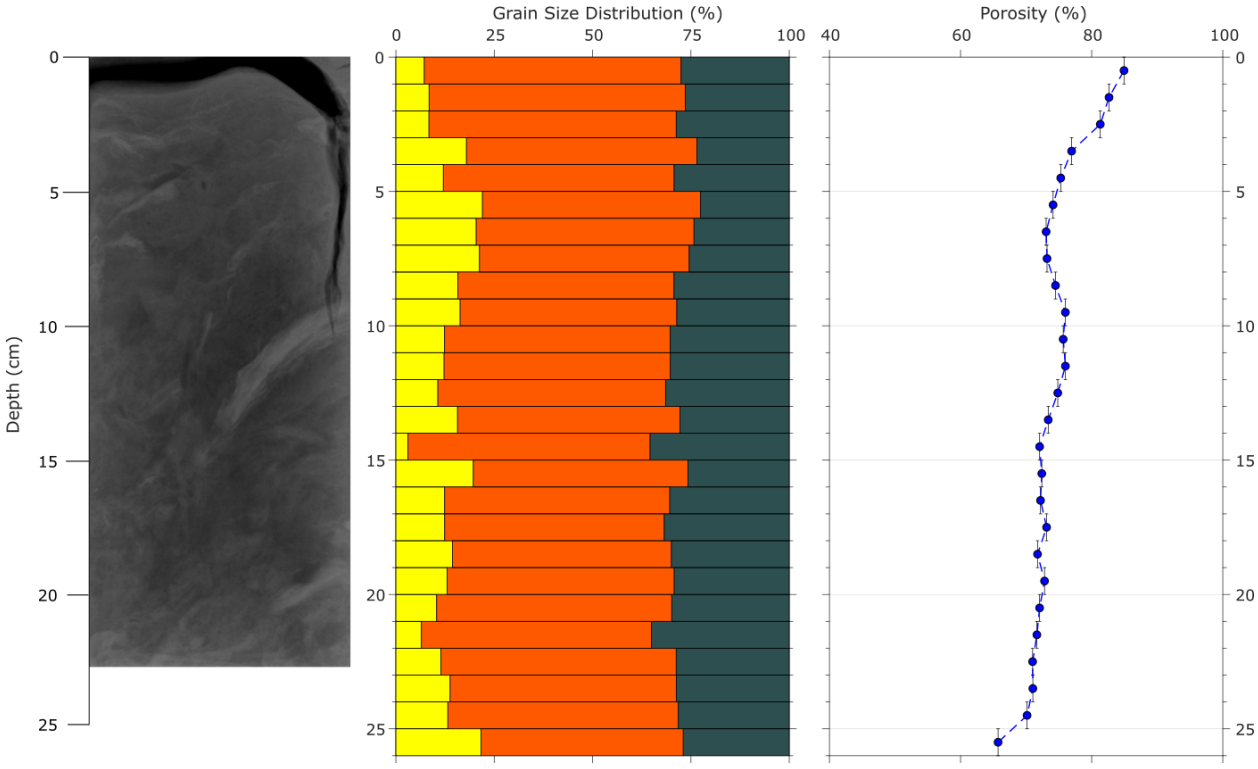
Grain Size Distribution (%)
Porosity (%)
Depth (cm)
0
25
50
75
100
40
60
80
5
10
15
20

J-04

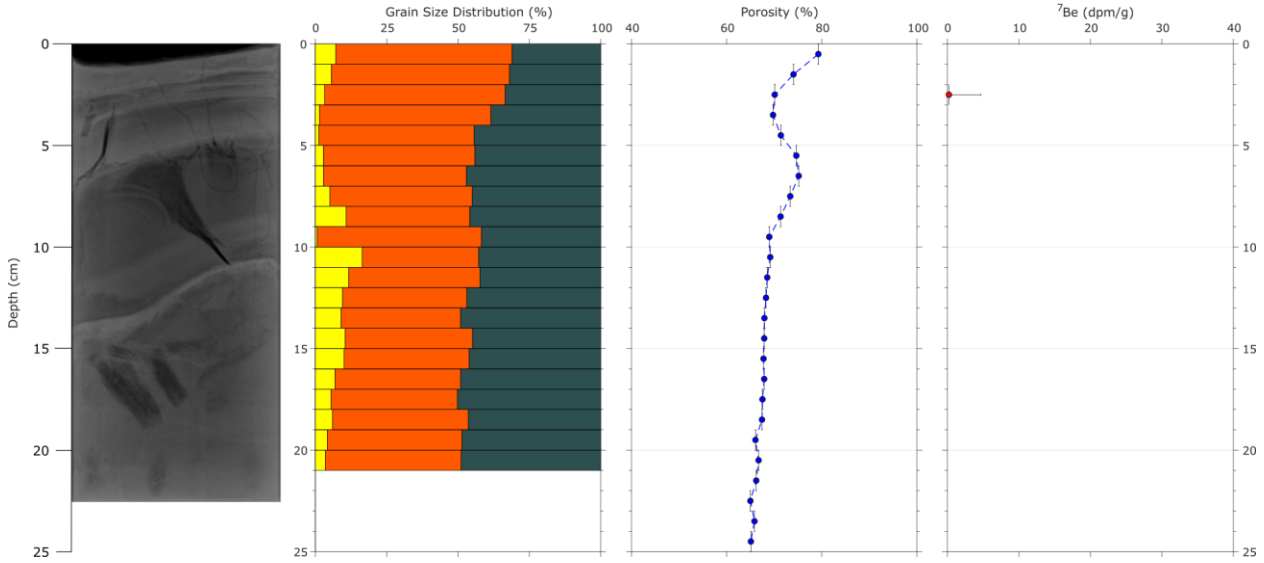
Grain Size Distribution (%)
Porosity (%)
^{7}Be (dpm/g)
Depth (cm)
0
5
10
15
20
25
0
25
50
75
100
40
60
80
100
0
10
20
30
40

J-06

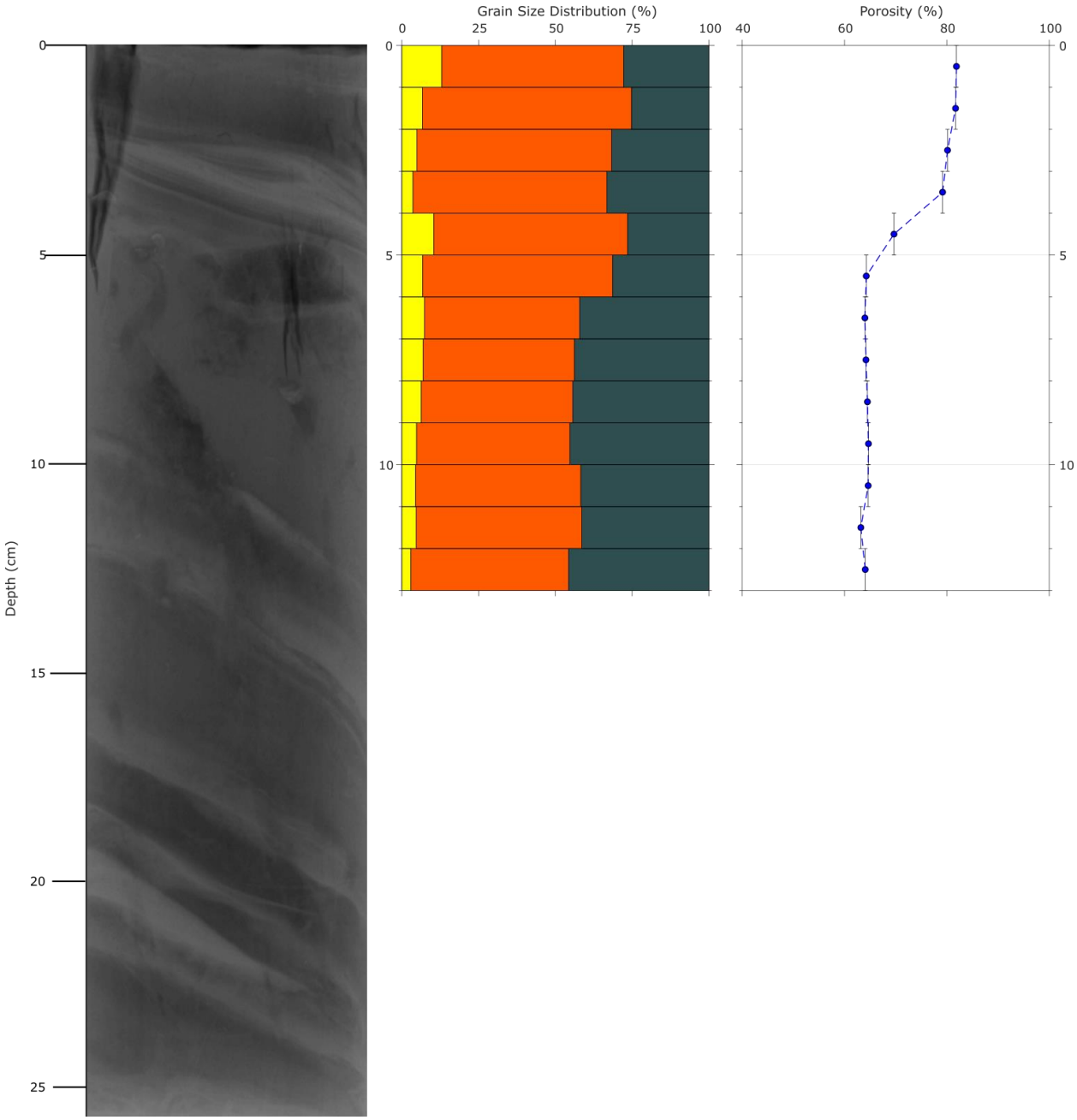
Grain Size Distribution (%)
0
25
50
75
100
Porosity (%)
40
60
80
100
Depth (cm)
0
5
10
15
20
25

J-12

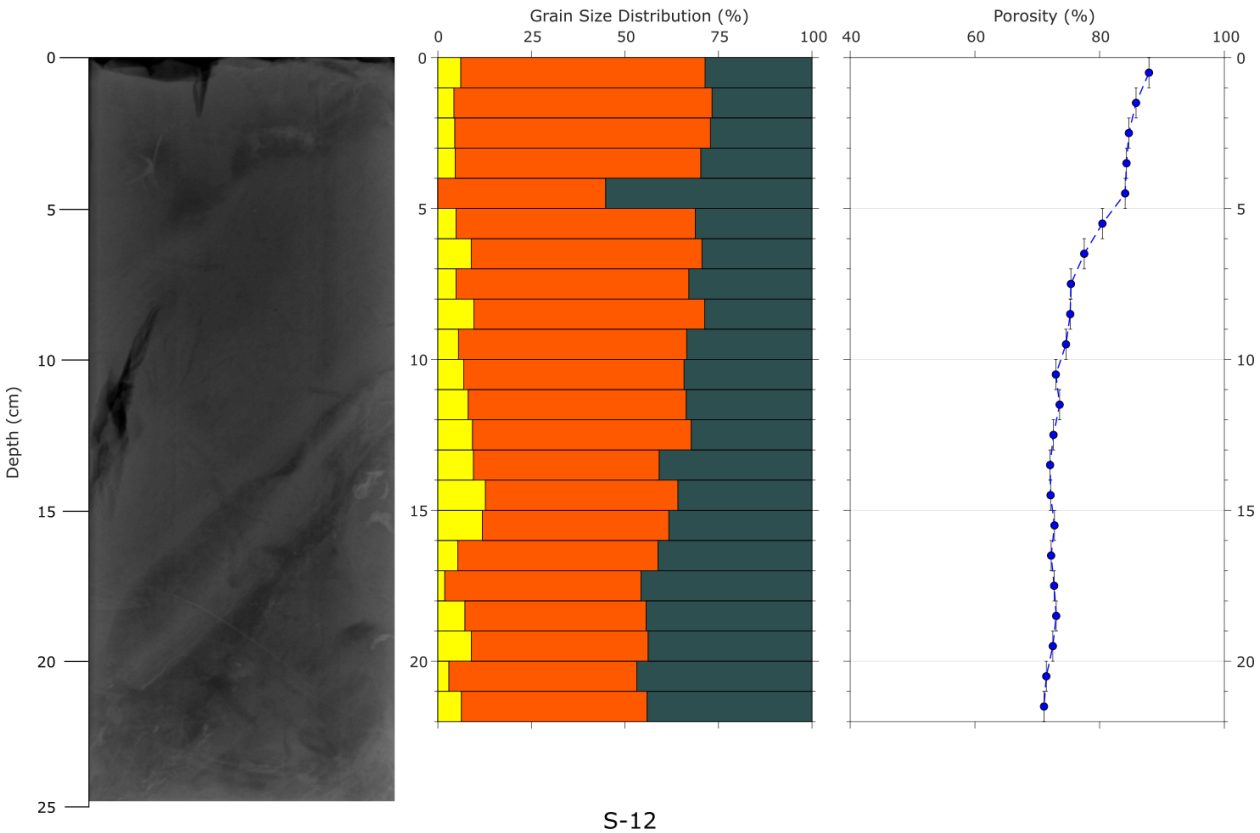
Grain Size Distribution (%)
Porosity (%)
Depth (cm)

S-12

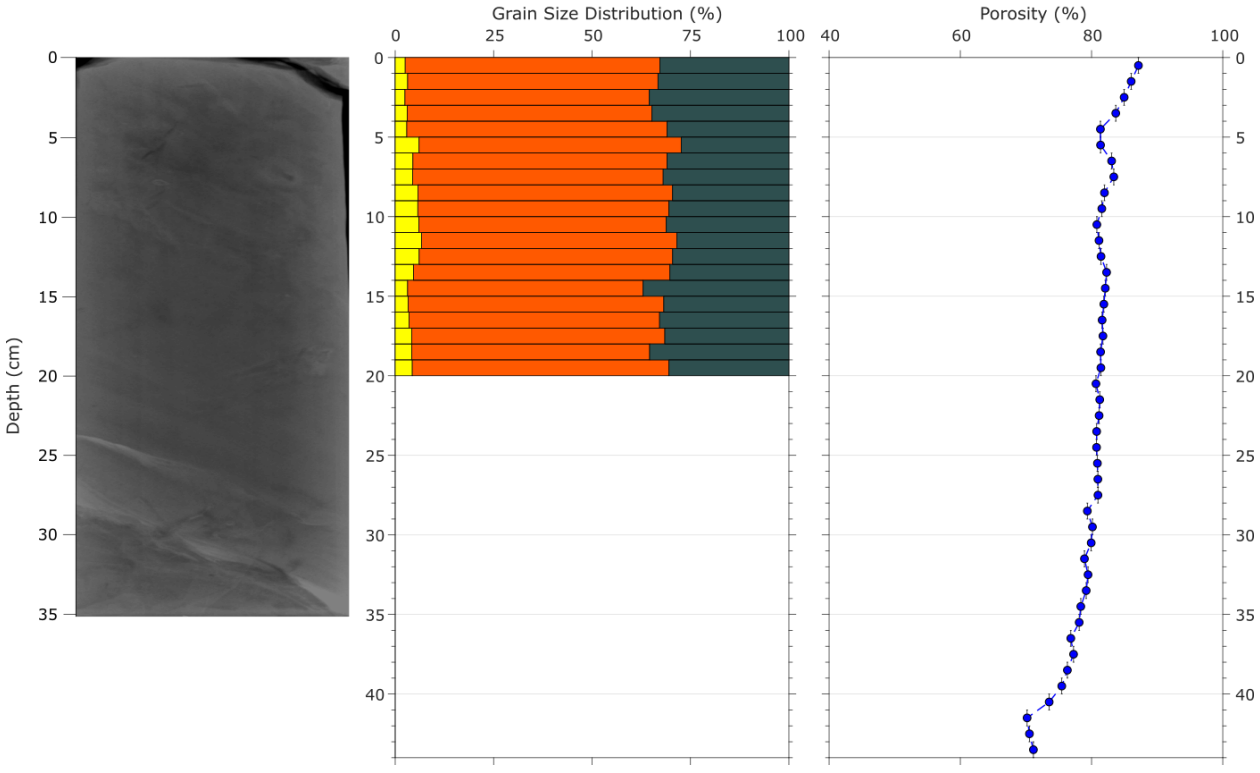
Grain Size Distribution (%)
Porosity (%)
Depth (cm)

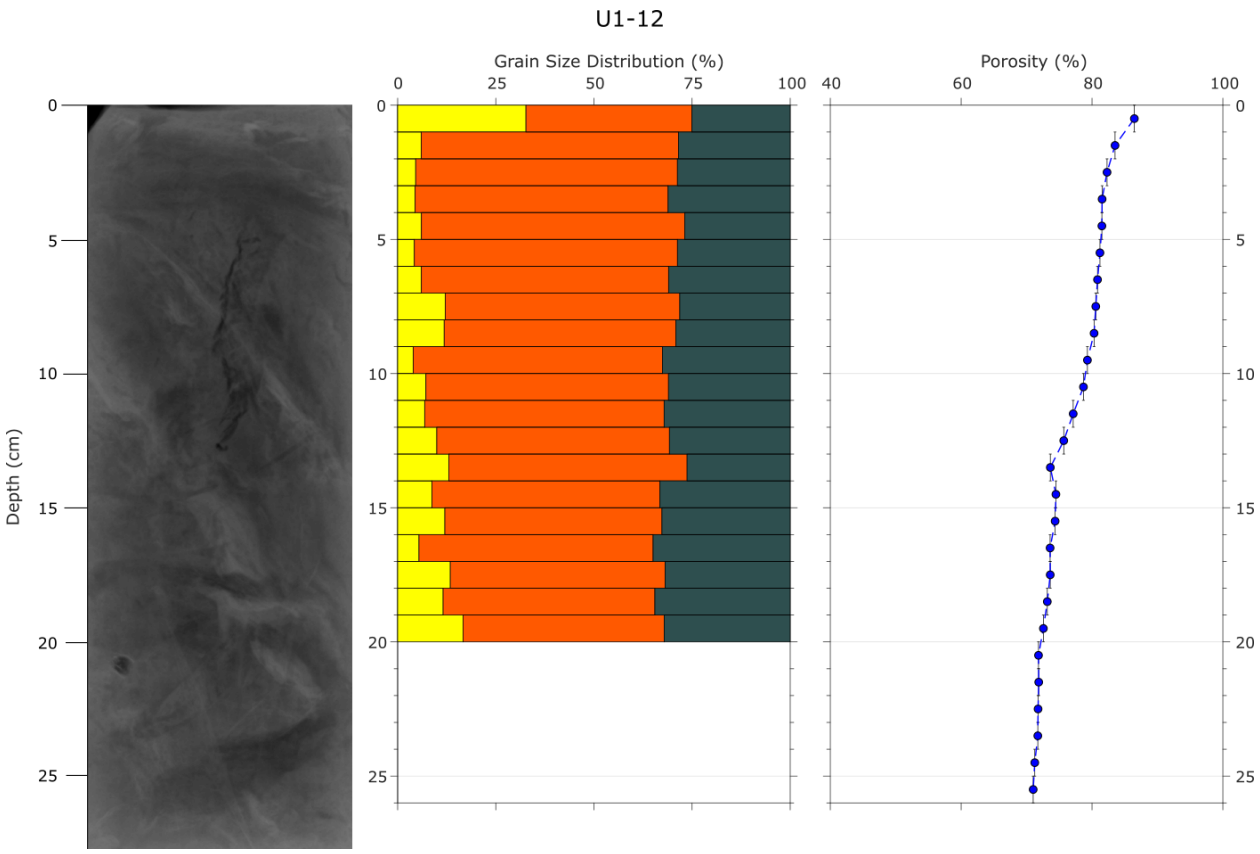
U1-12
Grain Size Distribution (%)
Porosity (%)
Depth (cm)
0
5
10
15
20
25
40
60
80
100

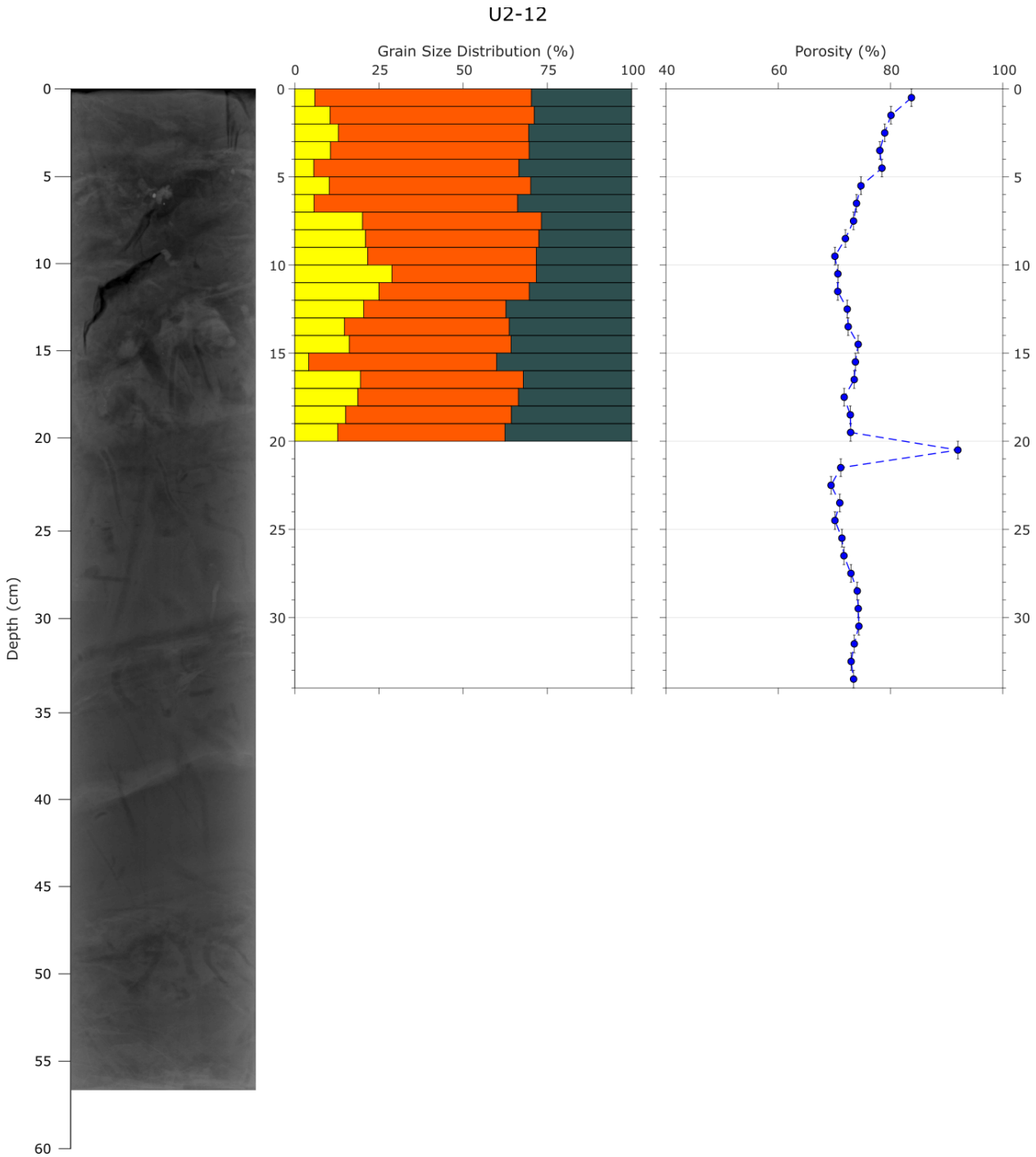
U2-12
Grain Size Distribution (%)
Porosity (%)
Depth (cm)
0
5
10
15
20
25
30
35
40
45
50
55
60
0
25
50
75
100
40
60
80
100

May 31, 2016 Boxcores

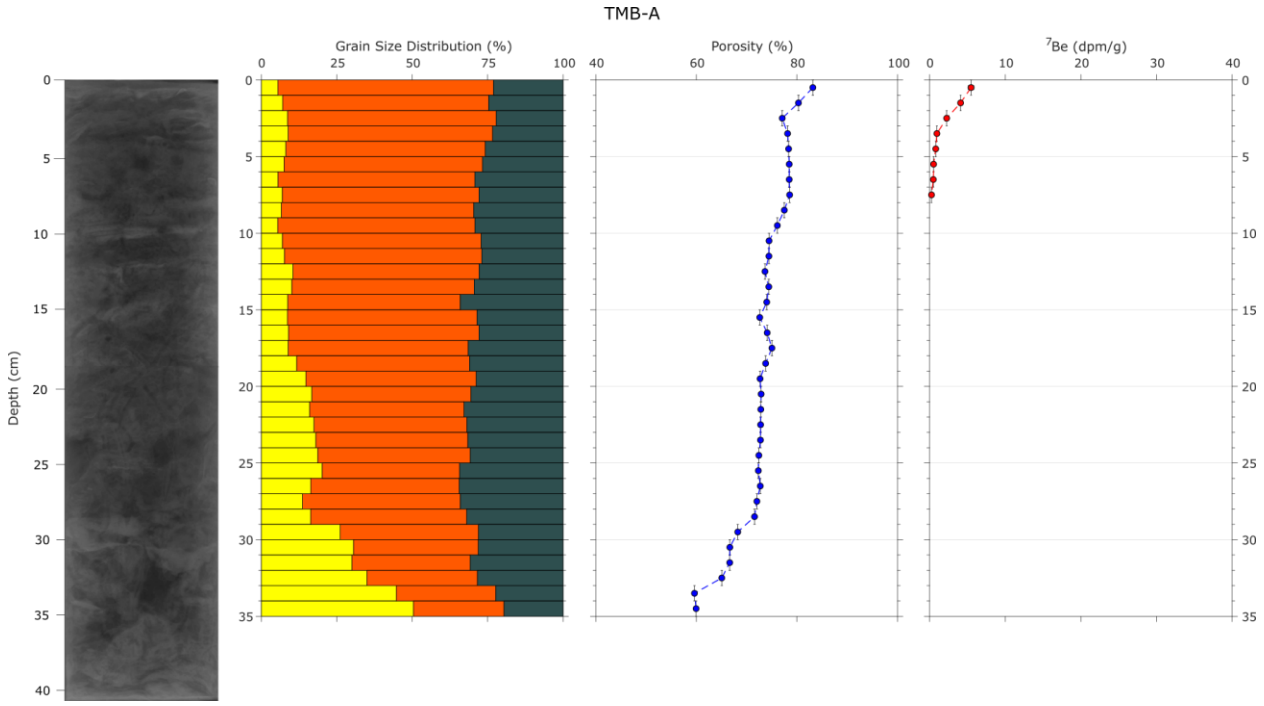

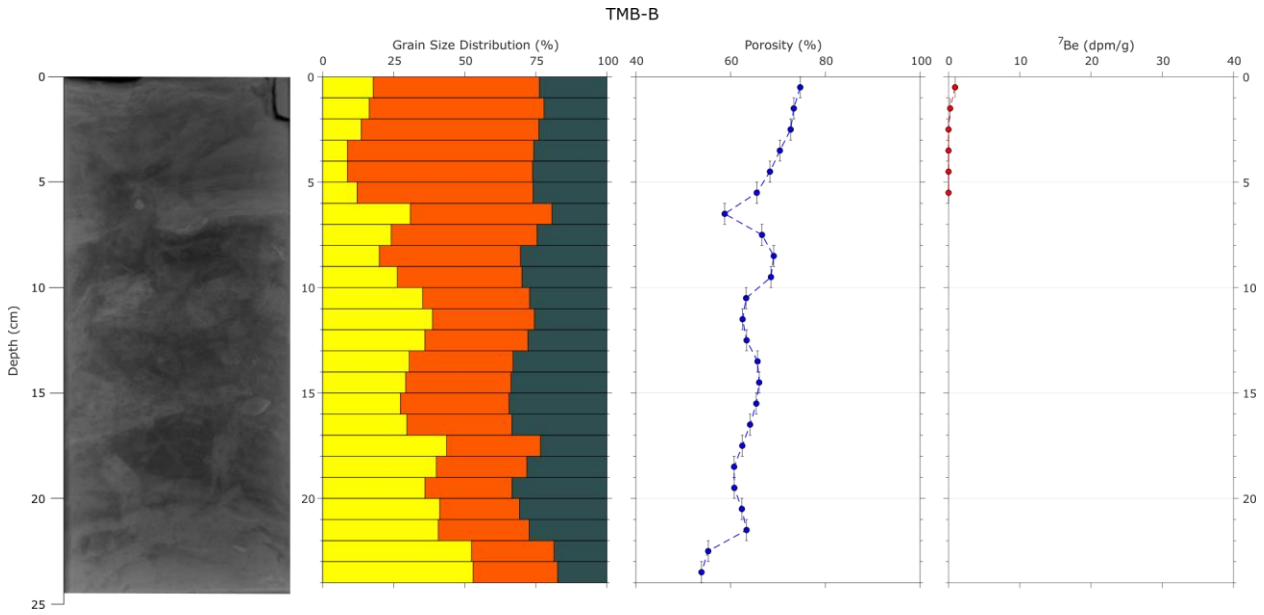
TMB-B
Grain Size Distribution (%)
Porosity (%)
^{7}Be (dpm/g)
Depth (cm)

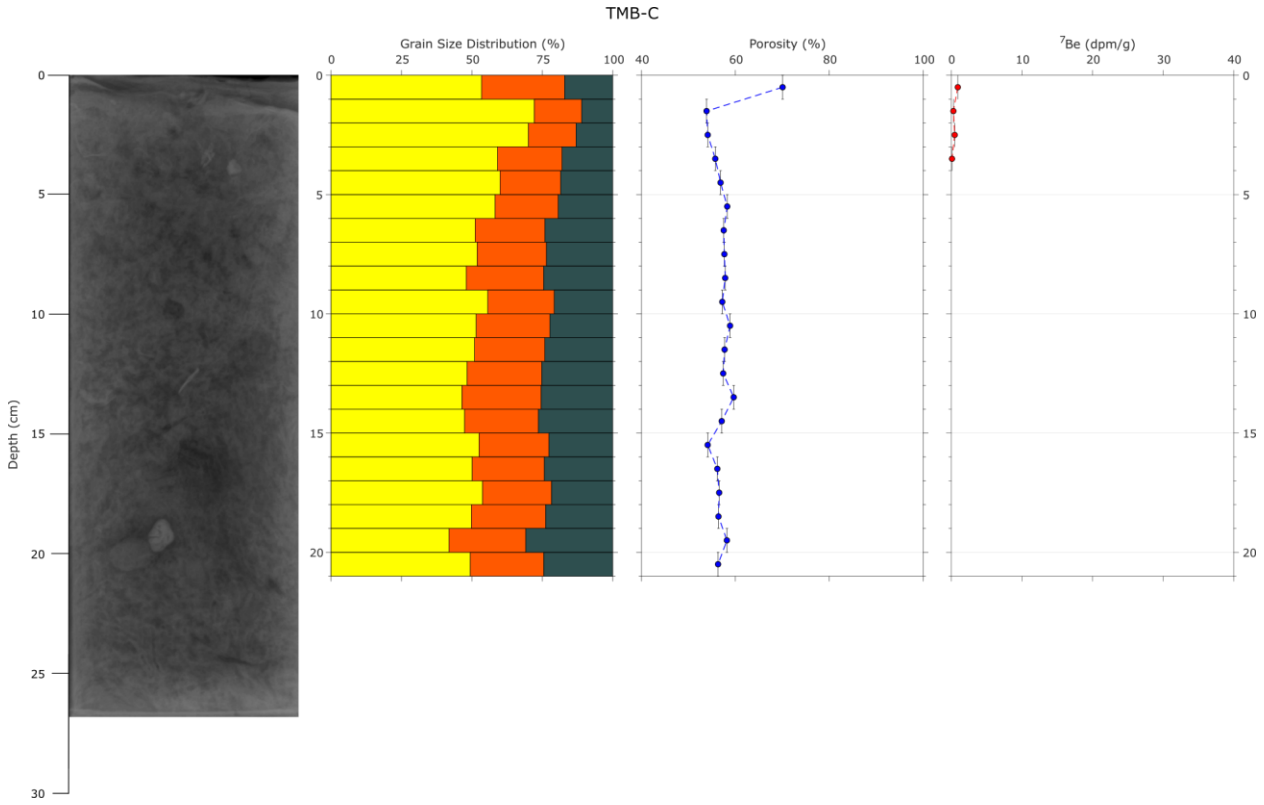
TMB-C
Grain Size Distribution (%)
Porosity (%)
^{7}Be (dpm/g)
Depth (cm)

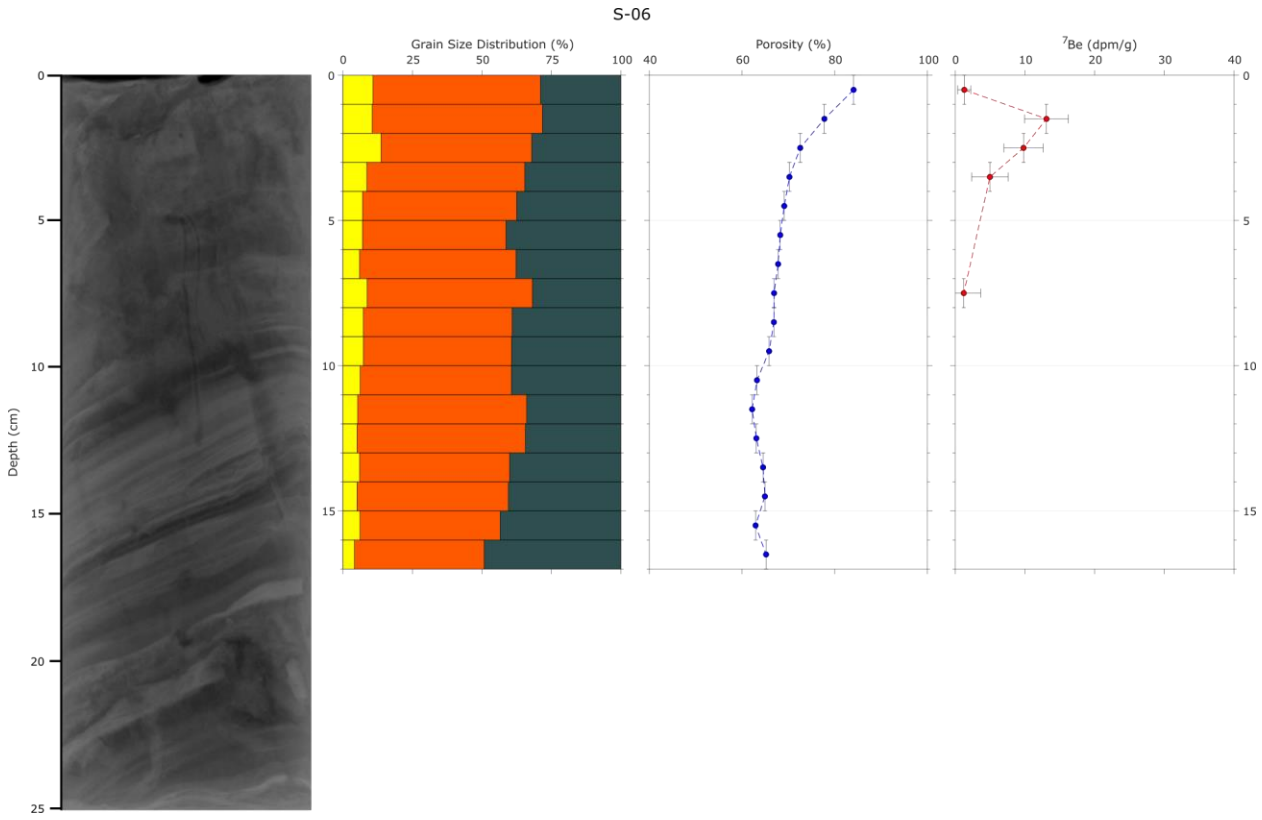
S-06
Grain Size Distribution (%)
Porosity (%)
^{7}Be (dpm/g)
Depth (cm)

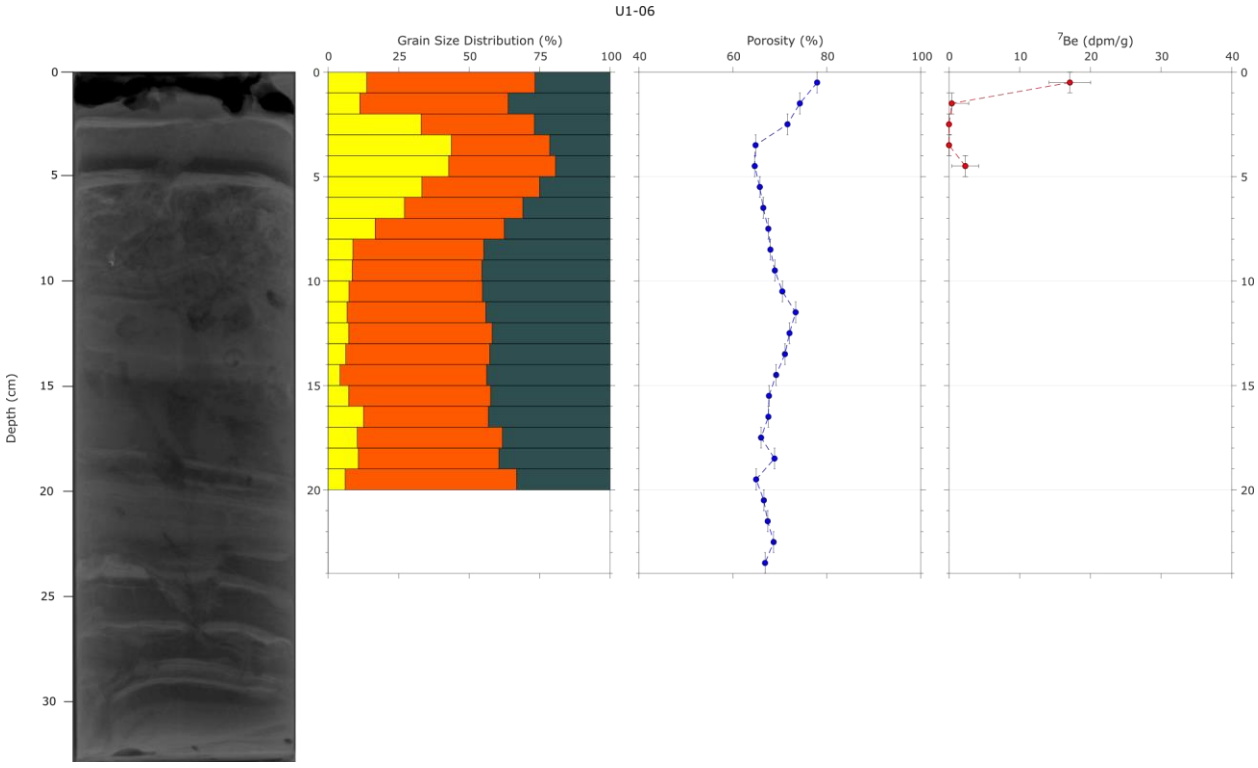
U1-06
Grain Size Distribution (%)
Porosity (%)
^{7}Be (dpm/g)
Depth (cm)

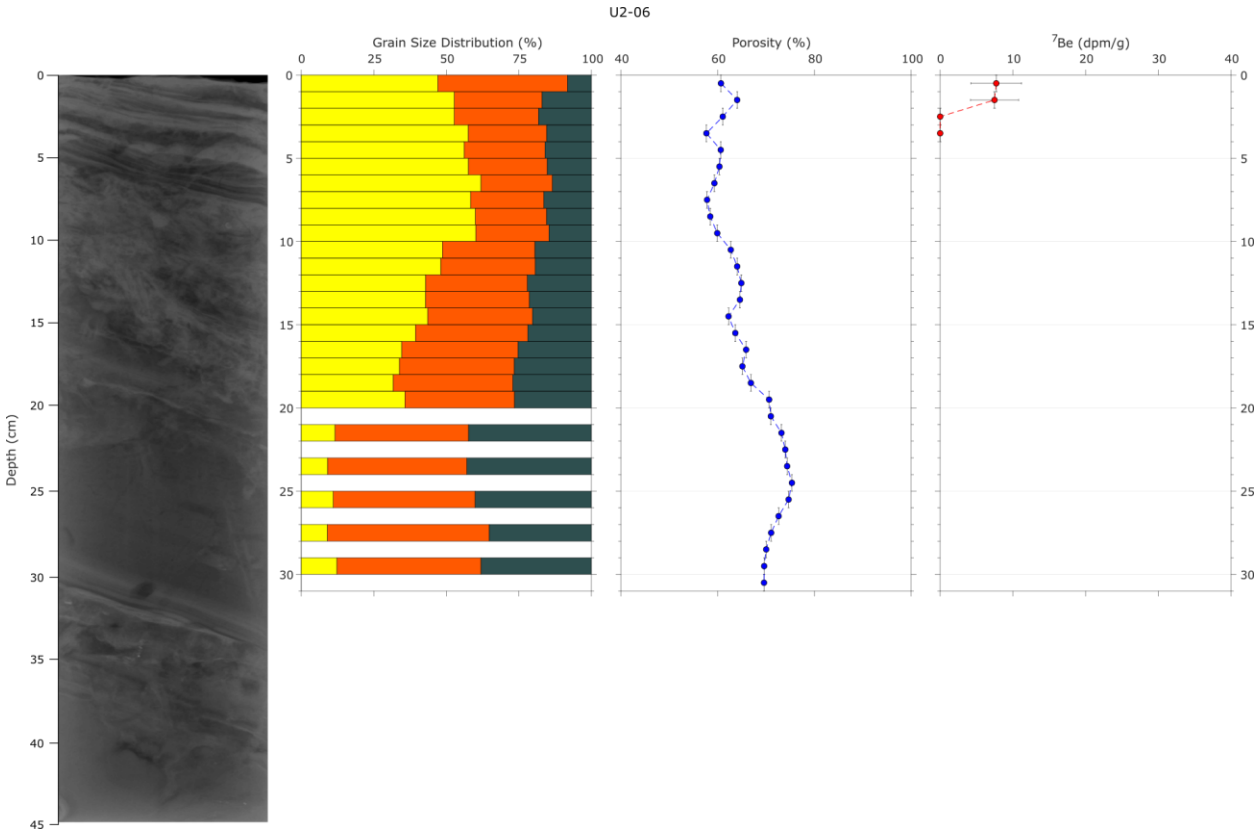
U2-06
Grain Size Distribution (%)
Porosity (%)
^{7}Be (dpm/g)
Depth (cm)

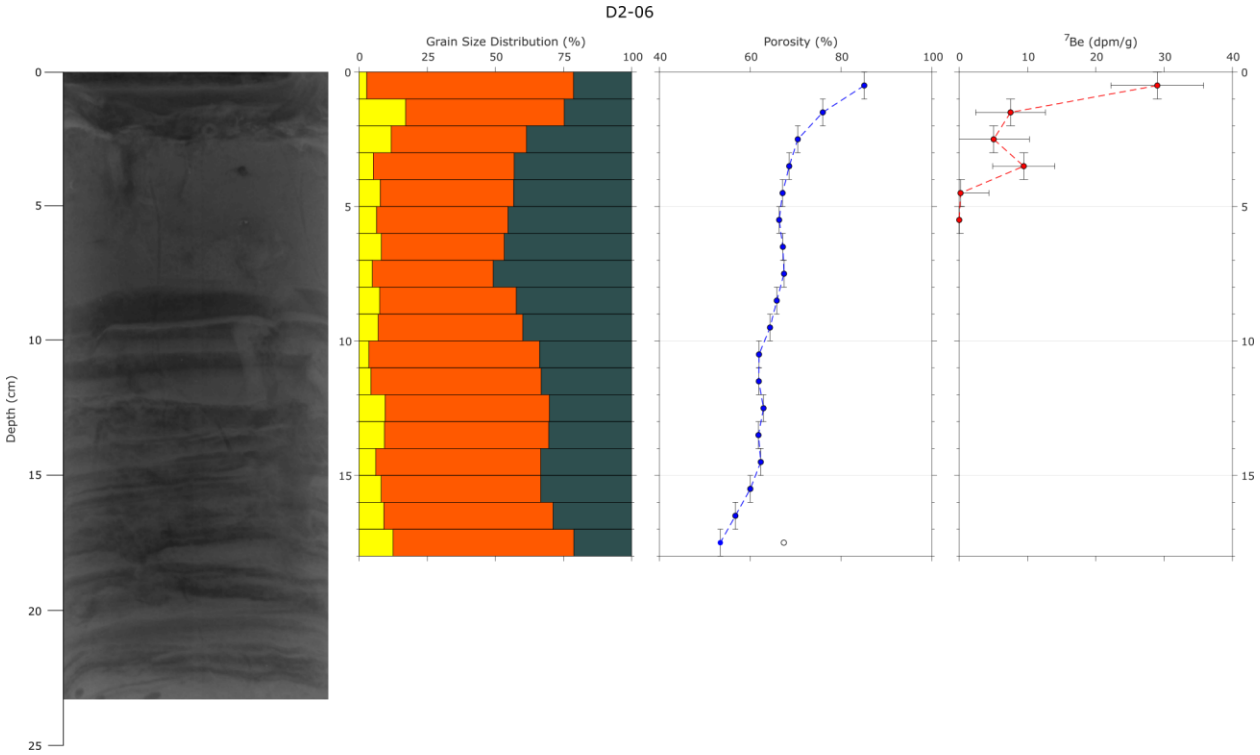
D2-06
Grain Size Distribution (%)
Porosity (%)
^{7}Be (dpm/g)
Depth (cm)

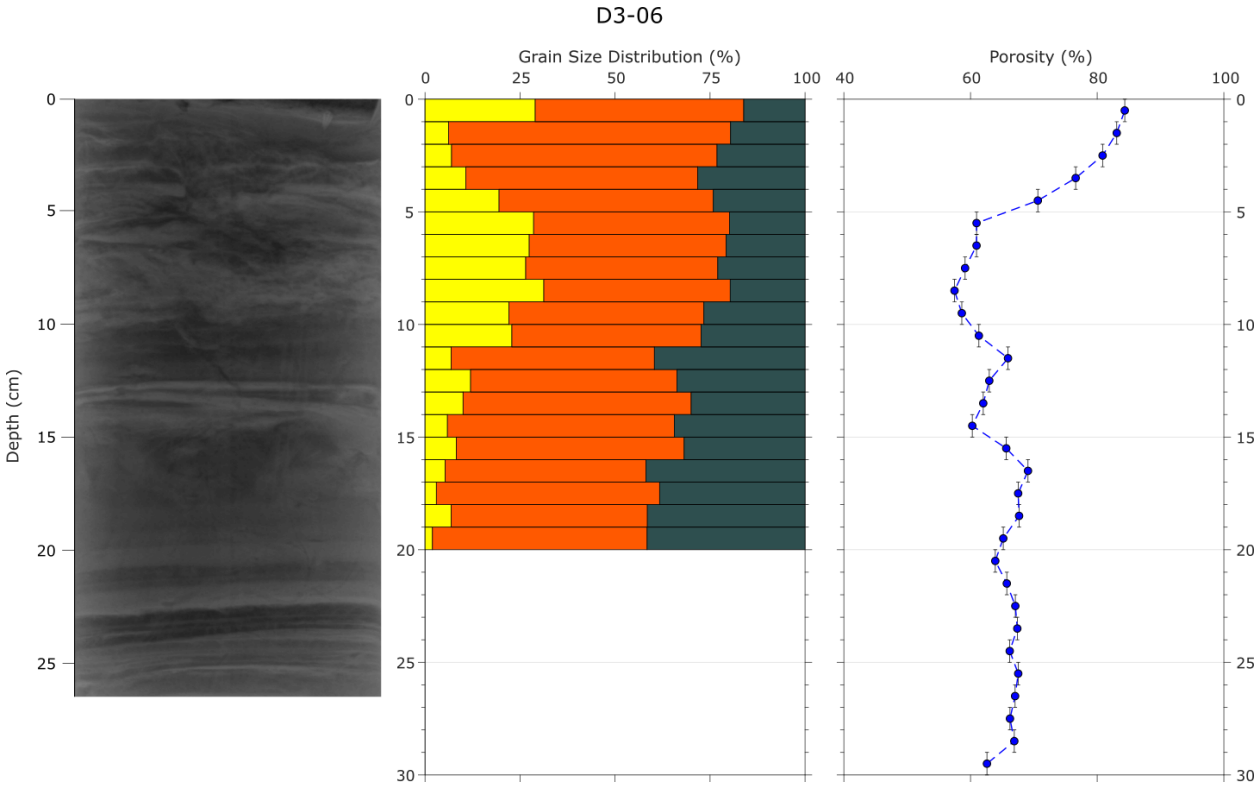
D3-06
Grain Size Distribution (%)
Porosity (%)
Depth (cm)

J-04

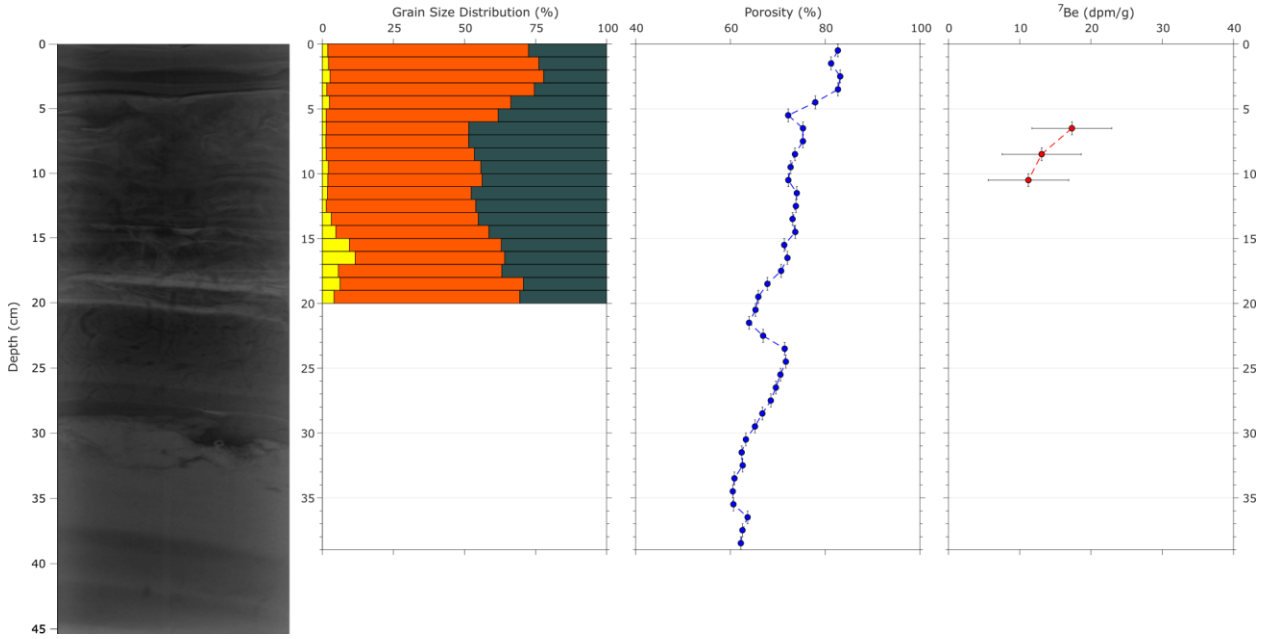
Grain Size Distribution (%)
Porosity (%)
^{7}Be (dpm/g)
Depth (cm)

J-06

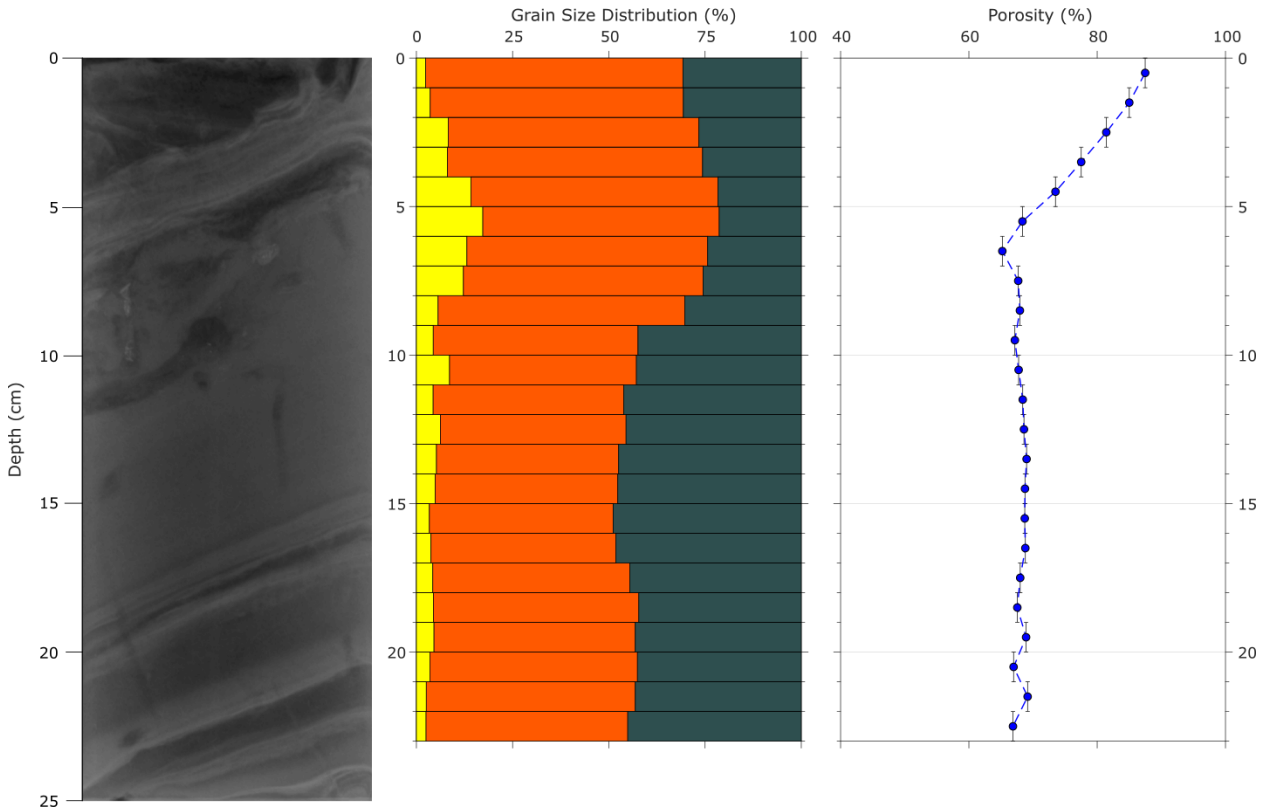
Grain Size Distribution (%)
Porosity (%)
Depth (cm)

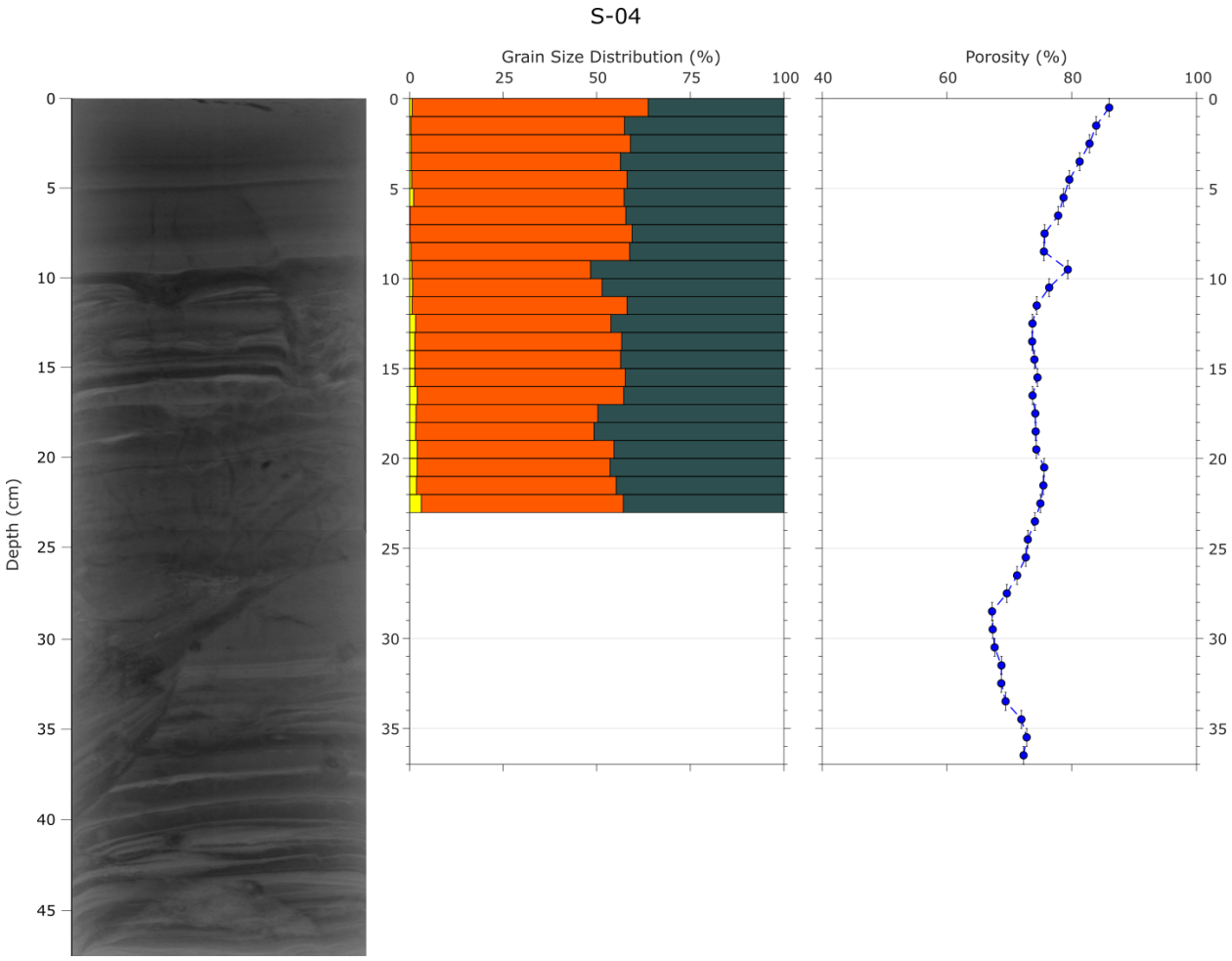
S-04
Grain Size Distribution (%)
Porosity (%)
Depth (cm)
0
25
50
75
100
40
60
80
0
5
10
15
20
25
30
35
40
45

S-06

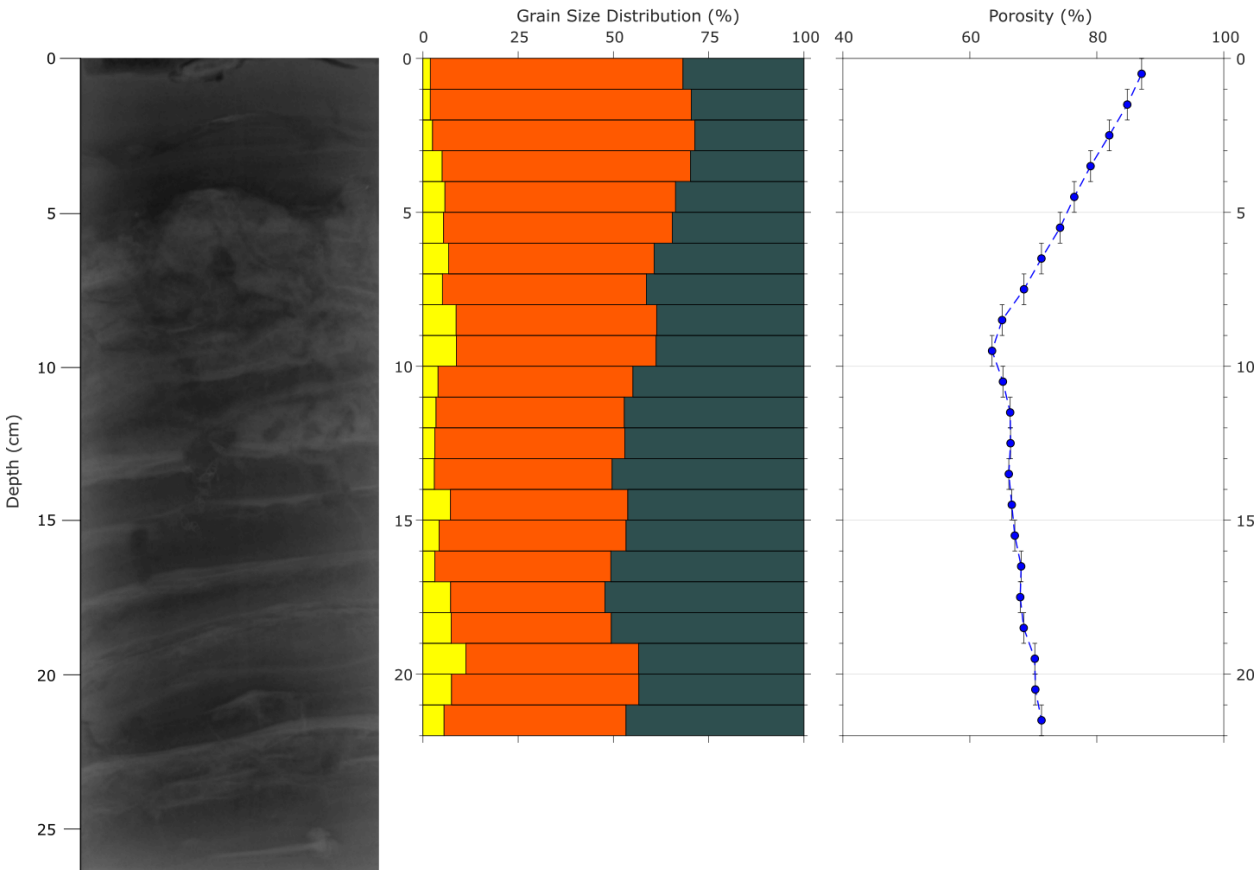
Grain Size Distribution (%)
Porosity (%)
Depth (cm)
0
5
10
15
20
25
40
60
80
100

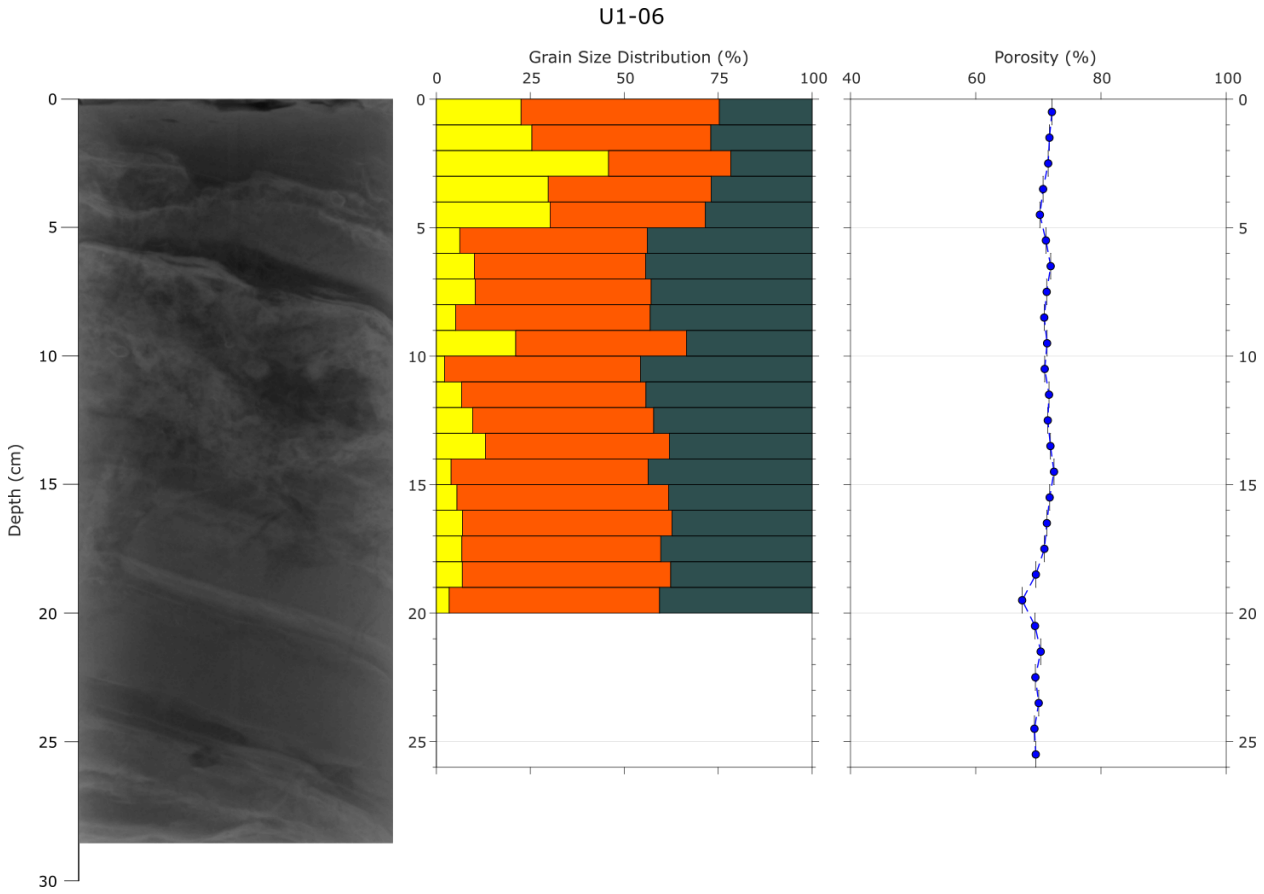
U1-06
Grain Size Distribution (%)
Porosity (%)
Depth (cm)
0
25
50
75
100
40
60
80
5
10
15
20
30

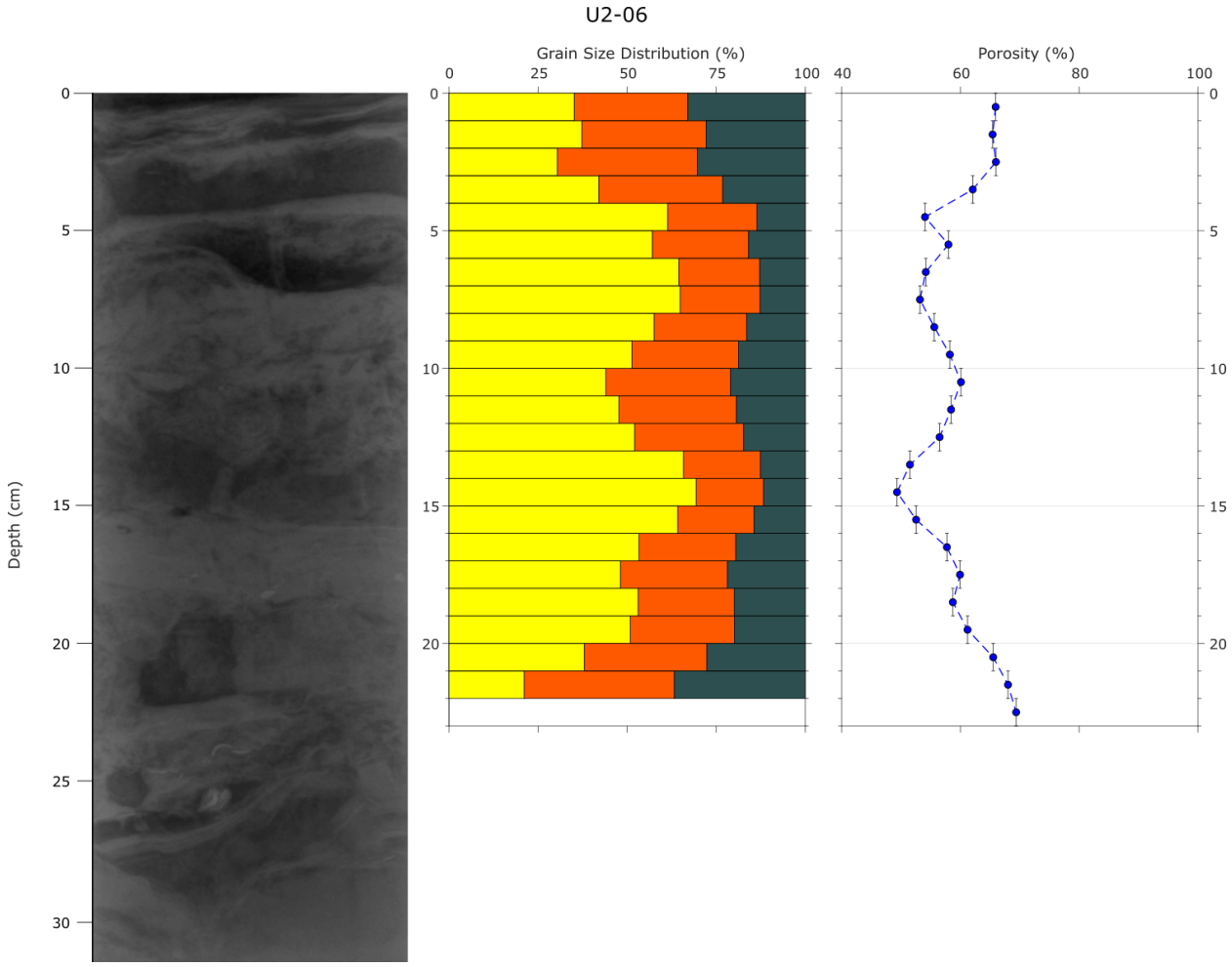
U2-06
Grain Size Distribution (%)
Porosity (%)
Depth (cm)
0
5
10
15
20
25
30
40
60
80
100

September 3, 2016 Boxcores

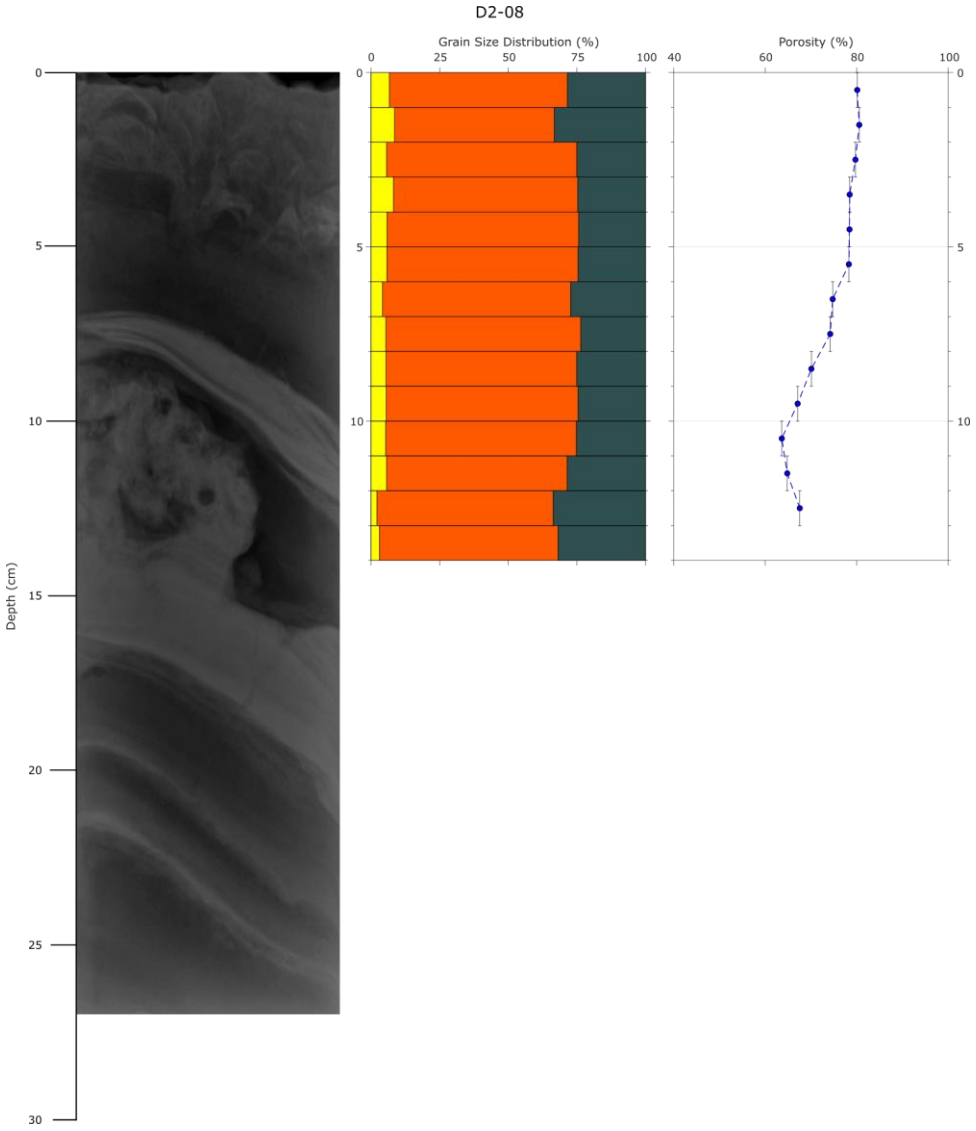

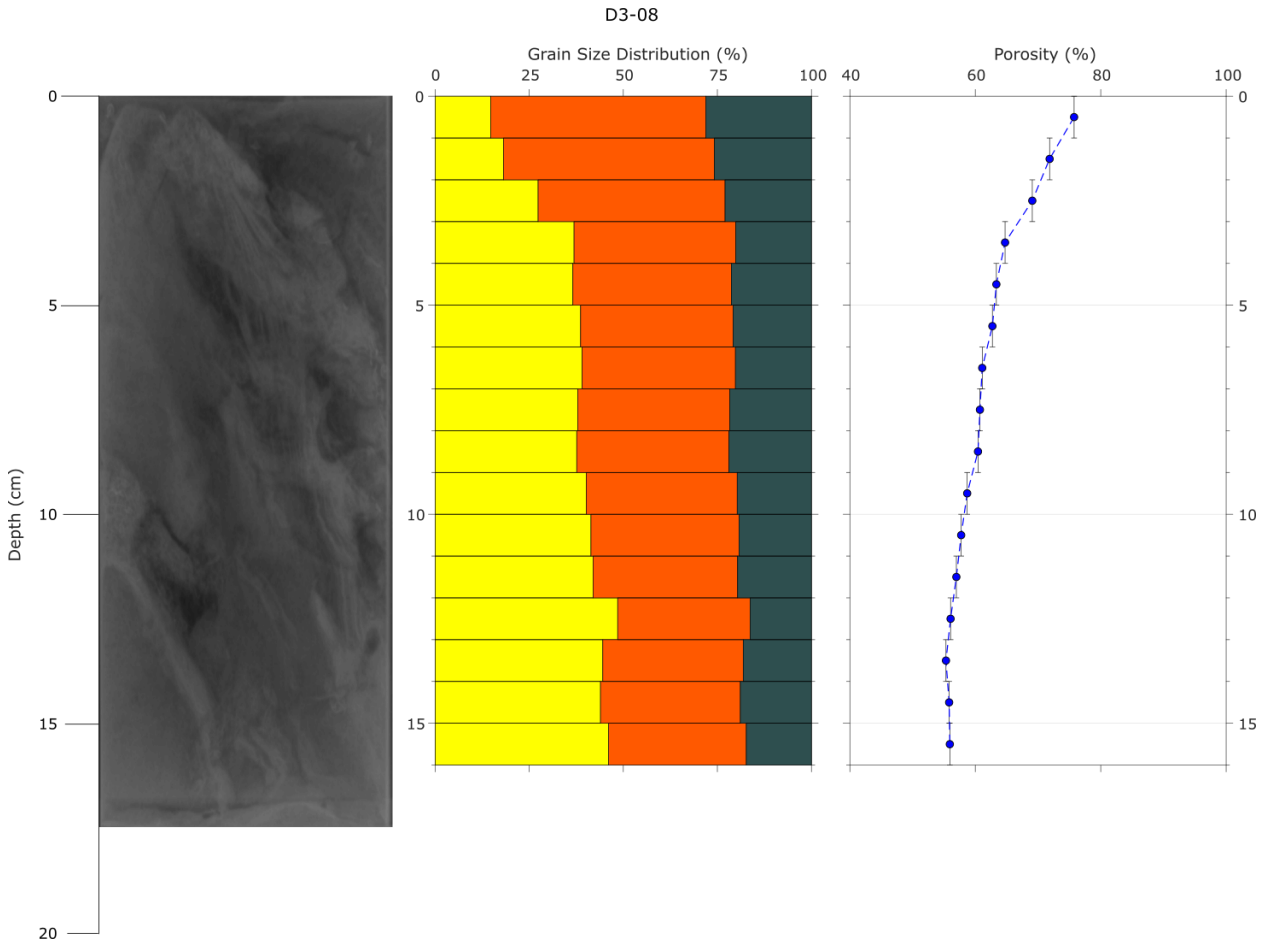
D3-08
Grain Size Distribution (%)
0
25
50
75
100
Porosity (%)
40
60
80
100
Depth (cm)
0
5
10
15
20

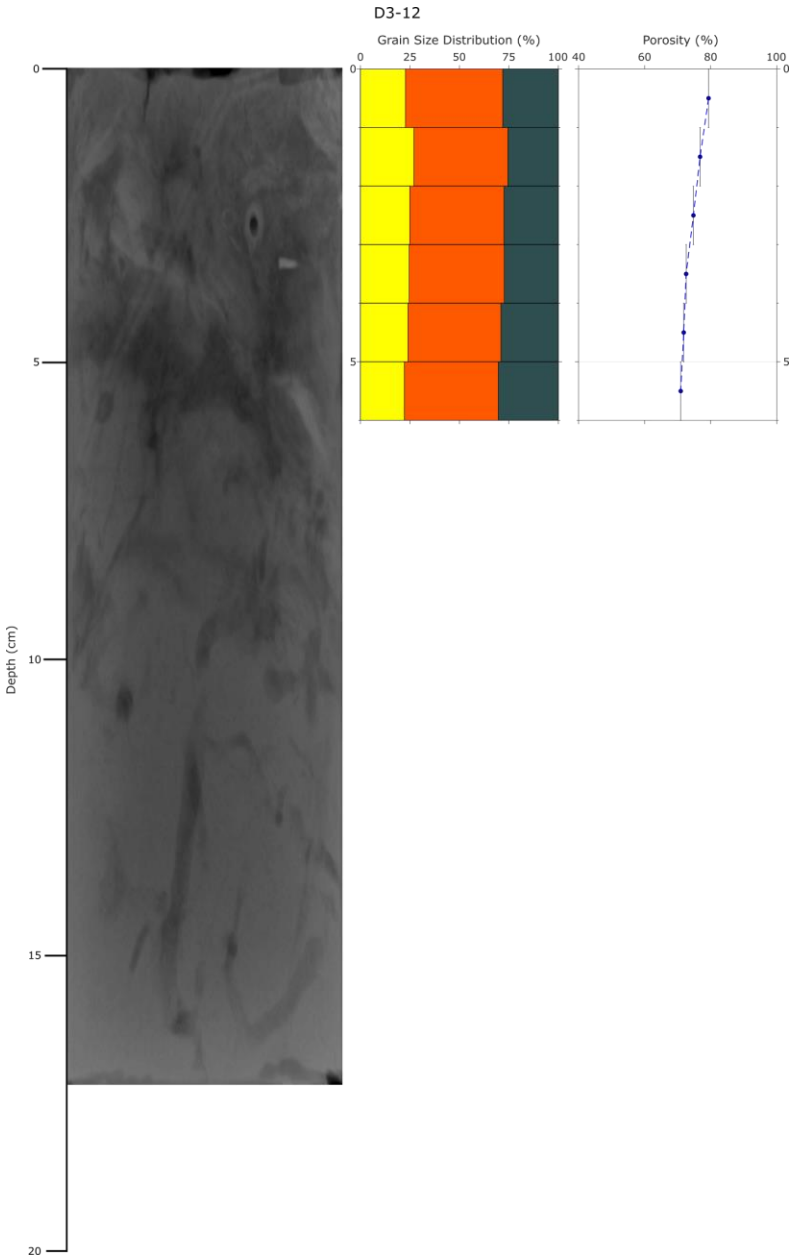
D3-12
Grain Size Distribution (%)
0
25
50
75
100
Porosity (%)
40
60
80
100
Depth (cm)
0
5
10
15
20

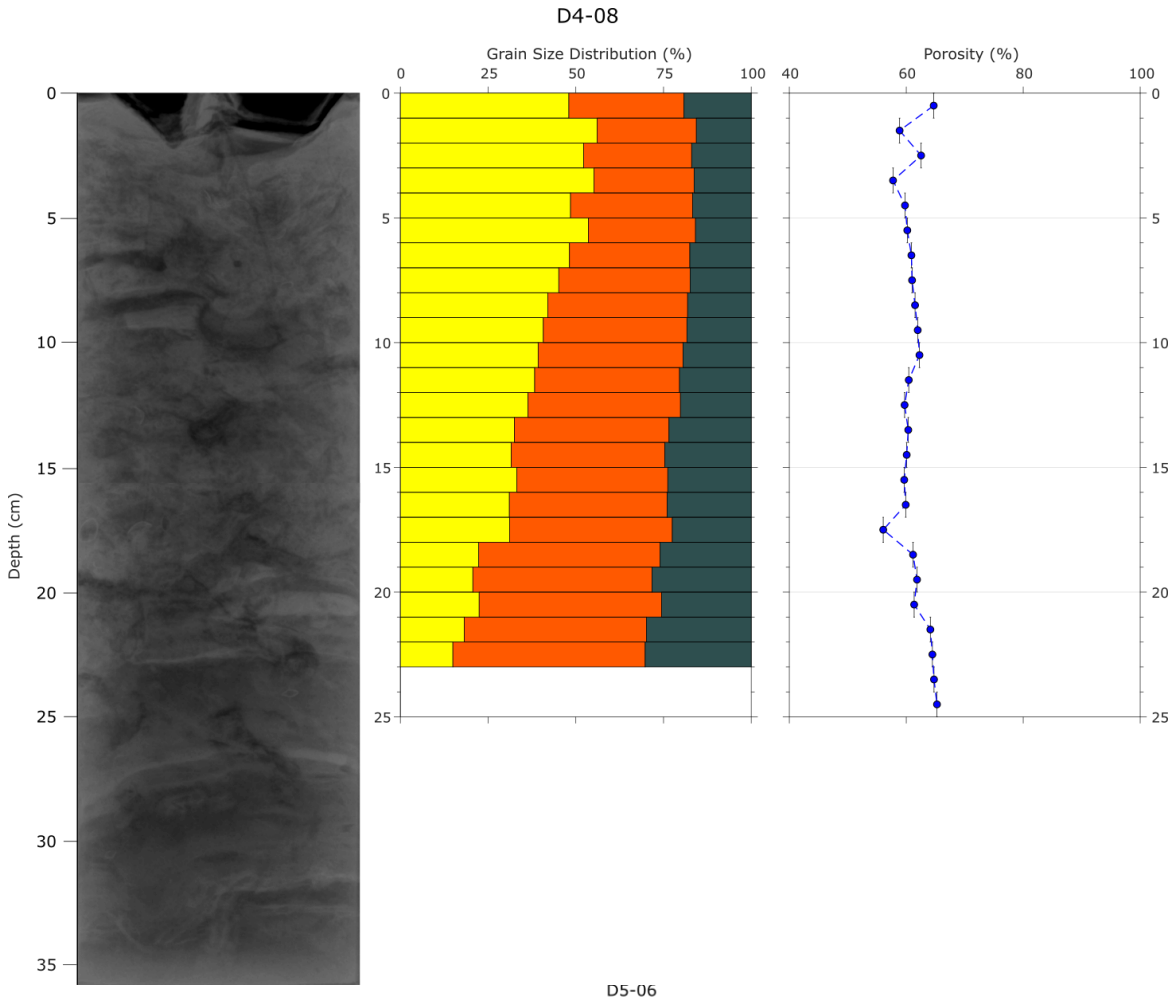
D4-08
Grain Size Distribution (%)
Porosity (%)
Depth (cm)

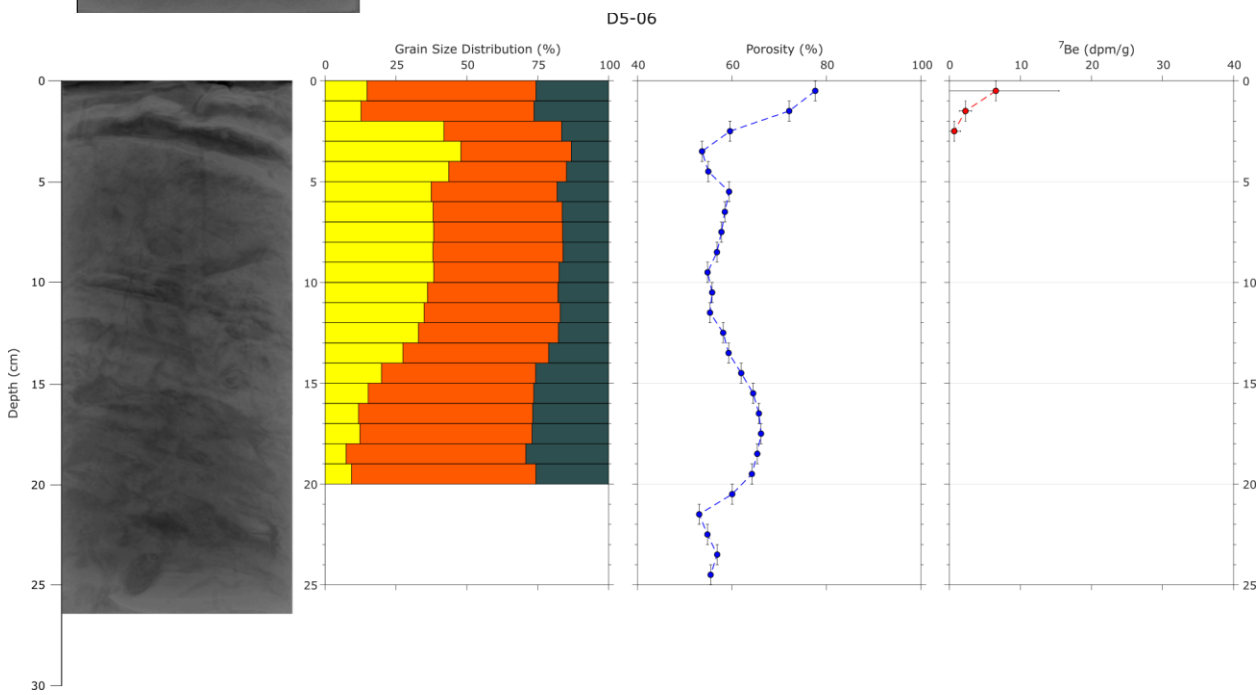
D5-06
Grain Size Distribution (%)
Porosity (%)
^{7}Be (dpm/g)
Depth (cm)

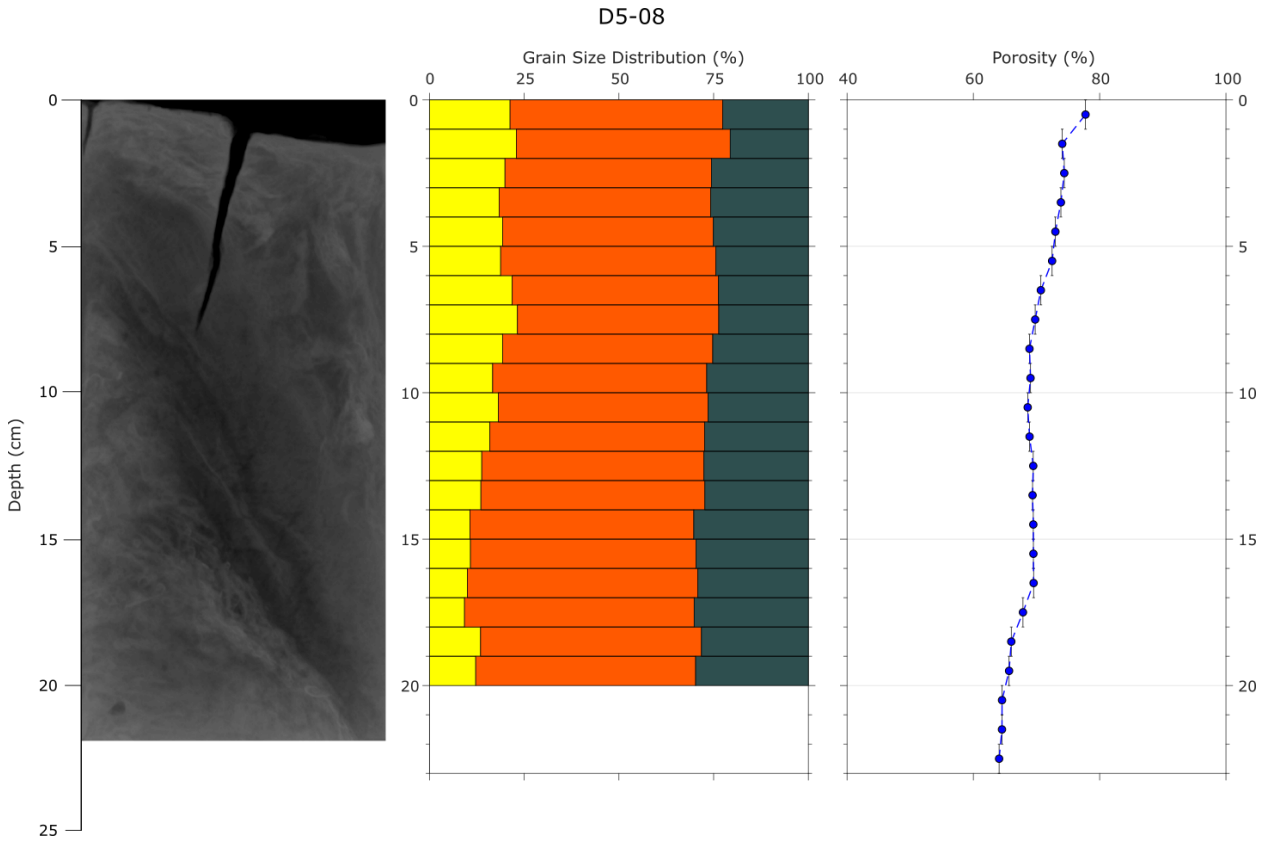
D5-08
Grain Size Distribution (%)
Porosity (%)
Depth (cm)
0
25
50
75
100
40
60
80
5
10
15
20

J-06

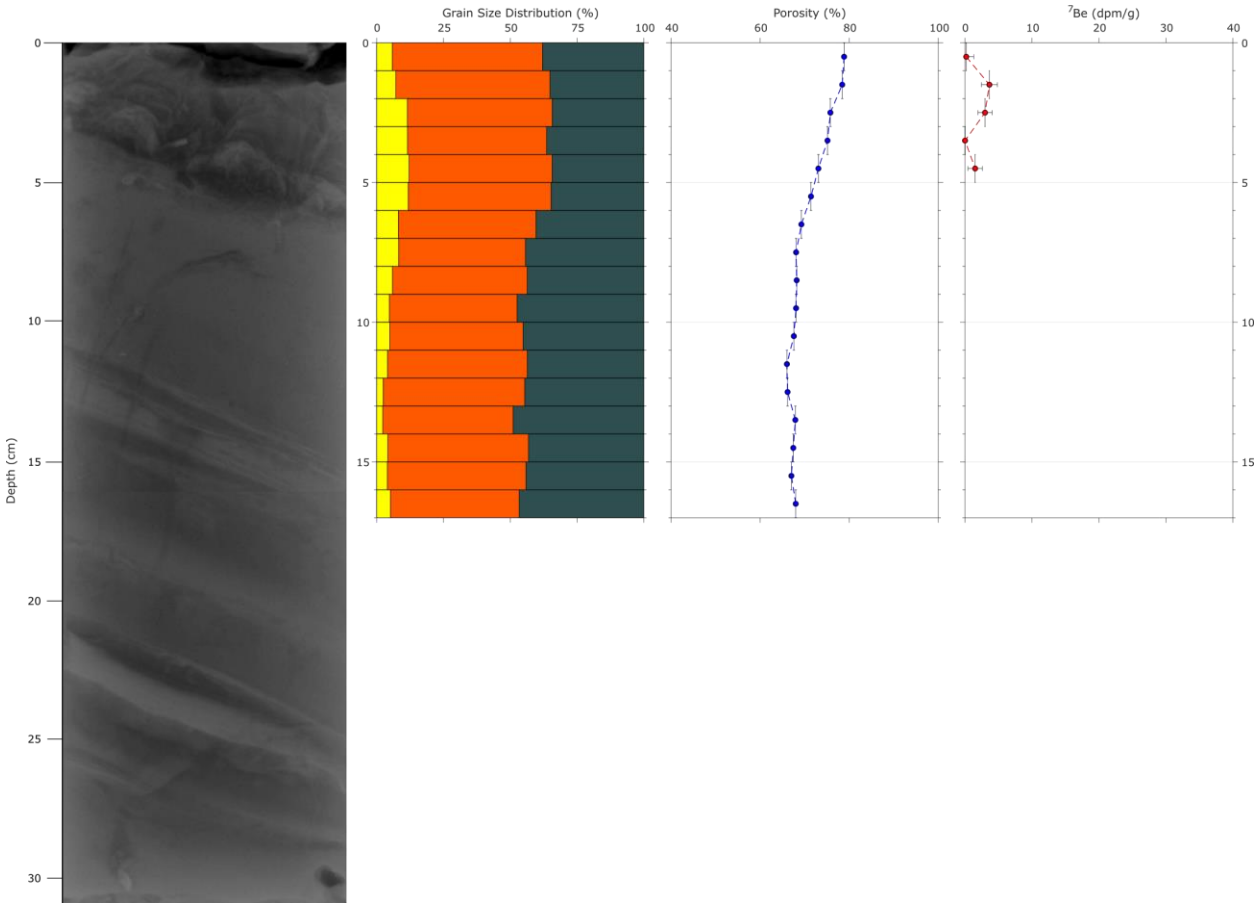

J-08

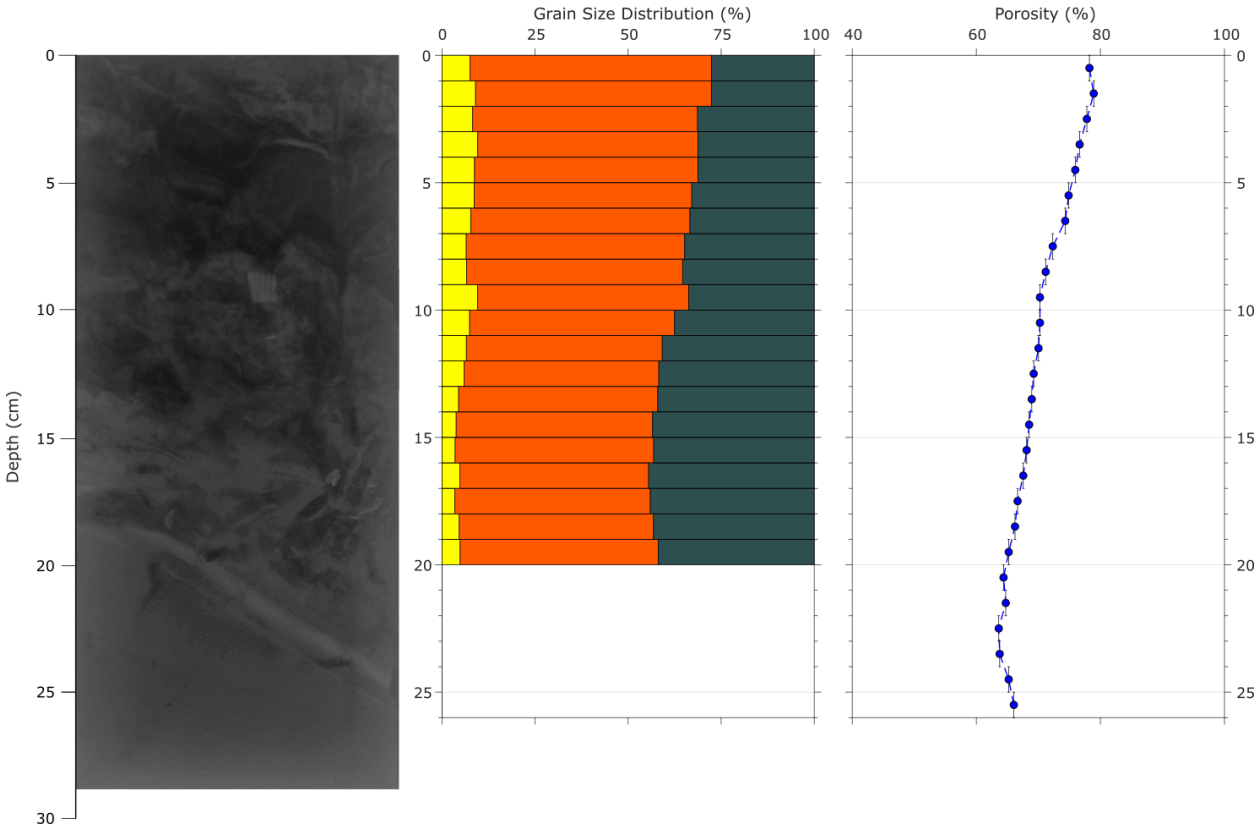
Grain Size Distribution (%)
Porosity (%)
Depth (cm)
0
5
10
15
20
25
30
40
60
80
100

S-06

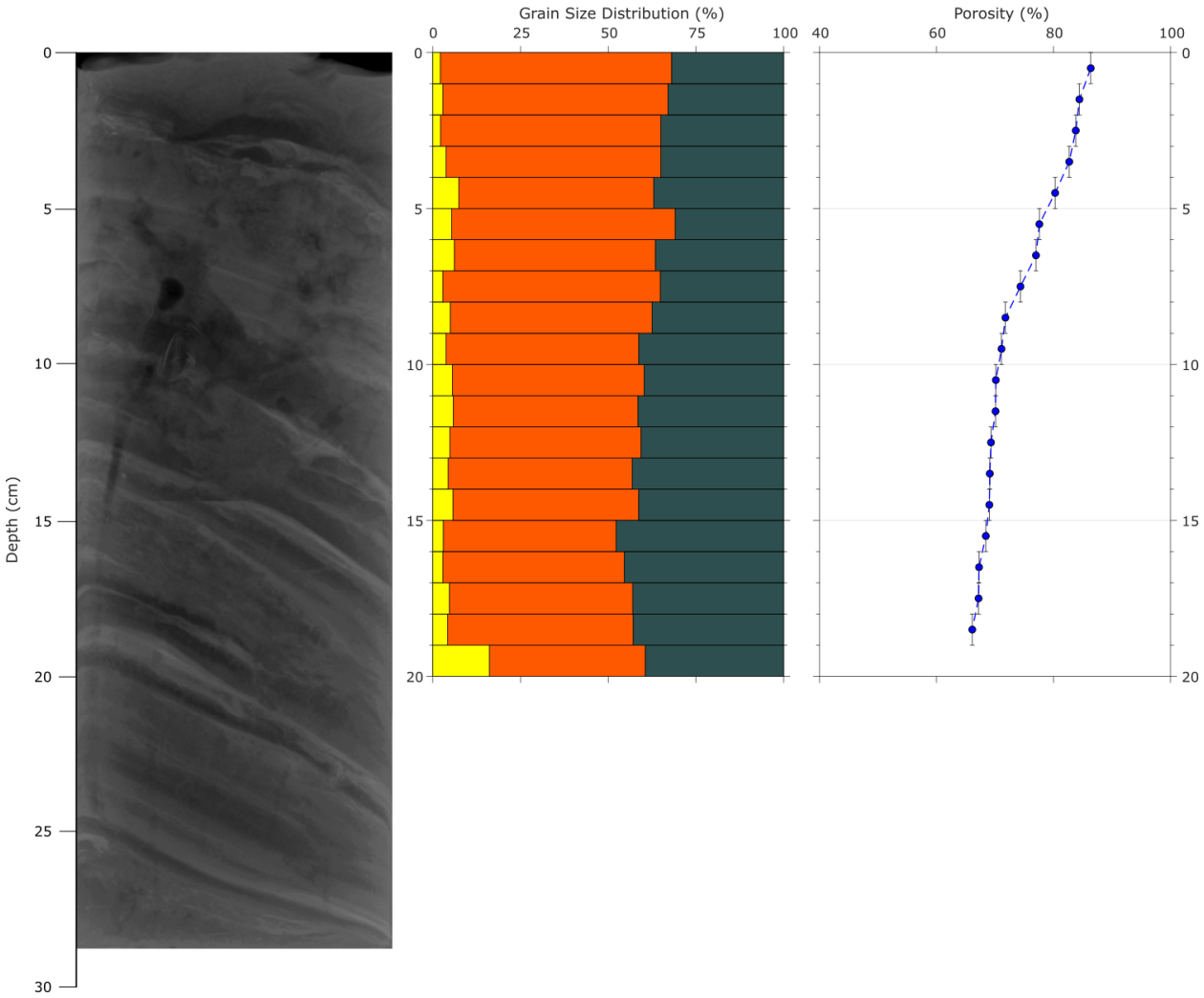
Grain Size Distribution (%)
0
25
50
75
100
Porosity (%)
40
60
80
100
Depth (cm)
0
5
10
15
20
25
30

S-12

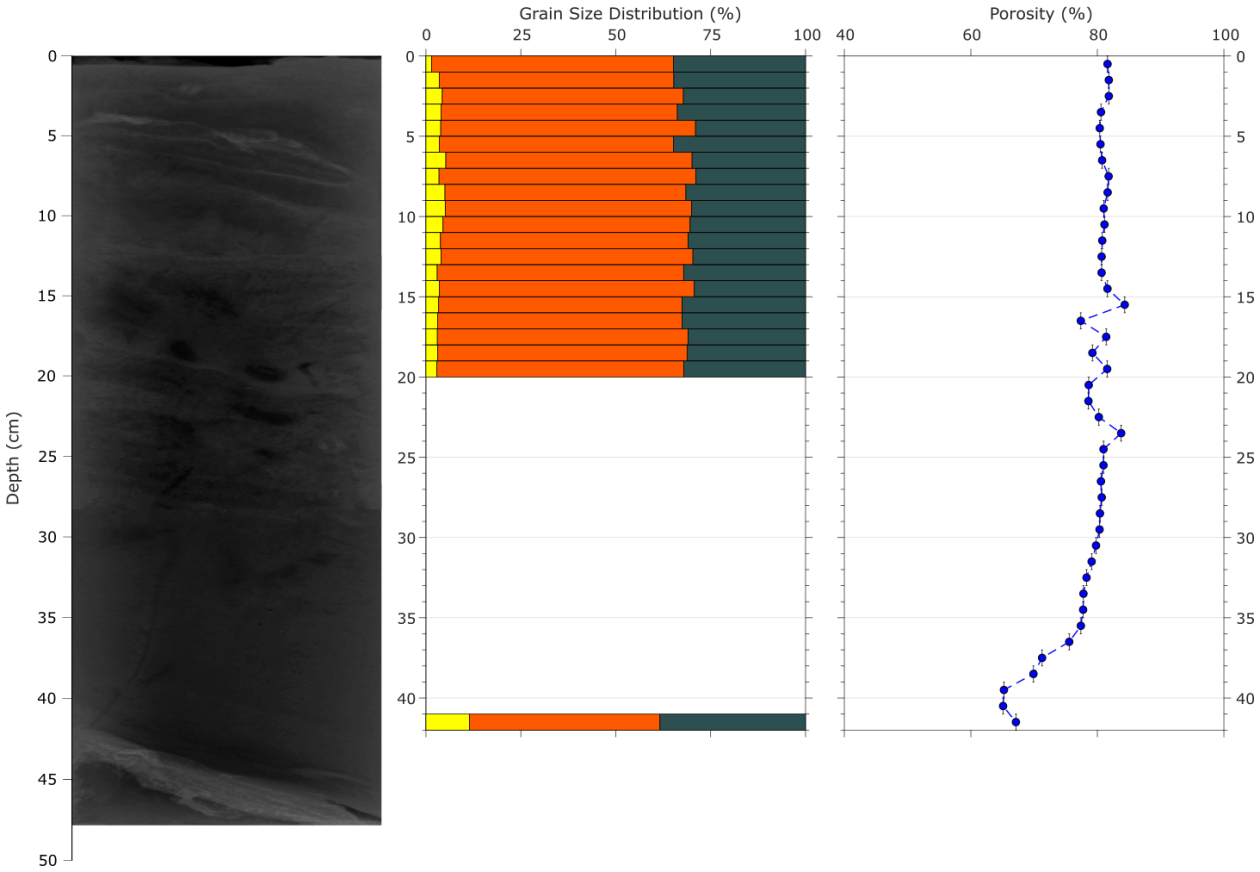
Grain Size Distribution (%)
Porosity (%)
Depth (cm)
0
5
10
15
20
25
30
35
40
45
50
0
25
50
75
100
40
60
80
100

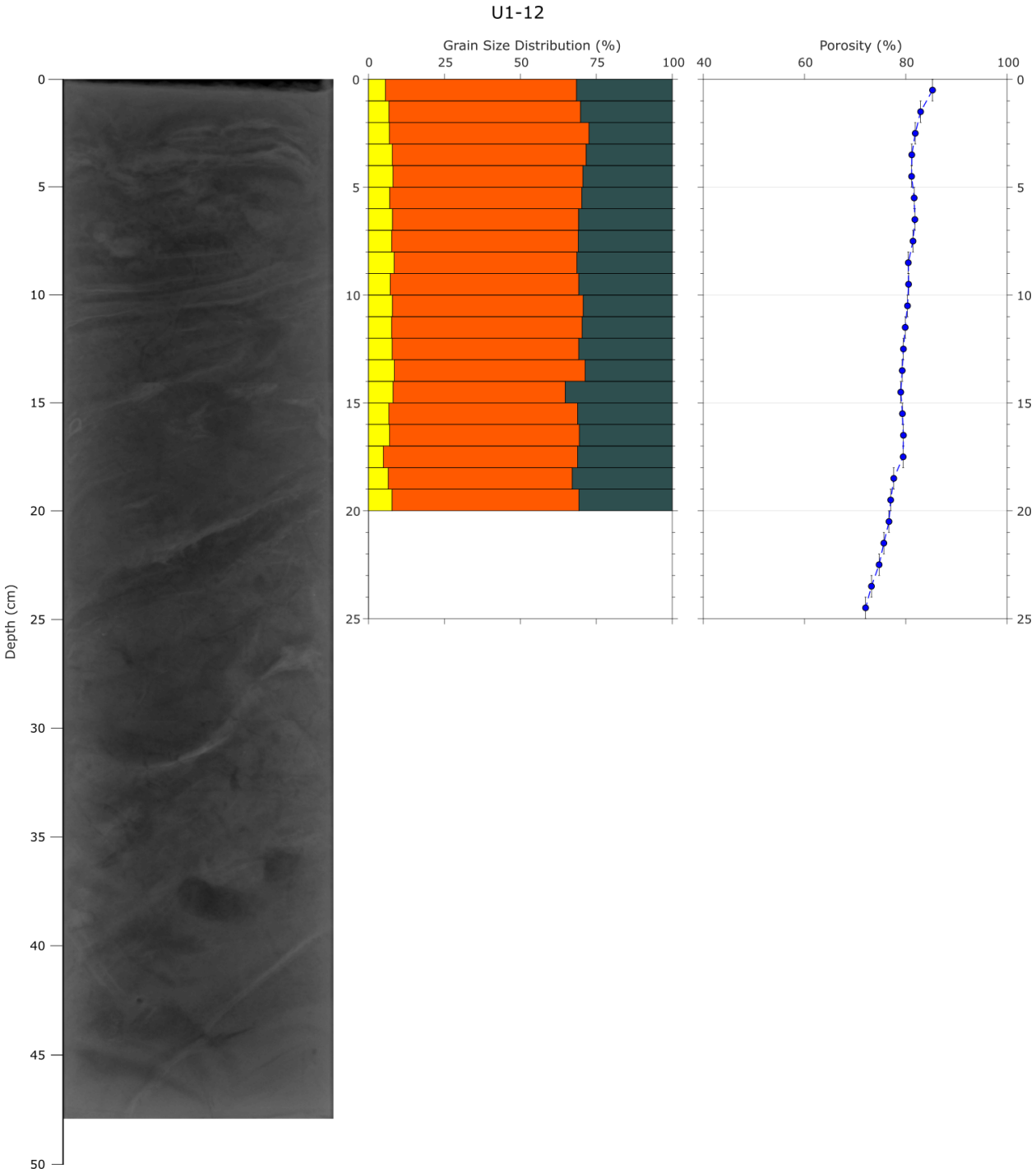
U1-12
Grain Size Distribution (%)
Porosity (%)
Depth (cm)
0
5
10
15
20
25
30
35
40
45
50
0
25
50
75
100
40
60
80
100